Technical University of Denmark - Spring 2006

Numerical modeling of the surf zone dynamics in Waimea Bay

Masters of Science Project

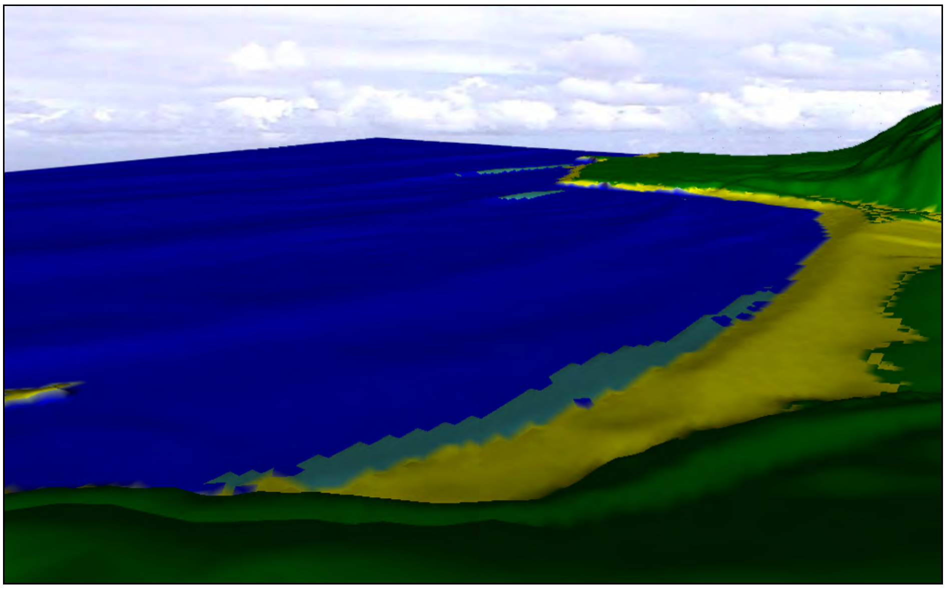

Student: ________________________________ Date ____________

S011250 Simon Brandi Mortensen

Supervisors:

Professor Per A. Madsen, MT, MEK, DTU

Professor Kwok Fai Cheung, University of Hawaii

Henrik Kofoed-Hansen, DHI Water & Environment

Acknowledgements

The University of Hawaii's Department of Ocean and Resources Engineering has most kindly hosted this research project under the supervision of Professor **Kwok Fai Cheung.** Professor **Per Madsen** from MEK DTU and **Henrik Kofoed-Hansen** from the DHI have been assisting as external supervisors. First of all I would like I would like to express my deepest gratitude to my three supervisors for allowing me to undertake this research project and for your kind help and assistance during the course of the study.

I would like to thank Professor **Geno Pawlak** for providing the necessary instruments and equipment for the field campaign and for his counseling and friendly coaching, and also Professor **Mark Merrifield** for his helpful advice on how to analyze the obtained field data.

Thank you to PhD student **Marion Chavanne** for teaching me how to calibrate the instruments and my deepest thanks to PhD student **Monte Hansen**, **Kimball Millikan** and PhD **Andrew B. Hebert** for obtaining the necessary permits and helping me carry out the underwater instrument deployment.

Thanks to PhD student **Volker Roeber** for providing me the surveyed Waimea Bay bathymetry data, to Professor **Jannette Frandsen** for lending me an extra computer for carrying out model simulations and to **Tyson Hilmer** for teaching me about digital video processing.

Thank you so much for your kind help and assistance.
My warmest Aloha to all of you.

Simon B. Mortensen
Denmark, July 25. 2006

1 Introduction

On the north shore of the Hawaiian island of Oahu located at 21°38’ W 158°03’ lies Waimea bay. During the winter months of November to March; Waimea Bay is frequently bombarded with long period groundswell with wave periods of typically 15-22 sec and wave heights ranging from 2 m to occasionally more than 10 m as measured by the Waimea wave buoy located 5.6 km offshore the bay in a water depth of 200 m.

figure 1 – Waimea Bay, North end

figure 2 – Waimea Bay, South end

The bay faces WNW (300°) and with the almost constant trade winds blowing from the east, Waimea bay is most often entirely sheltered from locally generated short period wind waves and therefore only subject to the long period groundswell usually originating from a direction of 300°-350°.

The almost rectangular shaped bay is only 640 m wide and 290 m long and with the exception of a reef situated along the north end of the bay and a few rocky outcrops along the south side of the bay, the bathymetry is fairly regular and mildly sloping with a average bottom gradient of 0.04.

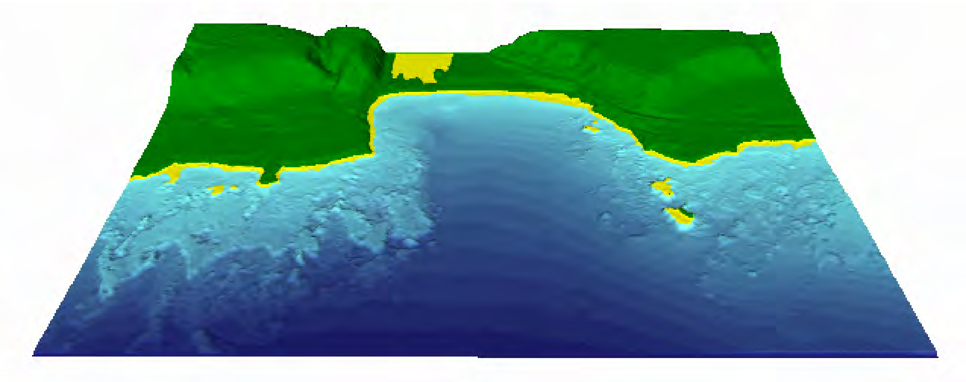

figure 3

The 2D-module of the MIKE21 BW software package developed by the Danish Hydraulic Institute is a state-of-the-art numerical modeling tool capable of modeling waves and wave driven currents in the coastal zone very accurately. The model uses the enhanced time-domain Boussinesq type equations initially presented in Madsen and Sørensen (1992) and later extended into the surf and swash zone as described in Madsen et al (1997a,b) and Sørensen et al (1998).

The main constraint of this enhanced Boussinesq model is that the maximum L_0/h ratio should be less than 0.5 and the bathymetry should be mildly sloping in order for the predictions to be reliable. Additionally the computational model domain should not be too extensive (in terms of the number of grid points) in order for the computational run-time to be within reasonable limits.
As a result it is clear that Waimea bay is an ideal location for assessing the performance of the MIKE21 BW model in a full-scale natural wave-environment.

The goal of this research project has been to use this enhanced Boussinesq model in an attempt to simulate the complex wave transformations and wave-driven current processes occurring in Waimea bay. For verification the model results are compared with field measurements obtained from a small-scale field campaign carried out as a part of this project, and the results of this comparison are thoroughly discussed and analyzed.

2 Governing Equations

The following chapter is based on the work presented in Madsen & Sørensen (1992), Madsen et al. (1997a) and Sørensen et al. (1998).

The 2D module of MIKE21 BW is based on the two dimensional Boussinesq equations with enhanced linear dispersion characteristics in a depth integrated flux-formulation presented in Madsen et al. (1997).

$$\frac{\partial \eta}{\partial t} + \frac{\partial P}{\partial x} + \frac{\partial Q}{\partial y} = 0 \tag{1.}$$

$$\frac{\partial P}{\partial t} + \frac{\partial}{dx}\left(\frac{P^2}{d}\right) + \frac{\partial}{dy}\left(\frac{PQ}{d}\right) + \frac{\partial R_{xx}}{\partial x} + \frac{\partial R_{xy}}{\partial y} + gd\frac{\partial \eta}{\partial x} + \psi_x + \frac{\tau_x}{\rho} = 0 \tag{2.}$$

$$\frac{\partial Q}{\partial t} + \frac{\partial}{dx}\left(\frac{Q^2}{d}\right) + \frac{\partial}{dy}\left(\frac{PQ}{d}\right) + \frac{\partial R_{yy}}{\partial y} + \frac{\partial R_{xy}}{\partial x} + gd\frac{\partial \eta}{\partial y} + \psi_y + \frac{\tau_y}{\rho} = 0 \tag{3.}$$

In this formulation d is the total water depth and P and Q are the depth-integrated velocities.

The terms ψ_x and ψ_y are dispersive Boussinesq type terms derived under the mild-slope assumption (ignoring higher order derivatives of $h(x)$) and enhanced to provide improved frequency dispersion characteristics by adopting a Pade expansion scheme in the truncation of the velocity terms instead of using Taylor expansion. These equations were first derived by Madsen and Sørensen (1992) and are expressed by:

$$\begin{aligned}\psi_x &= -\left(B+\frac{1}{3}\right)h^2\left(\frac{\partial^3 P}{\partial x^2 \partial t} + \frac{\partial^3 Q}{\partial x \partial y \partial t}\right) - Bgh^3\left(\frac{\partial^3 \eta}{\partial x^3} + \frac{\partial^3 \eta}{\partial x \partial y^2}\right) \\ &- h\frac{\partial h}{\partial x}\left(\frac{1}{3}\frac{\partial^2 P}{\partial x \partial t} + \frac{1}{6}\frac{\partial^2 Q}{\partial y \partial t} + 2Bgh\frac{\partial^2 \eta}{\partial x^2} + Bgh\frac{\partial^2 \eta}{\partial y^2}\right) - h\frac{\partial h}{\partial y}\left(\frac{1}{6}\frac{\partial^2 Q}{\partial x \partial t} + Bgh\frac{\partial^2 \eta}{\partial x \partial y}\right)\end{aligned} \tag{4.}$$

$$\begin{aligned}\psi_y &= -\left(B+\frac{1}{3}\right)h^2\left(\frac{\partial^3 Q}{\partial y^2 \partial t} + \frac{\partial^3 P}{\partial x \partial y \partial t}\right) - Bgh^3\left(\frac{\partial^3 \eta}{\partial y^3} + \frac{\partial^3 \eta}{\partial y \partial x^2}\right) \\ &- h\frac{\partial h}{\partial y}\left(\frac{1}{3}\frac{\partial^2 Q}{\partial y \partial t} + \frac{1}{6}\frac{\partial^2 P}{\partial x \partial t} + Bgh\frac{\partial^2 \eta}{\partial x^2} + 2Bgh\frac{\partial^2 \eta}{\partial y^2}\right) - h\frac{\partial h}{\partial x}\left(\frac{1}{6}\frac{\partial^2 P}{\partial y \partial t} + Bgh\frac{\partial^2 \eta}{\partial x \partial y}\right)\end{aligned} \tag{5.}$$

Where B is given by 1/15.

<u>Linear dispersion characteristics</u>

A small 1D study has been carried out in order to assess the governing equations linear dispersion characteristics. By only considering the x-direction, equation (1) can be simplified to:

$$\frac{\partial\eta}{\partial t}+\frac{\partial P}{\partial x}=0 \qquad 6.$$

Considering non-breaking wave conditions and ignoring bottom friction, equation (2) can be simplified to (by inserting equation (4)):

$$\frac{\partial P}{\partial t}+gh\frac{\partial\eta}{\partial x}-Bgh^3\frac{\partial^3\eta}{\partial x^3}-(B+\tfrac{1}{3})h^2\frac{\partial^3 P}{\partial x^2\partial t}-\frac{\partial h}{\partial x}\left(2Bgh^2\frac{\partial^2\eta}{\partial x^2}+\tfrac{1}{3}h\frac{\partial^2 P}{\partial x\partial t}\right)=0 \qquad 7.$$

By cross-differentiation and combination of (6) and (7) you get:

$$\frac{\partial^2\eta}{\partial t^2}-gh\frac{\partial^2\eta}{dx^2}+Bgh^3\frac{\partial^4\eta}{dx^4}-(B+\tfrac{1}{3})h^2\frac{\partial^4\eta}{\partial x^2\partial t^2}=\frac{\partial h}{\partial x}\left(g\frac{\partial\eta}{\partial x}+(2B+1)h\frac{\partial^3\eta}{\partial x\partial t^2}-5Bgh^2\frac{\partial^3\eta}{\partial x^3}\right) \qquad 8.$$

The solution to this equation can be expressed by:

$$\eta(x,t)=A(x)e^{i(\omega t-\varphi(x))} \qquad 9.$$

Where A is the wave amplitude, ω is the angular frequency and φ is the phase shift expressed by:

$$\frac{\partial\varphi}{\partial x}=k(x) \qquad 10.$$

By inserting (9) into (8) and assuming that A, h and k are only slowly varying functions of x, their spatial derivatives can be ignored and the linear dispersion relation is obtained given by:

$$\omega^2=\frac{3\left(gk^2h+Bgk^4h^3\right)}{3+k^2h^2+3Bk^2h^2} \qquad 11.$$

The linear dispersion relation derived from linear wave theory is given by:

$$\omega_{stokes}{}^2=g\cdot k\cdot\tanh(kh) \qquad 12.$$

From (11) and (12) the following ratio between the two is obtained and subsequently illustrated in figure 4.

$$\frac{\omega^2}{\omega_{stokes}{}^2}=\frac{3\cdot kh\cdot(1+\frac{1}{15}\cdot(kh)^2)\cdot\coth(kh)}{3+\frac{18}{15}\cdot(kh)^2} \qquad 13.$$

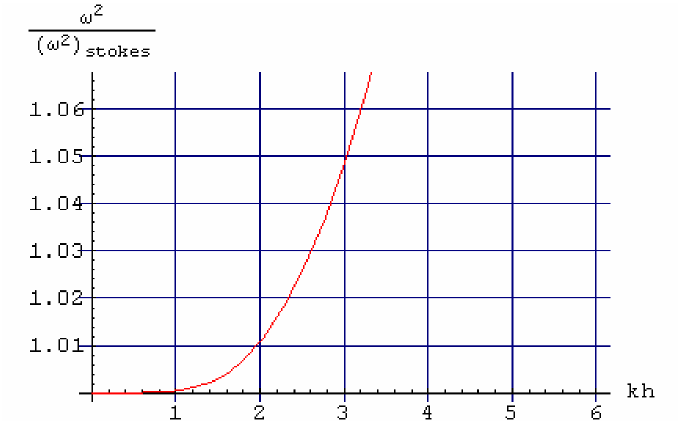

figure 4

From figure 4 it is observed how the governing equations show excellent linear dispersion characteristics up to a *kh* of about 1 after which is starts to grow increasingly inaccurate for larger *kh* values. The recommended maximum kh value in a Mike21 BW simulation is 3.15 *(DHI Software 2004)*, which in that case would correspond to a deviation of linear dispersion characteristics of 5.7%.

Wave breaking

The evolution equations have been extended to include the effects of wave breaking based on the concept of surface rollers, which is adapted from the breaking characteristics of a spilling breaker. The surface roller concept assumes that the effect of wave breaking can be modeled by imposing a volume of water (a roller) on the wave front (from the moment of breaking) traveling with the wave celerity c.

This change in the wave velocity profile leads to and excess in momentum, which is accounted for by the terms R_{xx}, R_{yy} and R_{xy} given by:

$$(R_{xx}, R_{xy}, R_{yy}) = \frac{\delta}{1-\delta/d}\left(\left(c_x - \frac{P}{d}\right)^2, \left(c_x - \frac{P}{d}\right)\cdot\left(c_y - \frac{Q}{d}\right), \left(c_y - \frac{Q}{d}\right)^2\right) \qquad (14.)$$

Here δ is the roller thickness and (c_x, c_y) are the wave/roller celerities.

In this model breaking occurs when the local wave steepness at the time t_B exceeds the initial breaker angle φ_B. After initial breaking the limiting gradient $\tan\varphi$ will gradually decay over time until reaching its terminal value of $\tan\varphi_0$. This decay is included in order to simulates the broken waves gradually transformation into a bore in the inner surf zone. The decay function is given by:

$$\tan\varphi(t) = \tan\varphi_0 + (\tan\varphi_B - \tan\varphi_0)\cdot\exp\left(-\ln 2\frac{t-t_B}{t_{1/2}}\right) \tag{15.}$$

Where $t_{1/2}$ is half time for the transition from φ_B and φ_B.

The toe of the roller is then defined as points satisfying the condition that the absolute value of the gradient equals the instantaneous local value of tanφ and that the gradient is negative in the direction of the wave propagation.

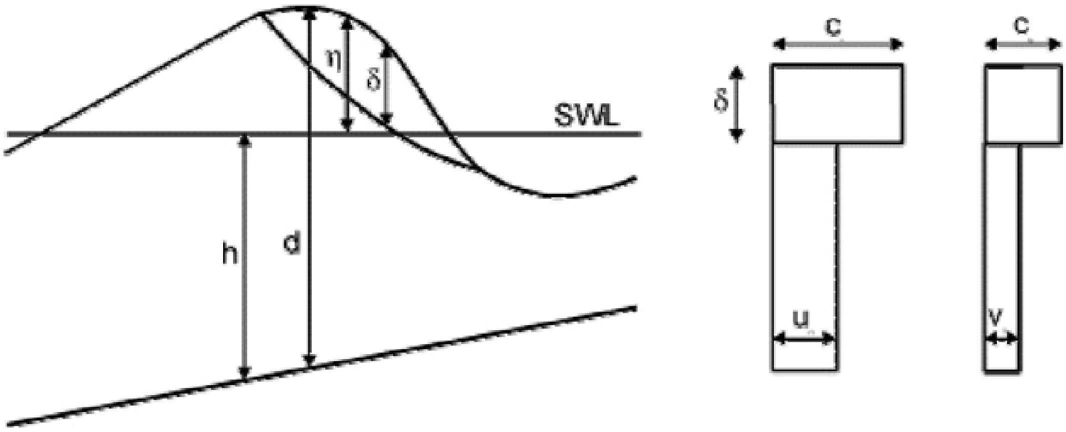

figure 5

In each toe point a tangent is imposed with the slope of tanφ and pointing in the opposite direction of the wave propagation as observed in figure 5. The roller thickness δ is then straight forwardly defined as the water above this tangent multiplied with the shape factor f_δ.

In nature wave breaking can be divided into 4 categories: Plunging, spilling, surging and collapsing. The breaker type can be determined using the surf similarity parameter given by:

$$\zeta = \tan\beta\sqrt{\frac{L_0}{H_b}} \tag{16.}$$

Where β is the beach slope, L_0 is the deepwater wavelength and H_b is the wave height at the break point. From Nielsen (2003) a table of the range of each breaker type is given.

Surf similarity parameter	**Breaker type**
4<ζ	Little or no breaking (Reflection)
2<ζ<4	Collapsing or surging breaker
0.4<ζ<2	Plunging Breaker
ζ<0.4	Spilling Breaker

table 1

It should be clear that each of these 4 types of breaking has different energy dissipation characteristics as well as visual appearance and behavior. As mentioned earlier the “roller concept” has been developed on the assumption of spilling breakers, which might provide an unsatisfying inaccurate prediction of energy dissipation if trying to simulate a surf zone containing one of the other 3 breaker types.

Wave celerity

The original Boussinesq model presented by Madsen et al. (1992) the wave celerity is calculated interactively from the local wave field. However as this feature can result in stability problems in the MIKE21 BW 2D-module the celerity is instead obtained from Sørensen et al (1997) given by a two dimensional expression of the linear formulation $c = 1.3\sqrt{gh}$:

$$\begin{pmatrix} c_x \\ c_y \end{pmatrix} = \begin{pmatrix} \frac{\partial\eta}{\partial x} \\ \frac{\partial\eta}{\partial y} \end{pmatrix} \cdot \frac{1.3 \cdot \sqrt{gh}}{\sqrt{\left(\frac{\partial\eta}{\partial x}\right)^2 + \left(\frac{\partial\eta}{\partial y}\right)^2}} \tag{17.}$$

Here η is the surface elevation and h is the still water depth. This linear celerity formulation has been shown to provide good results for regular waves, but it does not capture irregular wave phenomena like deceleration of the primary waves due to wave down-rush of long waves in the swash zone, which can be important in some model applications.

Bottom friction

The final terms in the evolution equations are the dispersive terms due to bottom friction which are given by:

$$(\tau_x, \tau_y) = \frac{1}{2} \cdot f_m \cdot \rho \cdot \frac{\sqrt{P^2 + Q^2}}{d^2}(P, Q) \tag{18.}$$

Here f_m is the friction factor, P and Q the depth integrated velocities and d the instantaneous water depth (d= h + η). However in the MIKE21 program interface the bottom selected in terms of the Chezy number C where:

$$C = \sqrt{\frac{2g}{f_m}} \tag{19.}$$

Hence:

$$\left(\tau_x,\tau_y\right)=\frac{1}{2}\cdot\frac{2g}{C^2}\cdot\rho\cdot\frac{\sqrt{P^2+Q^2}}{d^2}\left(P,Q\right) \tag{20.}$$

<u>Moving shoreline</u>

In order to be able to handle the moving boundary at the shore and gain the ability to simulate swash zone properties such as the wave run-up, the numerical model uses a method typically referred to as the "Slot technique" described in Madsen et al (1997). Using this approach the computational domain is extended artificially by introducing an artificial porous flow domain on the impermeable beach by introducing a permeable beach with very small porosity. Numerically the permeable beach is treated like water filled "slots" allowing waves to "propagate" into the beach slope and thereby handling the zero-water depth problem in the numerical calculations when trying to calculate a point based on a water point and a land point. The transition between the physical and porous flow regime is given by:

$$\gamma(z)=\begin{cases}1 & Z_L\le z\\ \varepsilon+(1-\varepsilon)\cdot e^{\beta(z-Z_L)/(Z_L-Z_B)} & Z_B\le z\le Z_L\end{cases} \tag{21.}$$

Here $\gamma(z)$ is the porosity, ε is the minimum value of γ, β is a constant shape factor defining the exponential transition between the physical and porous flow regime, z is the vertical coordinate, Z_L is the vertical location of the physical seabed and Z_B defines the lower limit of the porous region, which as minimum should be located offshore the swash zone which marks the limit for the fluctuation of the moving boundary.

The resulting effective water depth *A* can then be calculated as:

$$A(x,y,t)=\int_{Z_B}^{\eta}\gamma(z)dz \tag{22.}$$

Thus in the porous flow domain the water depth A is used in the depth-integrated momentum equations (1) and (2) instead of *d*. However as the porosity domain consists of a porous beach with clear water on top in the depth-integrated continuity equation can not be straight forwardly modified to include a depth-integrated porosity as this would lead to porous flow everywhere in this domain.

Instead (3) is modified by:

$$\alpha\frac{\partial\eta}{\partial t}+\frac{\partial P}{\partial x}+\frac{\partial Q}{\partial y}=0 \tag{23.}$$

Where:

$$\alpha(x, y, t) = \gamma(\eta) \quad (24.)$$

Where η is the surface elevation.

<u>The numerical scheme</u>

For the purposes of this study the differential equations used in the 2D-module of the MIKE21 BW is discretisized using a time-centered implicit scheme with variables defined on a space-staggered rectangular grid. The method is called the System21 scheme and is based on the Altering Direction Algorithm. The resulting system of finite difference equations is reduced to a tri-diagonal system, solved by the Double Sweep Algorithm as explained in Madsen (1992). However as the model is known to become unstable in regions with steep gradient introducing artificial oscillations, a simple unwinding scheme is applied in theses areas. The transition is set to occur when the absolute value of the second-difference of the local depth-integrated velocity grows larger than the first-difference of the local depth-integrated velocity.

When resolving the Boussinesq cross-terms the standard representation results in these terms to be back centering half a time-step, which will result in an artificial dissipation of waves traveling with an angle to the grid. As a result a linear extrapolation scheme has been used to avoid this effect. However this method of time-centering the cross-terms will sometimes result in model instability, which is accounted for in the model by incorporating a time-extrapolation factor, which can attain values between 0 and 1. A value of 1 represents a correct time centering and 0 represents a backward centering of the Boussinesq cross-terms.

3 Preliminary Study

Due to the extensive complexity of the modeling task at hand, a preliminary study has been carried out, where the most governing wave transformation processes has been modeled separately on simplified bathymetries using MIKE21 BW and the results compared with laboratory experiments. The preliminary study has been divided into 2 case studies.

- In case study 1 MIKE21 BW is used to model the cross-shore motion and breaking of regular and irregular waves on a plane sloping beach.
- In case study 2 MIKE21 BW is used to model the rip channel flow on an open beach and the circulation flow behind a breakwater.

The primary objective of these case studies is to carry out a proper assessment of how well MIKE21 BW deals with modeling each of these wave-induced processes individually using simplified model domains that allows the MIKE21 BW model predictions to be benchmarked with laboratory experiments.

The model setup and verification for both test cases in the preliminary study has been based on the work carried out in (Madsen et al. 1997 Part I-III).

3.1 Case 1 –Surf zone dynamics on a plane sloping beach

3.1.1 Mild slope, spilling breaker:

In the first part of this case study the wave-breaking module in MIKE21 BW is tested, by setting up a model, where directional monochromatic waves are set to propagate over a gently sloping bottom bathymetry.

As explained earlier the MIKE21 breaker module is based on the spilling breaker assumption.

For that reason it would be the most appropriate if the first model test in the assessment fulfilled this criterion.

(Stive 1980) has carried out wave tank experiments with regular waves with an initial wave height H of 0.145 m and a wave period T of 1.179 sec propagating on a beach slope of 1/40. The deepwater water depth h_{max} is 0.7 m. Under these conditions a spilling breaker should be expected.

The model is set to simulate this experimental study using at grid spacing dx of 0.05 m. A 2nd order stokes wave is set at the deepwater limit to represent the initial wave condition at the wave generation line.

The time step dt is set to 0.005 sec, which for the given corresponds to a Courant number of 0.26.

Offshore the wave generation line a sponge layer is placed to damp out all wave oscillations propagating offshore of it. The length of the sponge layer should be at least half the wavelength, which for the given T and h_{max} results in a wavelength L of 4 m. For convenience the length of the sponge layer L_{sponge} is set to 50 grid points (2.5 m) to assure that nothing is being reflected from the offshore back wall. The wave generation line is located at the toe of the slope.

After reaching the shoreline the beach continues to rise to an elevation h_{Beach} of 1.0 m, which corresponds to a horizontal beach length L_{Beach} of 40 m.

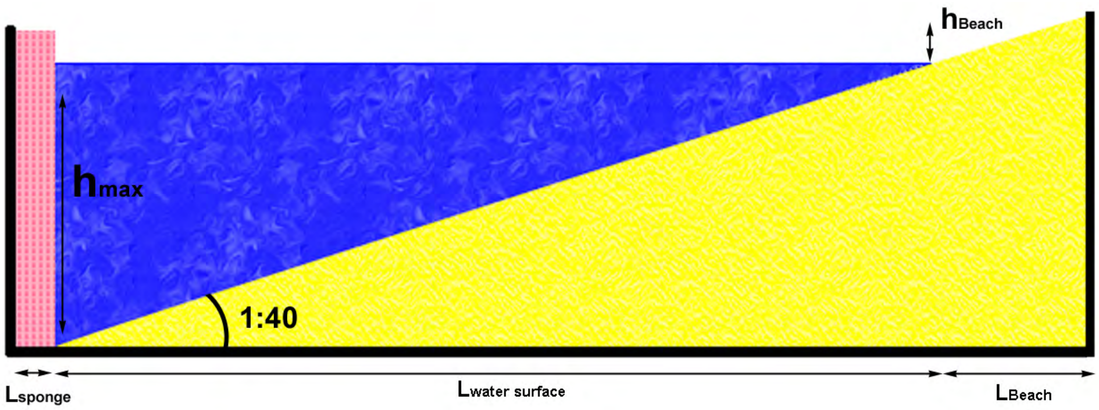

Figure 6

As explained earlier MIKE21 uses the slot technique to incorporate run-up, allowing water to propagate into the slope. So while the expected horizontal run-up should not reach more than in the order of 1 m, the unphysical propagation of water inside the slope extend much further. So the straight forward reason for choosing such a large beach area is simply to be absolute certain that the incoming waves do not get a chance to interfere with the back wall at the right boundary of the domain creating numerical instabilities and inaccurate model predictions.

Near the initial shoreline a low-pass filter is applied in order to damp out high-frequency instabilities and to dissipate the wave energy in the area where the surface roller cannot be resolved.

The simulation is run for 50.000 time steps (250 sec) in order to insure a proper development and stabilization of the wave setup.

When outputting and spatially plotting the wave height and the mean surface elevation (wave setup), it was quickly realizes that the position of the filter as well as the value of the filter coefficient itself had a significant influence on the model output. It was also discovered that different filter setups allowed for smaller slot widths than others and that the slot width itself also had some influence on the on the model output.

Influence of the filter coefficient value.

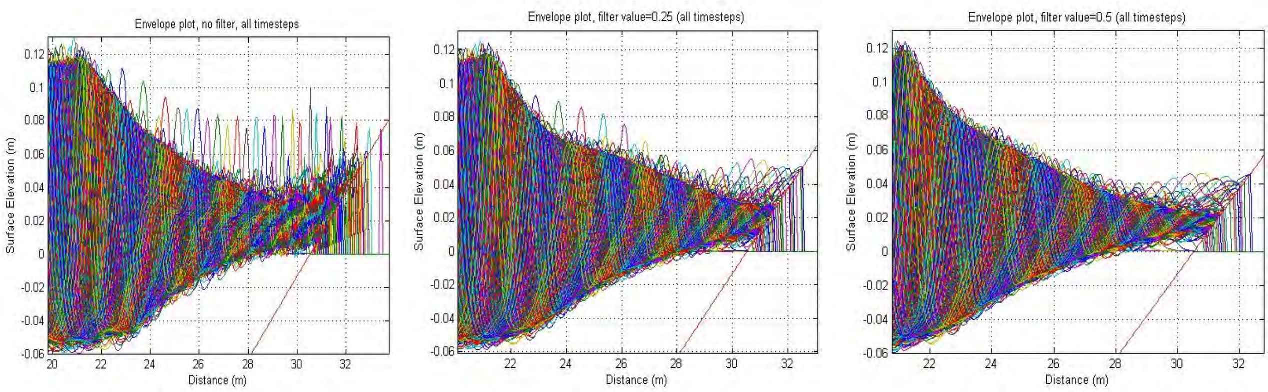

Figure 7

In Figure 7 envelope plots are made for 3 simulations using each using a different filter setup. For all 3 simulations a slot width *b* of 0.05 has been used.

The envelope plot to the left represents a simulation where no filter has been used. In the two other simulations presented in the center and right side plot, a filter with a filter value of respectively 0.25 and 0.5 have been applied. Both filters are applied in the surf and swash zone and start at 21.25 m, which is the first landward grid point following the determined breakpoint in the no-filter simulation. It is noticed how high frequency high amplitude oscillations are appearing in the surf and swash zone and how they are increasingly damped when the filter value is increased. With a filter value of 0.5 these oscillations have almost been entirely damped in the surf zone and only appear moderately in the swash zone close to the shoreline.

However an interesting observation was that the high-frequency high-amplitude oscillations in the surf zone only appear during the first couple of time steps. When plotting the last 20000 time steps of the 3 simulations, the envelope plots suddenly looks much more identical.

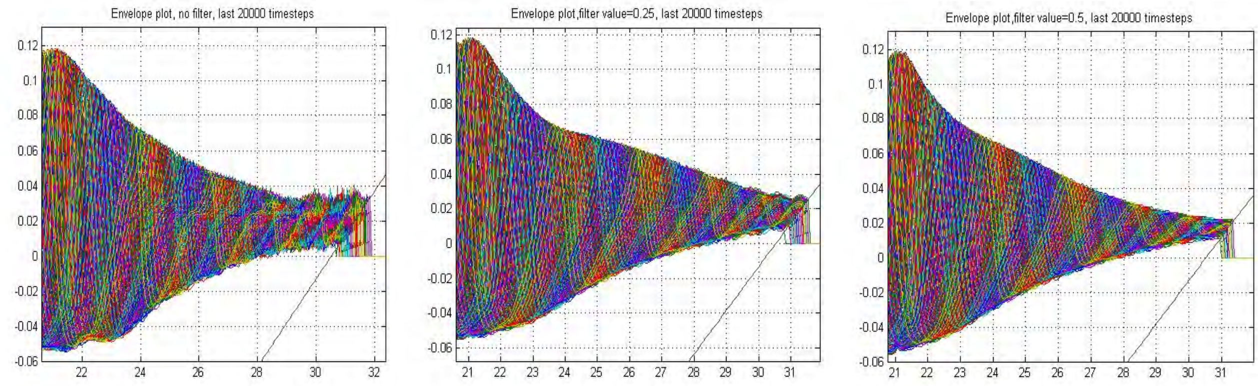

Figure 8

Gone are the high-frequency oscillations in the surf zone and now only the ones in the swash zone remains for the no-filter case and also to a minor degree for the case with a filter value of 0.25.
The conclusion is that the high-frequency high amplitude oscillations in the surf zone must be numerical instabilities that occur only during the first time steps until the model has reached quasi-static conditions, with a fully developed wave setup. As a result the high-amplitude instabilities in the surf zone does not contribute significantly to a distortion of the evolution of the outputted phase averaged wave height and setup in this region. But because the numerical instabilities can lead to model "blow-up" and e.g. limits the minimum slot width that can be used in the model, it is concluded to be the best approach to extend the filter into the surf zone.

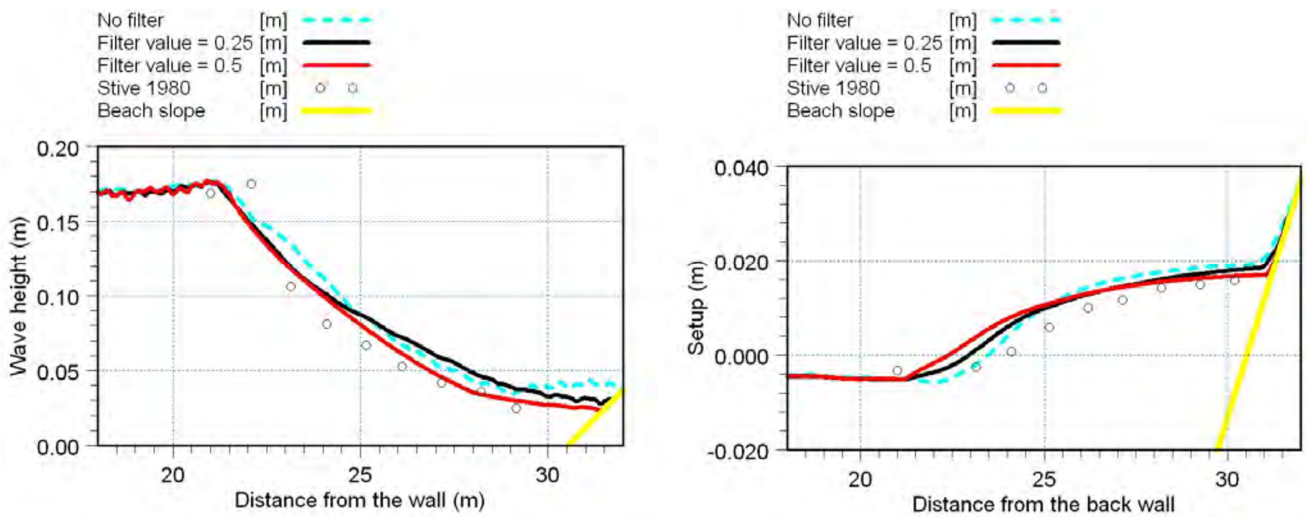

Figure 9

But meanwhile the lifespan of the numerical instabilities in the surf zone are short, it is noticed that high-frequency oscillations continue to exist in the swash zone near the shoreline, where the surface roller cannot be resolved. These can only be removed by applying the low-pass filter and from Figure 8 it can be concluded that the filter value should be 0.5 in order for the high-frequency oscillations to be removed correctly. When comparing to (Stive 1980) it can be observed how the model predicted wave height in the surf zone is overestimated if no filter is applied. The best wave height model prediction is obtained if a filter value of 0.5 is used. Also when it comes to modeling the wave setup a filter with a filter value of 0.5 provides the most accurate prediction of the maximum wave setup at the shoreline. However on the other hand the "no filter" model simulation seems to give a better prediction of the point of initiation of wave setup.

It is observed that the model predicts the wave breakpoint to occur to early when compared to (Stive 1980). In the simulation where no filter is applied the difference is 0.9 m and when a filter is used the difference is 1.1 m. The model predicted breakpoint can be shifted landwards by slightly increasing the initial breaking angle, but it would not improve the overall wave height prediction of the model.

The model predicts the horizontal shift between the breakpoint and the initiation of wave setup, which is in (Madsen 1997) explained as being caused as result of the initial conversion of potential energy into forward momentum flux.

The shift is 0.2 m for the simulations where a filter is applied and 0.85 m when no filter is used. From (Stive 1980) the horizontal shift is measured to approximately 1 m, so it could be suggested that the model provides better predictions if the filter is applied sufficiently landward of the breakpoint.

Influence of the filter position

Next step is to investigate how important the seaward extension of the low-pass filter into the surf zone is to model predictions. 3 model simulations with different offshore extensions of the filter have been carried out and are compared to the simulation, where no filter is used.

For all simulations the slot width is 0.05 and the filter value is 0.5. In the simulation where no filter is applied the wave breakpoint is noticed to be located at 21.2 m from the offshore back wall of the model.

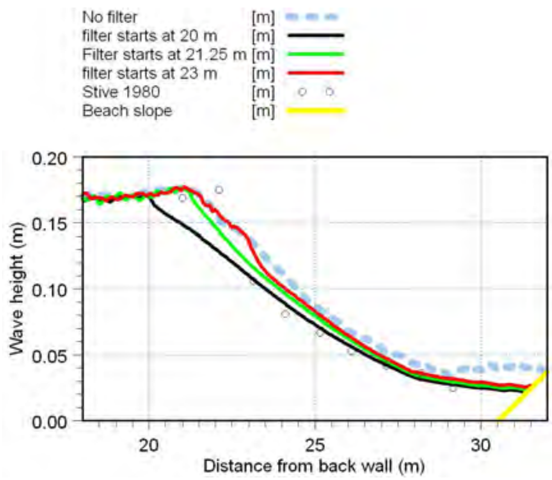

figure 10

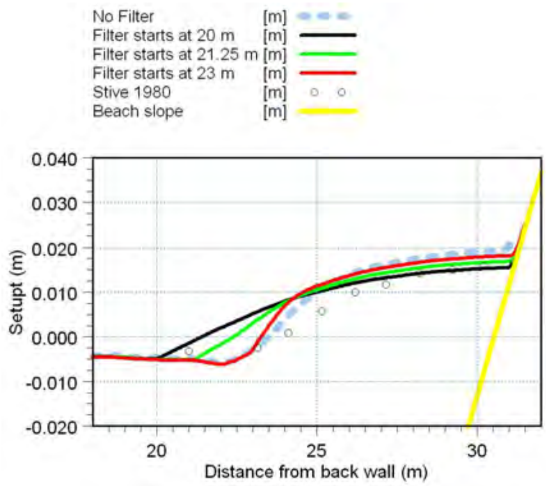

figure 11

It is clearly observed in figure 10 that if the filter is extended offshore (at 20 m) beyond the originally predicted breakpoint, it will lead to the breakpoint being predicted to be located at the new filter position, which of course is not correct. Locating the offshore limit of the filter landward of the breakpoint (at 23 m) does on the other hand not cause the predicted breakpoint to change (compared to the no-filter case).

However it is interesting to notice that when applying the filter just landward of the original breakpoint (occurring at 21.2 m), the new predicted breakpoint actually moves 0.25 m offshore.

From figure 11 it is observed how the placement of the filter also strongly affects the starting location of the wave setup. When the filter is applied offshore the original breakpoint the location of the wave setup also moves offshore corresponding to the original starting location (where no filter is uses). When the filter is applied just landward of the original breakpoint the breakpoint moves slightly offshore and so does the starting location of the wave setup. Applying the filter further landward from the original breakpoint (at 23 m) does not change the starting location of the wave setup compared with the no-filter simulation.

Finally it is noticed how the starting location of the wave setup is horizontally shifted landwards compared to the respective wave breakpoint for all 4 simulations.

For the simulation where the filter is applied at 20 m, the shift is 0.15 m. When the filter is applied at 21.25 m just landward of the original breakpoint, the shift is 0.2 and for the simulation with the filter starting at 23 m the shift is 0.85 m just as when no filter is applied.

It is clear that the offshore extension of the filter has a major influence on how large this horizontal shift is as predicted by the model.

When compared to (Stive 1980), the best wave height model prediction is obtained with a filter located at 21.25m just landward of the break point. When the filter is applied offshore the original breakpoint the model breakpoint prediction becomes completely wrong significantly decreasing model accuracy. If the filter is not applied, the wave height in the swash and inner surf zone is predicted inaccurately and the model easily becomes unstable. If the filter is applied at 23 m the breakpoint remains unchanged at 21.2 m. The wave height for this simulation is predicted fairly well with the exception of the area just landward of the breakpoint, where no filter is present.

Like in the previous study the initiation of wave setup is less well predicted if the filter is applied immediately landward of the breakpoint but on the other hand provides the most accurate prediction of the maximum wave setup near the shoreline. If the filter is applied at 23 m (1.8 m landward of the breakpoint) the point of initiation is the same as when no filter is used, but the prediction of the maximum setup is more accurate near the shoreline compared with the no filter case. If the filter is applied offshore the original breakpoint, the initiation of wave setup is predicted inaccurately offshore, and even though its prediction of maximum setup is the most accurate in the study compared to (Stive 1980), this is not interpreted as a suggestion of good model performance, but rather due to improper damping by the incorrectly placed filter.

From this study it can be concluded that the overall best model performance is obtained if the filter is placed sufficiently landward of the original breakpoint. The filter should cover the swash zone and not be extended further into the surf zone than strictly necessary to assure a stable model run.

Influence of the slot width

If for some reason the filter is not applied or if using a smaller filter value, this poses a lower limit to the allowed slot width in order to avoid blow-ups. 3 simulations using the same filter starting at 21.25 m and a filter value of 0.5 has been carried out and the results presented in Figure 12.

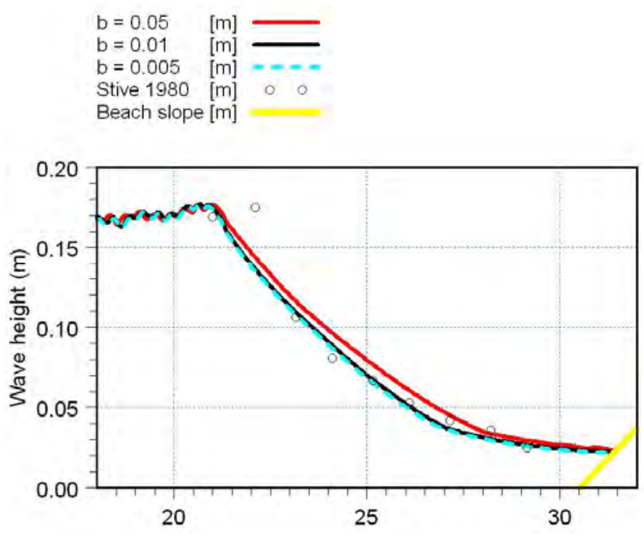

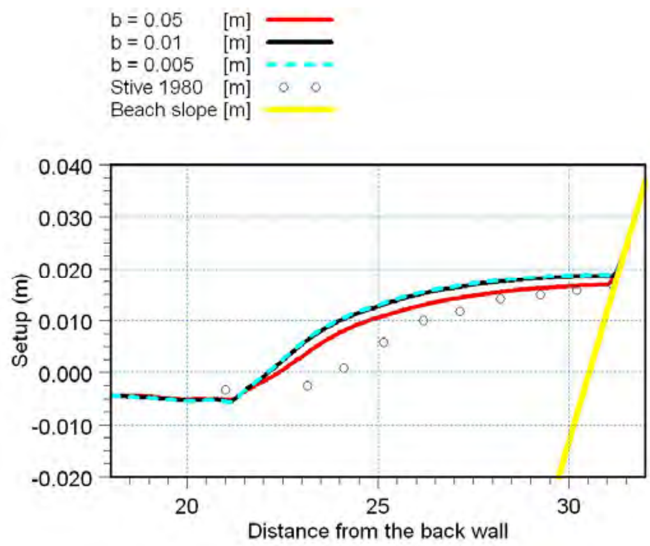

Figure 12 **Figure 13**

It is noticed how a slightly better prediction of the wave height if a slot width of 0.01 or smaller is used. However the model predicted magnitude of the wave setup becomes larger and deviates further from the experimental results by (Stive 1980) compared to the simulation where the slot width is 0.05.

The explanation is that as the water filled slots in the slope are increased; more water is allowed to propagate and be "lost" in the slope making the system less physical, which e.g. results in an underestimation of the magnitude of wave setup, even though this prediction is closer to the experimental results. There seem to be no difference between model results carried out with a slot width of 0.01 and 0.005. It is recognized that a smaller slot width can lead to model instability and eventually blow-up, but it should always be attempted to use a small a slot width as possible in order to make the computational domain (and thereby model predictions) as physical as possible.

3.1.2 Mild slope, spilling breaker

Another quite similar test case has been carried out in order to compare model performance with laboratory experiments carried out by Hansen & Svendsen (1984). The model setup consists of a rectangular flume with a horizontal section with a water depth of 0.36 m followed by a plane sloping beach of 1/34.25. The input wave condition uses is a monochromatic wave with a period of 2.0 seconds and a wave height of 0.12 m. Calculating the surf similarity parameter yields a spilling breaker in the flume. However it is noticed that the applied wave condition yields a highly non-linear solution at the model offshore boundary and as a result a Cnoidal wave has been used as input in the model.

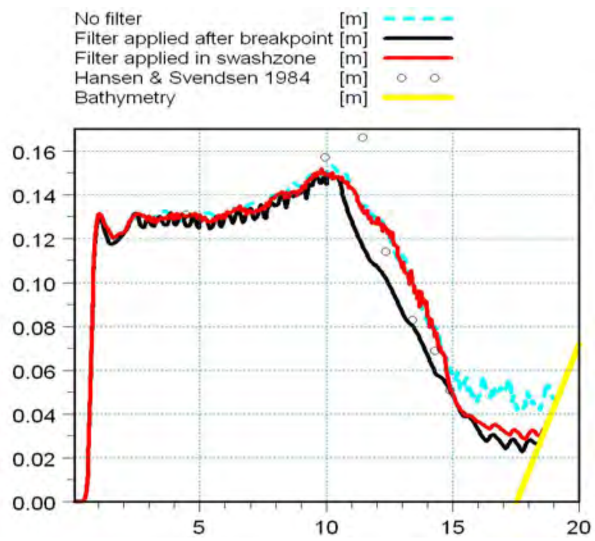

figure 14

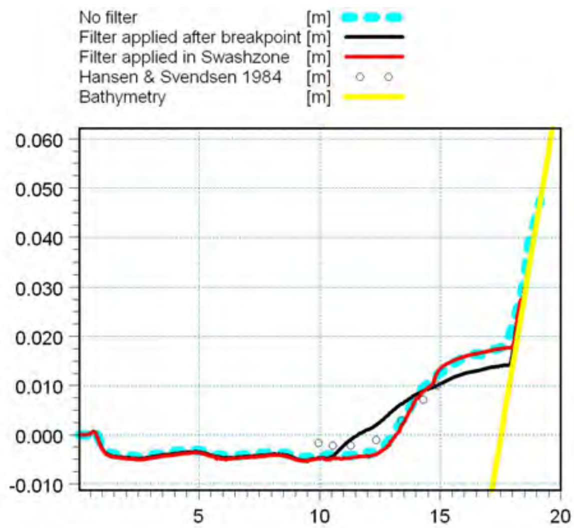

figure 15

From figure 14 and figure 15 it is again confirmed that the best agreement with laboratory data is obtained when applying a filter in the swash zone and how a misplaced filter near the actual break point results in an inaccurate prediction of the break point and the initiation of setup. As a result only the simulation containing a filter applied in the swash zone (the red line) will be commented in the following paragraph.

For this simulation it is noticed that the model predicts the initial shoaling very well in agreement with Hansen & Svendsen (1984) and also the surf zone is well predicted by the model. However it is noticed that the shoaling just offshore of the breakpoint is notably underestimated by the model, which is assumed to be a result of the models limited capability in handling non-linear shoaling. Non-linear shoaling is a combination of linear shoaling and an energy transfer to higher order harmonics. The Boussinesq model used in this study has proven to have excellent linear shoaling characteristics up to a *kh* of 3.15 for the primary wave harmonic but due to the same kh-limitation it generally underestimate the magnitude of the higher order harmonics. As an example the 2nd order harmonic is underestimated with more than 10% for a *kh* larger than 0.5. In comparison the *kh* for this simulation is 1.1 near the breakpoint and as so the underestimated shoaling at this location would be expected.

3.1.3 Steep slope, plunging breaker

Yet another simulation has been carried out to test the models capability in modeling a surf zone containing plunging breakers. As recalled the breaker module in the model was originally designed to deal with spilling breakers, but as a plunging breaker is expected to be dominant when modeling the surf zone dynamics in Waimea Bay, it was found important to pre-assess the model performance in such conditions.

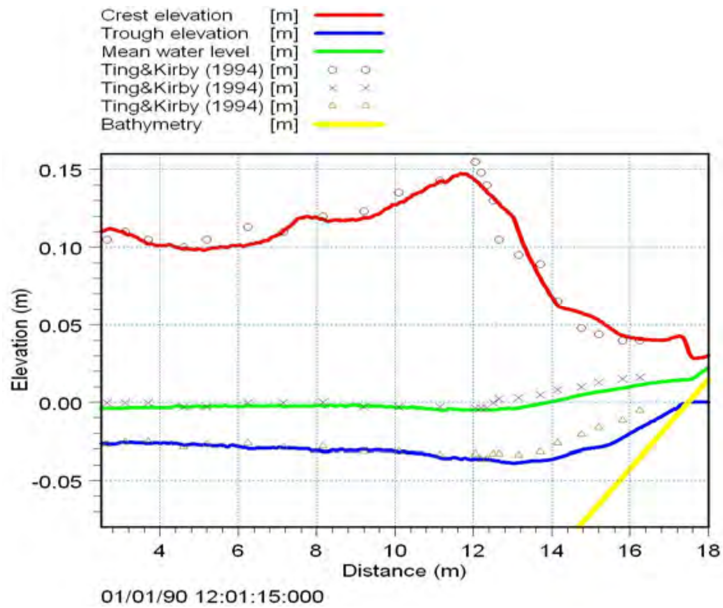

figure 16

A model simulation has been set up based on a laboratory experiment conducted by Ting & Kirby (1994) in a rectangular flume with a water depth of 0.4 m followed by a beach slope of 1/35. The wave conditions consist of monochromatic waves with period of 5.0 sec and a wave height of 0.125 m. In the model Cnoidal waves has been used to provide the offshore input. The grid spacing and time step is the same as for previous simulations. In order to account for the spilling breaker the initial breaker angle has been adjusted from 20° to 25° and the half-time cut-off from 1 sec (T/5) to 0.5 sec (T/10). The surface roller shape factor has been set to 2.

From figure 16 it is noticed how the break point is very well predicted and also the non-linear shoaling characteristics are much better compared to figure 14 in the previous simulation. The explanation is that the wave numbers are much smaller for this simulation (kh_{max}=0.26) thus the higher order harmonics near the break point are much better estimated compared to the previous simulation. Overall the agreement between Ting & Kirby (1994) and model results are most satisfying and contributes to the overall justification for using the present model to simulate the surf zone dynamic in Waimea Bay.

3.1.4 Propagation and breaking of irregular wave train

The input wave time-series used in the Waimea Bay model simulation is obtained from a measured surface elevation time-series provided by an ADCP placed at the location of the model offshore boundary. The resulting input wave time-series in the model will resemble an irregular wave train that will go through a large number of complex transformation processes while propagating through the domain.

Due to the complexity of the 2D-modeling task at hand, it was found reasonable to first assess Mike21 BWs capability to simulate some of these processes (such as triad-interactions and bound harmonic releases due to breaking of irregular wave-trains) in a 1D environment using a simplified bathymetry.

In a laboratory study by Mase (1994) a bichromatic input was applied in a rectangular wave flume consisting of a flat section with a water depth of 0.47 m followed by a sloping beach of 1/23. In the experiment the bichromatic input were all given expressed by:

$$\eta = a \cdot \cos(2\pi \cdot f_1 t) + a \cdot \cos(2\pi \cdot f_2 t)$$

Where

$$f_1 = \left(1 + \frac{\Delta}{2}\right) \cdot f_m \qquad f_2 = \left(1 - \frac{\Delta}{2}\right) \cdot f_m$$

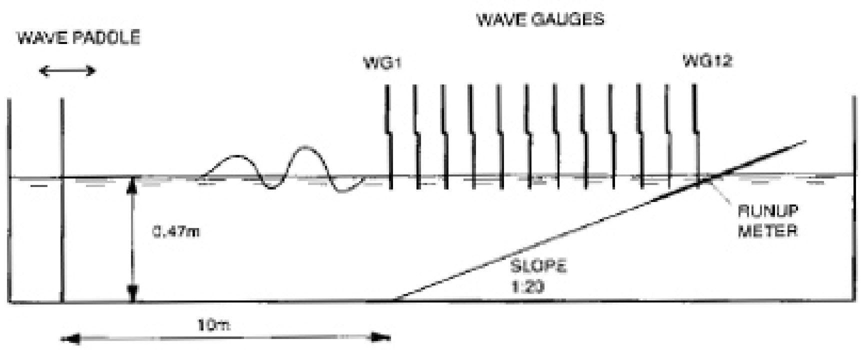

figure 17

Along the beach slope 12 wave gauges were positioned to measure the surface elevation time-series at each of these respective locations. The model was started at WG1 using the measured time series at this location to generate the model input condition. Subsequently the predicted time-series at WG 8, WG 10 and WG12 was compared with laboratory experiments. The experimental test case used for the comparison had an input bichromatic wave condition using Δ=0.2 (WP2) and f_m = 0.3 Hz, which would result in plunging breakers in the model.

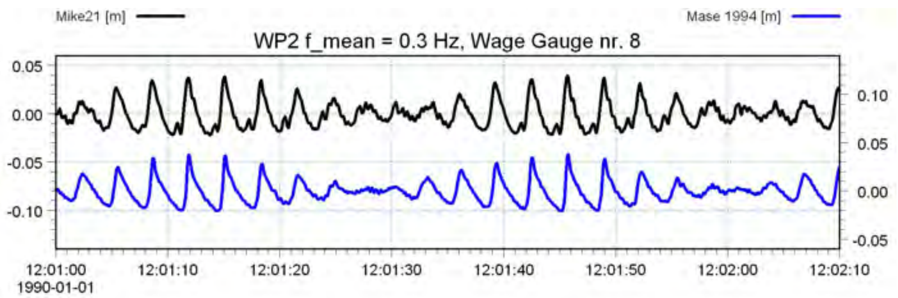

figure 18

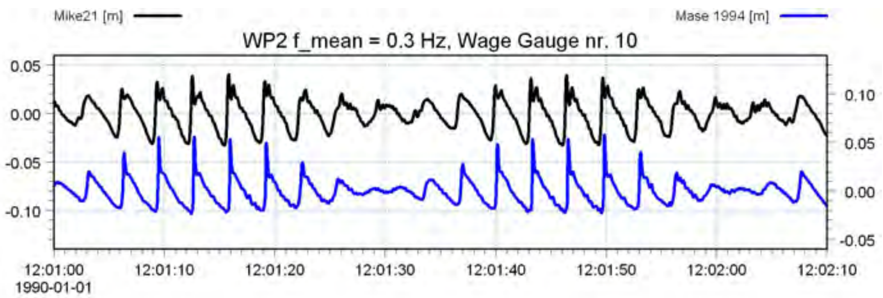

figure 19

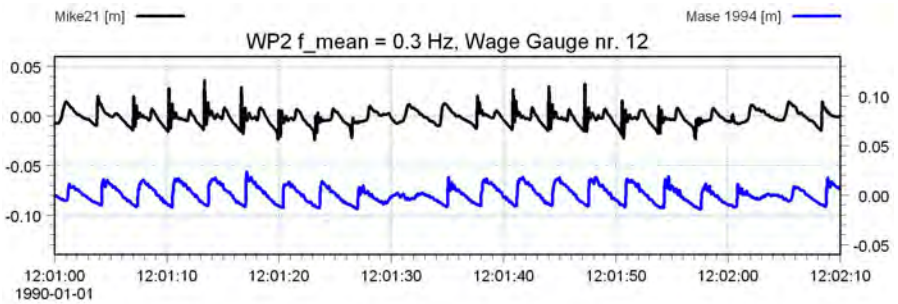

figure 20

From figure 18, figure 19 and figure 20 it is observed how a good agreement between experimental data and model results are maintained throughout all 3 benchmarking locations, which indicates that processes such as non-linear energy transfer to bound higher order harmonics and dissipation of the irregular wave train due to breaking is well simulated by the model.

3.2 Case 2 – 2D simulation of wave induced horizontal current circulations

3.2.1 A detached breakwater

In this section a 2D simulation modeling the wave transformation processes and wave induced current circulation around a detached breakwater has been carried out. The model setup builds on a laboratory study originally carried out by Hamm et al. (1995) and consists of 30x30 m basin starting off with a 4.4 m wide horizontal section with a water depth of 0.33 m followed by a sloping beach with a gradient of 1/50 until reaching the shoreline. From here the emerged beach has a slope of 1/20. Located 9.33 m from the shoreline a detached breakwater is placed being 6.66 m long and 0.87 m wide. The system is exposed to a monochromatic wave input with wave period of 1.69 sec and a wave height of 0.08 m.

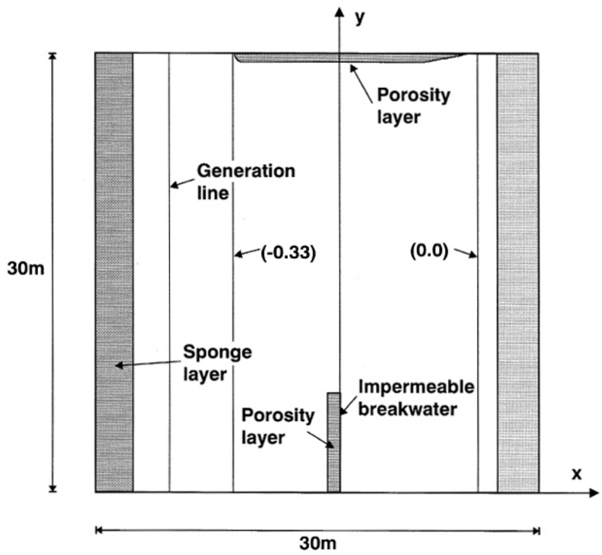

figure 21

The wave basin has been used to generate the model domain using a grid size of 0.05 m and a time step of 0.02 sec. Behind the wave generation line a 2.5 m wide sponge layer (50 grid points) has been applied to prevent wave reflection from the offshore back wall. A porosity layer enclosed on 3 sides by an impermeable wall is used to simulate partial reflection from the detached breakwater. Also a porosity layer at the upper boundary has been used to damp out eventual reflection and prevent instabilities in this area. The reflection coefficient used for this is 0.85. The breaker module has been set to simulate spilling breakers and the moving shoreline module uses a slot depth of 0.33

m and a slot width of 0.02. A filter is applied in the swash zone extending out to a water depth of 0.067 m. The filter coefficient used is 0.5 as for previous simulations.

The bottom friction factor used in the model was given by a Chezy number of 65 corresponding to a f_m of 0.005.

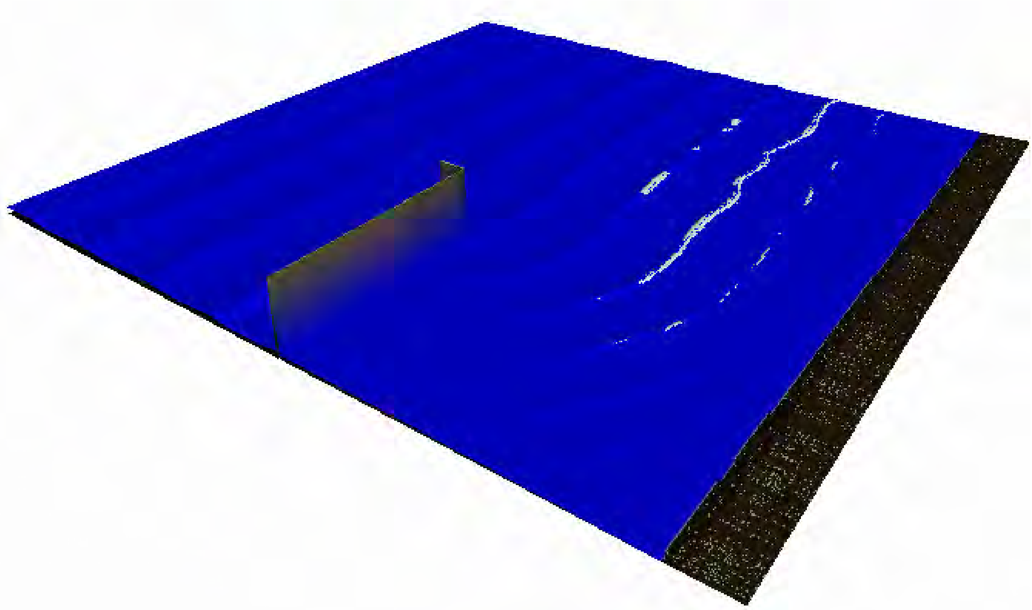

figure 22

A Boussinesq wave input has been applied at the offshore wave generation line and the simulation is carried out for 80000 time-steps (947 wave periods) and the phase-averaged properties (currents, wave heights) are calculated on the basis of the last 10000 time-steps (118 wave periods). Subsequently the wave height profiles behind the breakwater are compared to the laboratory results at 4 locations. Also a comparison of the circulation current behind the breakwater is carried out.

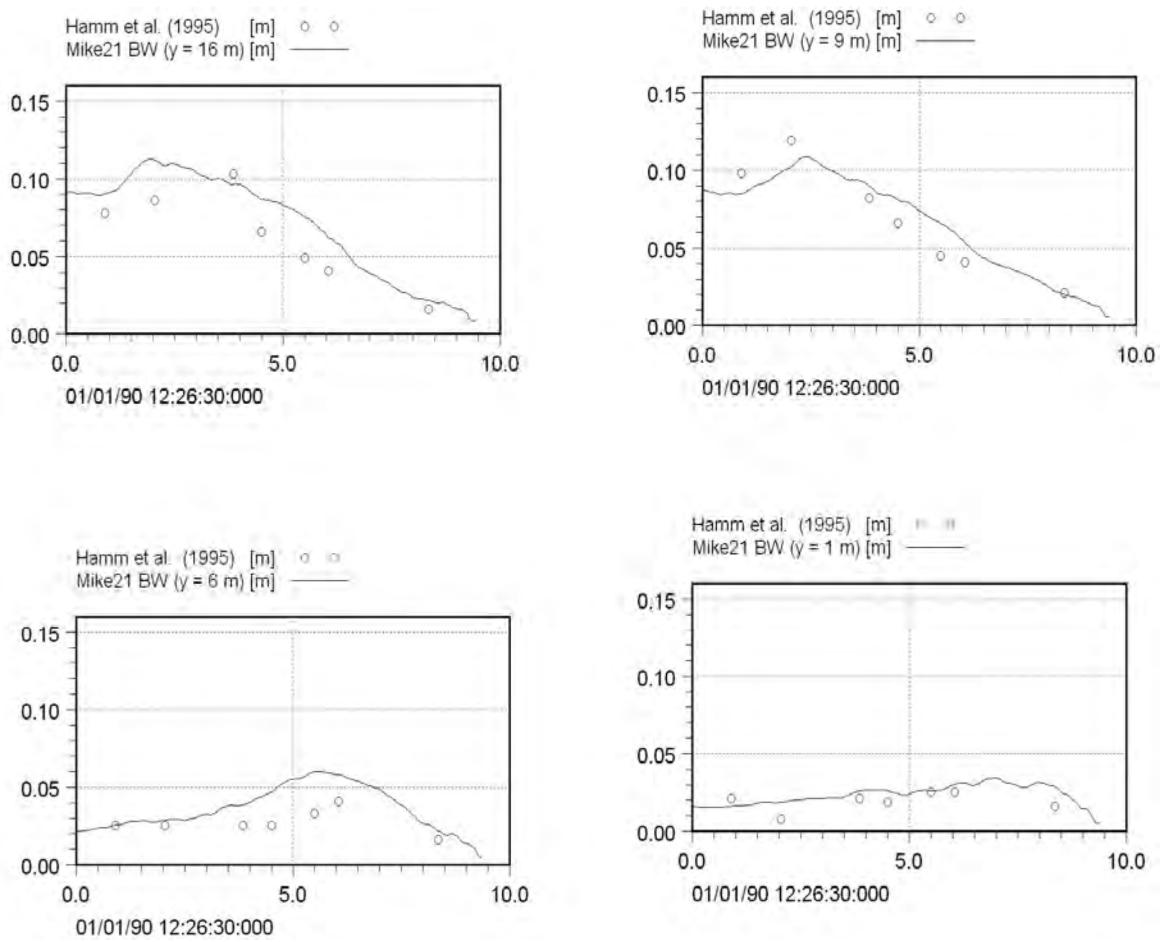

figure 23

From figure 23 a decent agreement between model results and laboratory experiments is observed. Due to the significant velocity gradients near the breakwater it was found that simulation wave height predictions were quite sensitive to a variation in bottom friction. Also the way the partial reflection was handled at the offshore side of the breakwater and at the upper model boundary showed to have some minor influence.

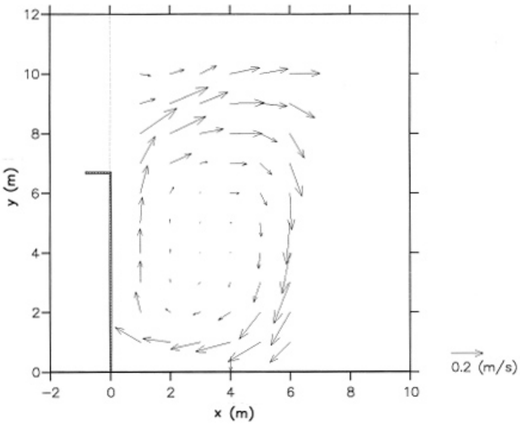

figure 24 – circulation current, Hamm (1995)

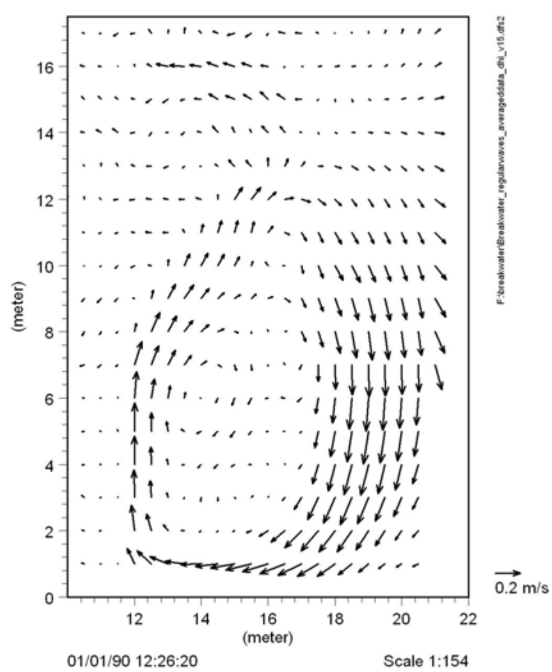

figure 25 – Circulation current, Mike21 BW

From the circulation current comparison it is observed how there exists an excellent agreement between the current circulation plot predicted by the model and the one measured by Hamm (1995) as the only notable difference is that the circulation structure appear to be extending slightly further out from the breakwater in comparison with laboratory measurements. Notice how the predicted return current (near y= 16 m) causes small inundations in the breaker fronts in figure 22 as the opposing current causes result in a wave steeping and thereby an offshore shift of the breakpoint at this location.

3.2.2 Rip current

In a laboratory experiment originally carried out by Hamm (1992) and presented in Sørensen et al. (1998), a 30 x 30 m wave basin has been used to simulate the rip-current generation on an open beach.

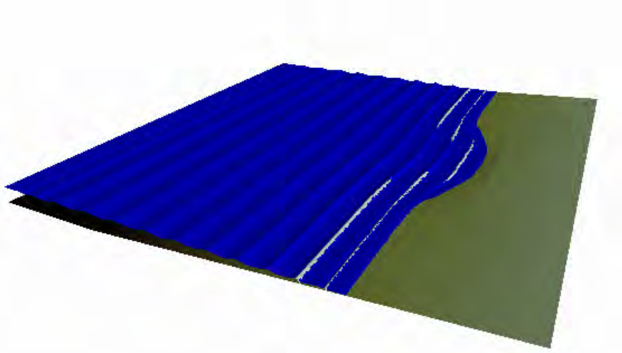

In the last 2D-simulation in the preliminary study, a simulation has been carried for this setup and the results compared to the experimental data.

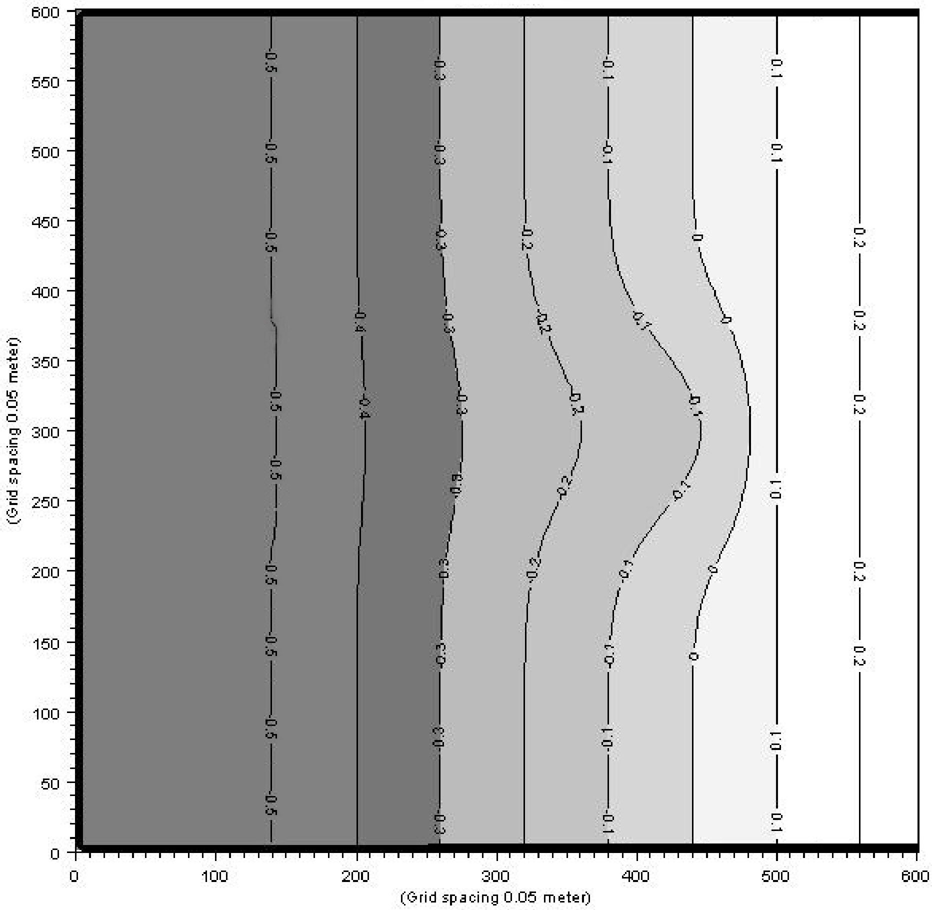

Figure 26

The model domain consists of a 7 m horizontal section with a water depth of 0.5 m followed by a sloping beach of 1/30. A small extravagation is made in the middle of the beach to represent the typical bottom feature of a rip channel. The grid size is 0.05 m and the time-step is 0.01 sec. The wave input is monochromatic with wave period of 1.25 sec and a wave height of 0.07 m. behind the wave generation line a 2.5 m sponge has been applied to prevent reflection from the offshore boundary. A filter has been applied in the swash zone extending out to a water depth of 0.035 m using a filter value of 0.5. In the moving shoreline module a slot depth of 0.5 m and a slot width of 0.05 are used and the wave breaker module is set to simulate spilling breaking. In order for this simulation to remain stabile it was found necessary to reduce the time-extrapolation factor to 0.5. The bottom friction was set to a Chezy number of 35 corresponding to a f_m of 0.016.

The simulation was carried out for 80000 time-steps (640 wave periods) and the wave height distribution and wave-induced currents were calculated on the basis of the last 10000 time-steps (80 wave periods).

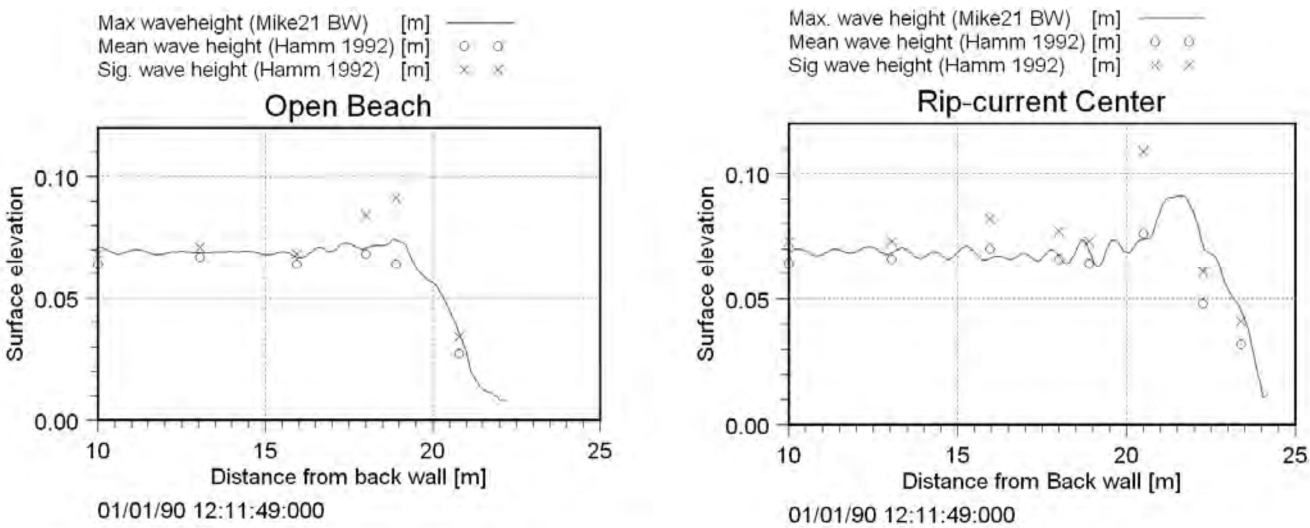

figure 27

figure 27 shows a good agreement between predicted wave height and model results. However it is acknowledged that the break point is predicted to occur slightly landward of what was experienced in the experiments by Hamm (1992). The explanation is expected to be due to small disagreements in domain bathymetry compared to the laboratory test case.

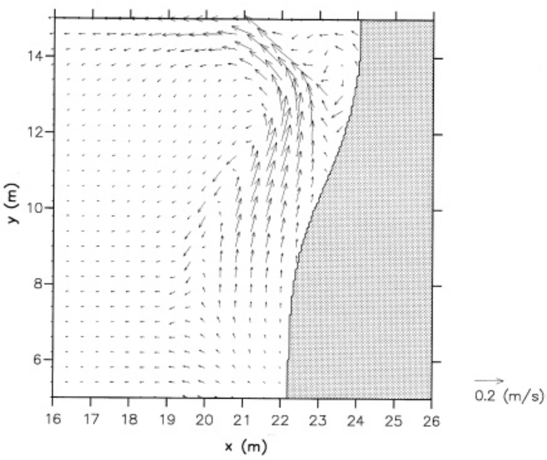

figure 28 – Sørensen et al. (1998)

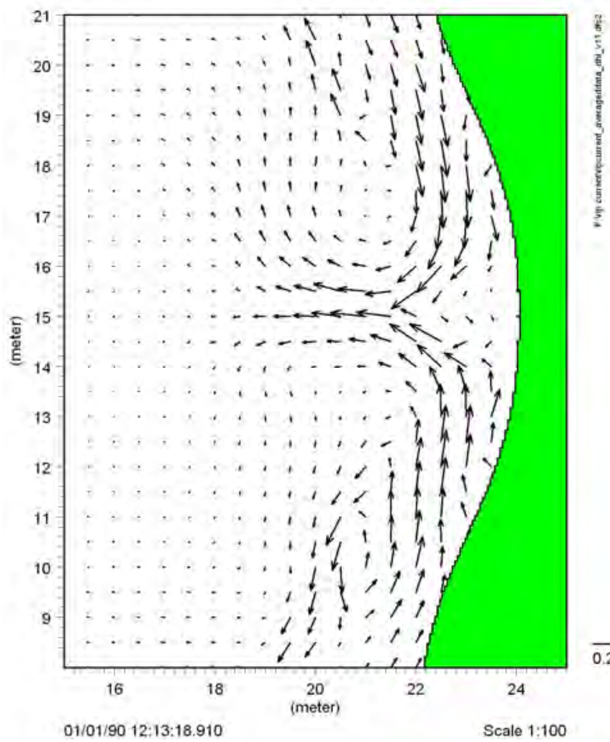

figure 29 – Current model simulation

The laboratory study by Hamm (1992) did not include a survey of the generated rip current so instead the rip current obtained in this study (figure 29) has been compared with Sørensen (1998) that previously used the Boussinesq model to simulate the same case study, which is presented in figure 28. From the two figures above it is observed that the predicted velocities are with in the same magnitude and the overall agreement is very good.

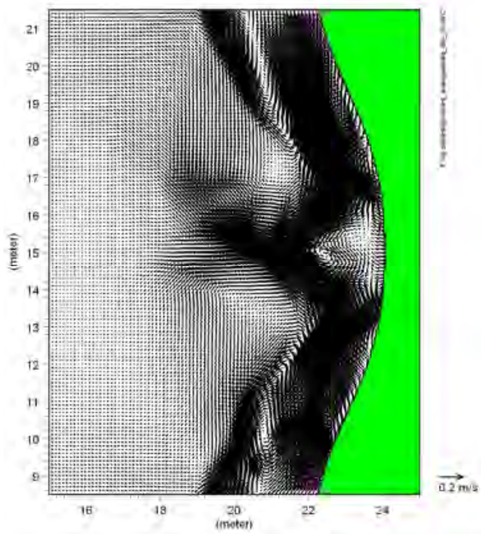

figure 30

However from figure 30 it is observed how the predicted rip current profile is slightly asymmetrical in spite of the symmetrical model domain. Apart from suggesting that this might be the result of small instabilities in the numerical computations no definitive explanation for this phenomenon could be given in this paper.

4 Waimea Bay

4.1 The Field Campaign

In order to provide real case offshore boundary conditions for the Waimea Bay model simulation and in order to be able to calibrate and assess the model predictions inside the bay, a small-scale field campaign was initiated.

The simple purpose of this field campaign was to gather simultaneous time-series data of the surface elevation and wave driven velocities inside the bay and at a suitable offshore location during an event of long-period wave conditions (pop: a swell event).

4.1.1 Offshore boundary considerations

The first important decision was to be made on where to put the instrument located offshore of the bay. As the wave time-series data gathered at this location will define the offshore boundary condition for the model, two important conditions have to be satisfied.

- The *kh*-ratio as this location should not exceed 3.15 in order to keep the linear dispersion characteristics of the enhanced Boussinesq equations within their limit of accuracy *(DHI Software 2004)*. Here *k* being the wave number and *h* the still water depth.
- When dealing with an irregular wave time-series as offshore boundary condition in the MIKE21 BW model, the surface elevation signal is decomposed into all its harmonic components, where each will be sent into the computational domain as free waves. As a result the bound higher-order harmonics in a non-linear signal will instead be treated as free waves causing boundary conditions to be resolved incorrectly. As a result the location of the offshore boundary should be located in sufficiently deep water where the wave condition for the desired swell event can be assumed to be linear.

As the desired offshore wave spectrum is expected to be narrow banded (no presence of short period wind-waves) with wave periods ranging from 13-20 sec, the constraint of the possible offshore water depth given by the *kh*-limit is by far exceeded by the limit of the maximum size of the domain (number of grid-points) and the depth limitations of the instruments. Considering the conservatively expected minimum wave-period to be 10 seconds, the model allowed deep-water limit is as deep as 78 m. However the number of grid-points required extending the model from the shoreline into a water depth this deep would make computational run-time unrealistically large not to mention the practical difficulties associated with mounting an instrument at this location.

In the end it is the instrument available for deployment that sets the deepwater limit for the offshore boundary. The 1200kHz ADCP Workhorse Sentinel (Acoustic Deepwater Current Profiler) made available for this field campaign is a bottom-mounted instrument that has a max absolute water depth limit ($d = h + \eta$) of 25 m. The ADCP is produced by *Teledyne RD Instruments.*

As large waves are common at this location during a regular swell event the water depth of the ADCP deployment was chosen to be 21 m in order to assure that the instruments depth limitation would not be an issue during sampling.

With the depth of offshore boundary decided, it was investigated if linear wave conditions could be assumed at this location. Linear wave conditions can be assumed if following two conditions are satisfied *(Nielsen 2003)*.

$$\frac{H \cdot L^2}{d^3} << 1 \quad \textit{(Ursell's parameter)} \tag{25.}$$

and

$$H/L << 1 \qquad \textit{(wave steepness ratio)} \tag{26.}$$

The wave heights *H* experienced in a typical swell event ranges between 1 to 4 m with periods ranging from 10-20 seconds corresponding to wavelengths (at h = 21 m) between 156-277 m.

As observed the wave steepness condition is satisfied easily, but unfortunately this is not the case for the criterion posed by the Ursell’s number that for these wave conditions ranges from 2.62 to more than 33.

As a result it is clear that it would not be possible to achieve pure linear conditions at the offshore boundary as even the best case scenario still would be weakly non-linear.

With this information in mind it was decided to try to launch the field campaign for a small sized swell event assuming that the non-linearities at the offshore boundary could be considered as weak and insignificant not resulting in significant distortion of the model results. Additionally it was decided that the duration of instrument deployment should be at least1-2 days in order to assure that at least somewhere within this time span, the wave conditions would satisfy the condition of being only weakly non-linear.

4.1.2 Placing the instruments

In addition to the ADCP placed at the model offshore boundary, two *Nortek* Current Profilers (AquaDopps/AQDPs) has been assigned to measure the wave conditions inside the bay. Due to the very limited number of instruments available for this study it was decided to place all three instruments along the bay-normal centerline and focus on capturing the wave transformations occurring from offshore into shallow water along this line. As mentioned earlier the ADCP is deployed offshore in 21 m of water. The first AQDP is deployed at the bay entry in a water depth of 10.7 m and the last AQDP is placed approximately in bay middle in 7.4 m of water. These 3 locations will from now on be addressed Station 1, 2 and 3.

An overview of the instrument deployment is illustrated in figure 31:

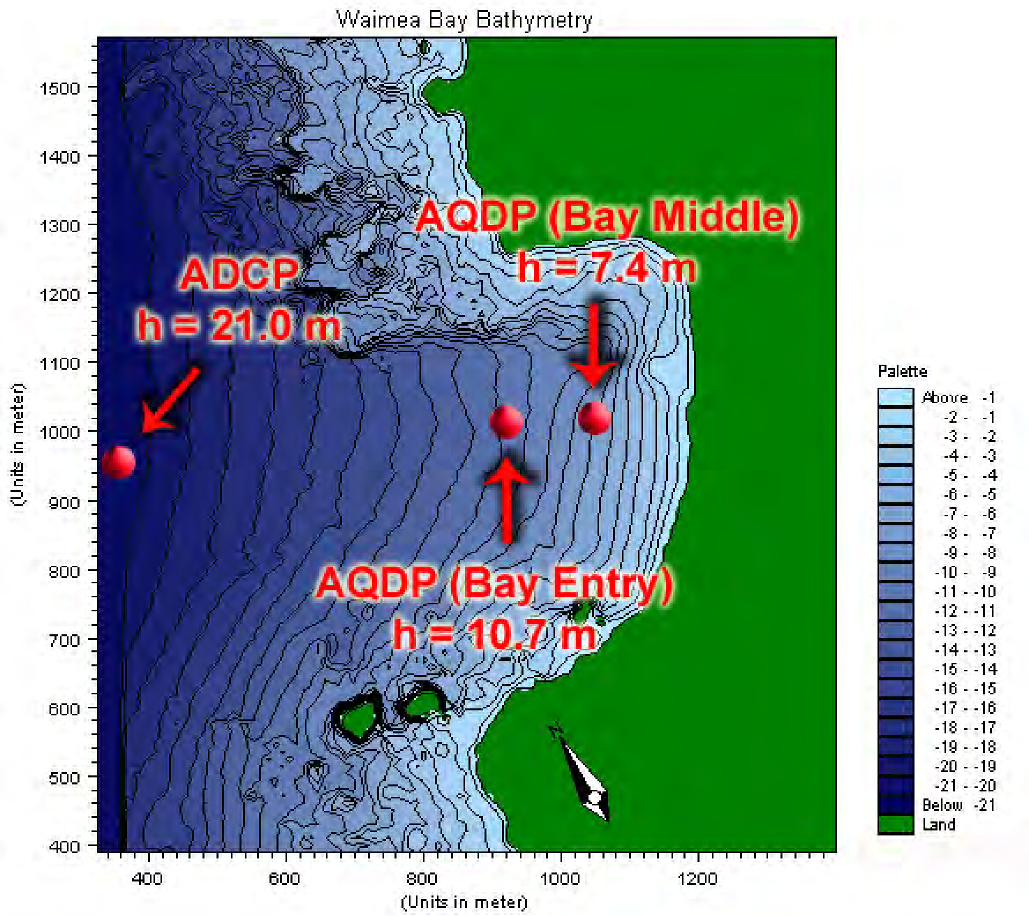

figure 31

Instrument	Latitude	Longitude	Mean Water Depth
ADCP	N 21.64356	W 158.07115	21 m
AQDP 1 (Bay Entry)	N 21.64134	W 158.06622	10.7 m
AQDP 2 (Bay Middle)	N 21.64069	W 158.06508	7.4 m

table 2

From figure 31 it is quickly noticed that the location of the ADCP is not entirely in-line with the two Aqua Dopplers. The simple explanation for this is a drifting boat anchor during deployment of ADCP that caused the instrument in being placed slightly downwind of the planned location. However this small displacement is of course not expected to be of any relevance whatsoever.

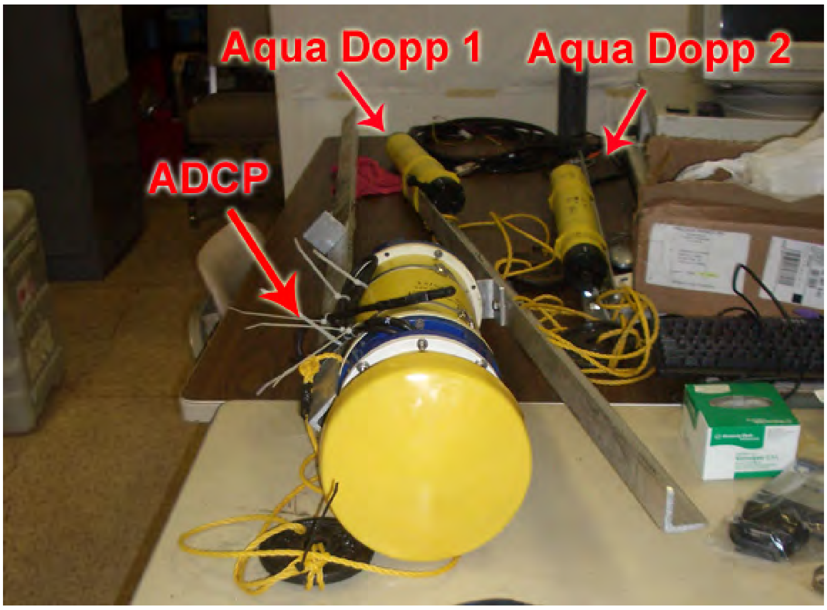

Above: Instruments ready for deployment

The ADCP and AQDP 1 were each mounted on an angular iron that was pressure drilled approximately 1.5 meters vertically into the sand bottom to keep them stable and slightly elevated above the sea bed in order to prevent eventual burial by moving sand. The angular irons were made of aluminum in order not to disturb the instruments internal compasses and were equipment with flaps to prevent them from rotating after deployment. AQDP 2 was designed to be mounted horizontally and was fixed to two aluminum rods that were pressure drilled into the sand bottom.

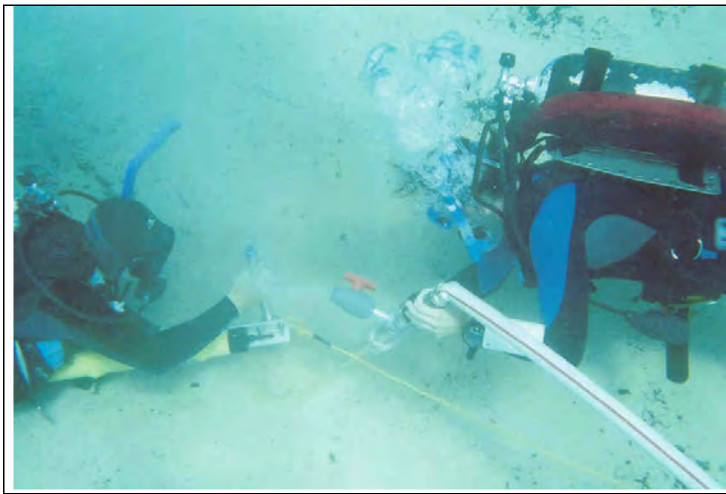	
Pressure-drilling the aluminum rods into the bottom.	Mounting AQDP 2 in 7.4 m of water.

During the 48 hours of deployment no notable migration or burial of any of the instruments were experienced.

4.1.3 The acquired field data

Due to busy department schedules and the time required obtain the necessary permits for deploying instruments in Waimea bay, the field campaign was originally scheduled to be carried out in the beginning of March 2006. But in this month the island of Oahu experienced the worst series of flooding events in 30 year, which caused septic tanks on the north shore to overflow and spill into the ocean causing health hazardous conditions (for the divers) in Waimea Bay for more than 40 day.

Final diver preparations before deployment of AQDP 2 in the bay middle.

Drifting anchor problems during the offshore deployment of the ADCP.

By the time conditions in the bay had turned to normal in April the chances of a decent swell event (that normally only occurs during the winter months) had become very slim. But luckily a late season swell suddenly showed up on the weather charts so that on Tuesday April 18, the field campaign could be initiated and the instruments deployed in calm oceans and timed to start sampling on Wednesday morning where a the swell was predicted to arrive.

The instrument started measuring at 9 am Wednesday morning and collected wave and current data for the following 48 hours. All three instruments was set to their maximum sampling frequency of 1 Hz allowing for a 10-20 point resolution of each wave, which was considered to be satisfactory. The data collected by all 3 instruments were stored in binary files from which the hydrodynamic pressure at the instrument location at the bottom and the two depth-averaged velocity components could be extracted using the bundled software from the instrument manufacturers.

4.1.4 Post-processing the field data.

The surface elevation is outputted in terms of a pressure time-series in dBar (10^{-1} bar) measured by a sensor located on each of the 3 bottom-mounted instruments.

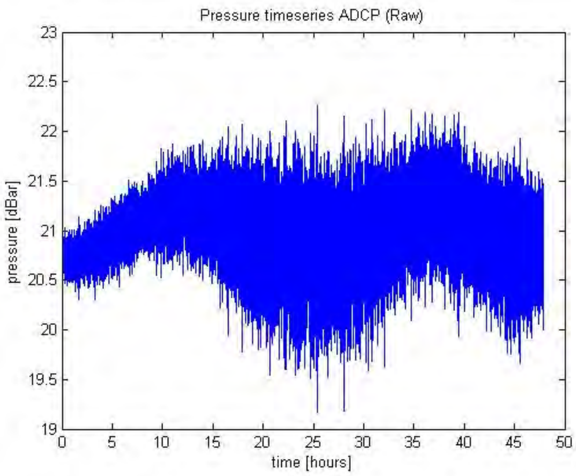

figure 32

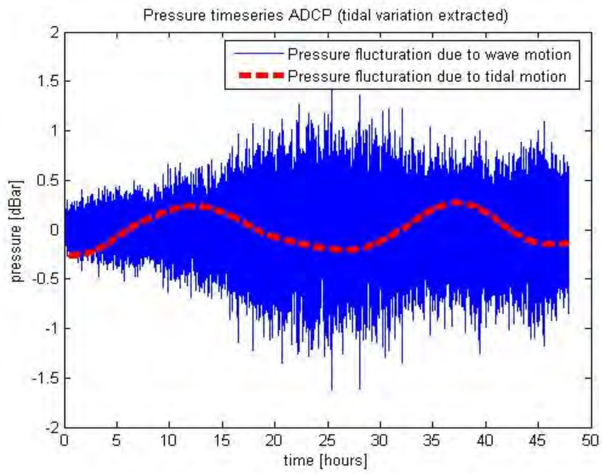

figure 33

Using the block-averaging scheme (block size: 30 minutes) the fluctuations due to tidal motion is removed from the raw pressure time-series and the oscillating pressure component p^+ extracted from the signal for further processing.

For a linear wave the relation between the surface elevation η and p^+ at an arbitrary location in the water column is given by:

$$\frac{p^+(z,t)}{\rho \cdot g} = \eta(t) \cdot \frac{\cosh(k \cdot z)}{\cosh kh} \Rightarrow G_N(k_i) = \frac{1}{\rho \cdot g} \cdot \frac{\cosh k_i \cdot h}{\cosh(k_i \cdot z_1)} \tag{27.}$$

Here h is the positive still-water depth (measured from the seabed), z_1 is the positive distance from the pressure sensor to the seabed, G_N is the linear transfer function and k_i is the wave number obtained from the linear dispersion relation expressed by:

$$(2\pi \cdot f_i)^2 = g \cdot k_i \cdot \tanh(k_i \cdot h) \tag{28.}$$

In order to calculate the actual surface elevation using this equation, a Fourier transform (FFT) of the p^+ time-series is used to decompose the signal into harmonic components for which the linear transfer function can be applied to calculate the surface elevation contribution from each respective harmonic. Finally the resulting surface elevation time series is obtained by merging the individually modified harmonics.

$$\eta(t) = a_0 + \sum_{n=1}^{N} \left(a_n \cdot \cos(f_n \cdot 2\pi \cdot t) + b_n \cdot \sin(f_n \cdot 2\pi \cdot t)\right) \cdot G_N(k_n) \tag{29.}$$

Here a_n and b_n are the real and imaginary components of the complex amplitudes obtained from the Fourier transform and f_n is the corresponding frequency ranging from $1/f_{Ny}$ to f_{Ny}, where f_{Ny} is the Nyquist frequency given by 0.5 Hz (half the sampling rate of 1 Hz).

Special consideration had to be given on where to apply the frequency cutoff corresponding to the parameter *N*. G_N is an exponential growing function and for larger values of f_n it will lead to artificial amplification of high-frequency noise existing in this end of the frequency domain. As a result a reasonable frequency cut-off must be introduced. With the model *kh* limit of 3.15 the minimum wave period that can be resolved correctly at the 3 instrument respective locations (starting from offshore) are T_{min}={5.2 sec, 3.7 sec, 3.1 sec}. In this study it was decided to use the model limitation for the frequency cutoff. Hence, $f_{cut\text{-}off}$ ={0.19 Hz, 0.27 Hz, 0.32 Hz} for the 3 locations.

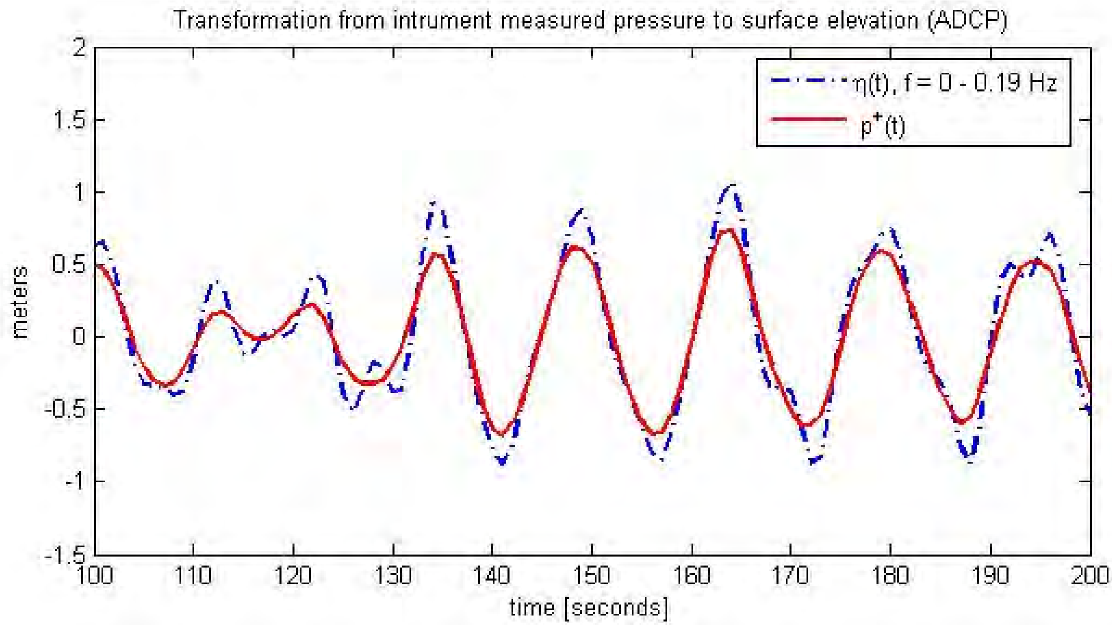

figure 34

In figure 34 it is observed how the transfer function amplifies contributions from the higher order harmonics revealing a wave train significantly more irregular in shape than what visually could be observed from the raw pressure time-series. However it should be made clear that effects such as instrument noise and not to mention the mathematical difficulties associated with resolving the finite nature of the measured time-series always provide some contribution to the harmonic amplitudes. While these effects are hardly felt in the lower range of the frequency domain, they hold the potential to significantly distort the signal by even just small contributions to the small harmonic amplitudes for the higher frequencies close to the cut-off (*Smith 1999)*. As a result a careful assessment has been made of each spectrum in order to assure that the defined frequency cut-off for the 3 locations were acceptable estimates and only included frequencies that was part of the wave signal.

The spectral wave peak period *Tp* is straightforwardly determined as the maximum harmonic amplitude occurring in the wave-spectrum and is as such a measure for at what frequency that contains the most energy. In order to obtain a distinguishable spectral distribution while still keeping a fine frequency resolution, the frequencies are stored into bins of each 0.01 Hz wide, while the FFT size is set to 4096 (using zero padding) corresponding to a frequency resolution Δf of $2.44 \cdot 10^{-4}$ Hz.

The integral wave parameters (H_{mean}, H_{sig}, H_{max}) and the wave peak period can now be calculated for the 48-hour field campaign. All these are calculated in 1-hour segments starting Wednesday morning at 9 am. The integral wave parameters have been calculated using the zero-upcrossing method.

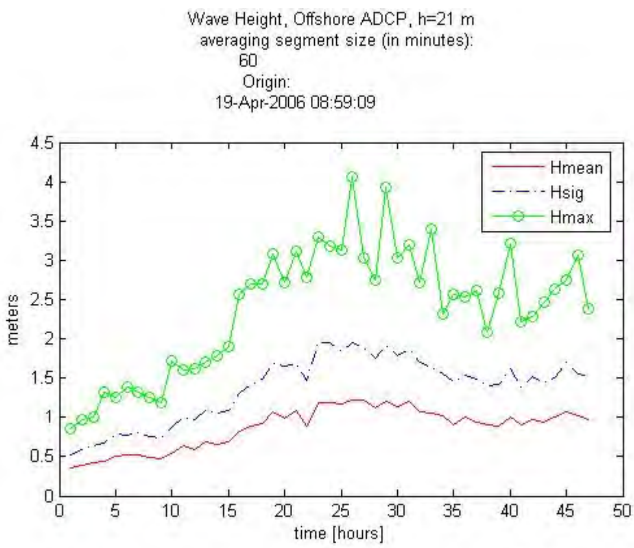

figure 35

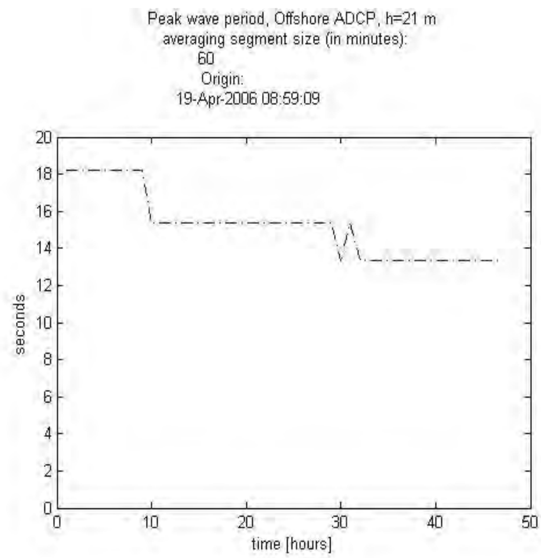

figure 36

On figure 35 it is observed how the size of the waves builds through Wednesday reaching its peak late Thursday morning and then slowly declining in size until Thursday evening after which the wave size remains constant through to Friday morning where the Field Campaign ended. Upon the initial arrival of the swell event Wednesday morning the spectral peak wave period is 18.2 seconds, which drops to 15.4 on Wednesday evening and finally to 13.3 sec Thursday evening. The decaying trend in wave-period is a typical pattern for a swell event and is very common in Hawaiian waters. The swells reaching the islands are most often generated thousands of kilometer away by powerful storms generating waves with a broad spectrum of wave periods. As given by linear wave theory the speed of wave in deep water will depend entirely on its period as given by:

$$c_0 = \frac{g \cdot T}{2 \cdot \pi} \tag{30.}$$

As a result the fraction of the generated waves with a longer period will travel faster and arrive earlier than as a result a swell event in Hawaii (lasting typically 2-5 days) would usually begin with long period forerunners and subsequently experience a downward trend in wave period until the end of the swell event.

The mean wave directions (also from 1 hour intervals) are calculated from the two velocity components measured by the ADCP.

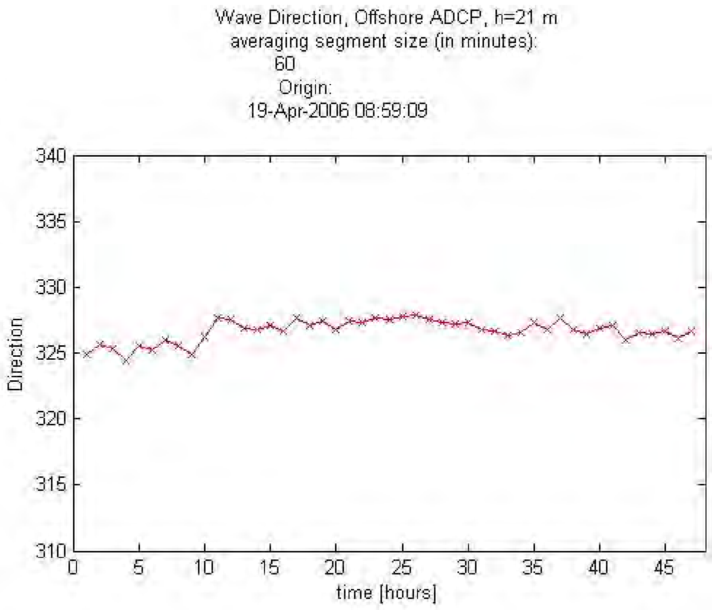

figure 37

As the monitored swell origins from a storm thousands of kilometers away, the dominant wave direction usually only changes a very few degrees during this event. From figure 37 it is observed how the mean wave direction is 325 degrees on Wednesday morning changing to 327 degrees Wednesday evening.

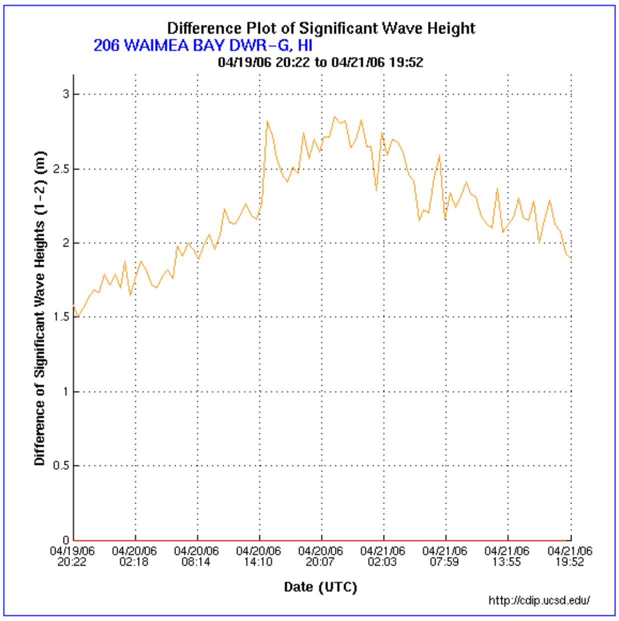

figure 38

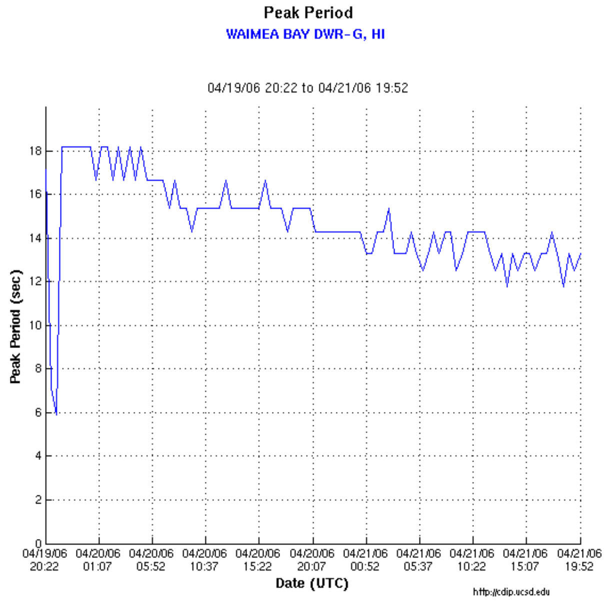

figure 39

Finally the wave statistics calculated for the ADCP is compared with the concurrent wave statistic taken at the Waimea buoy located 5.6 km northwest of the ADCP in 200 meters of water. The buoy data is publicly accessible and can be found on the Coastal Data Information Program’s home page (see references).

It is observed that there exists a very good agreement between the wave peak periods and the trend in significant wave height is also in good in good agreement, with the one calculated for the ADCP. The explanation for the significant drop in wave height between the two locations, could were well be due to extensive refraction between the two locations.

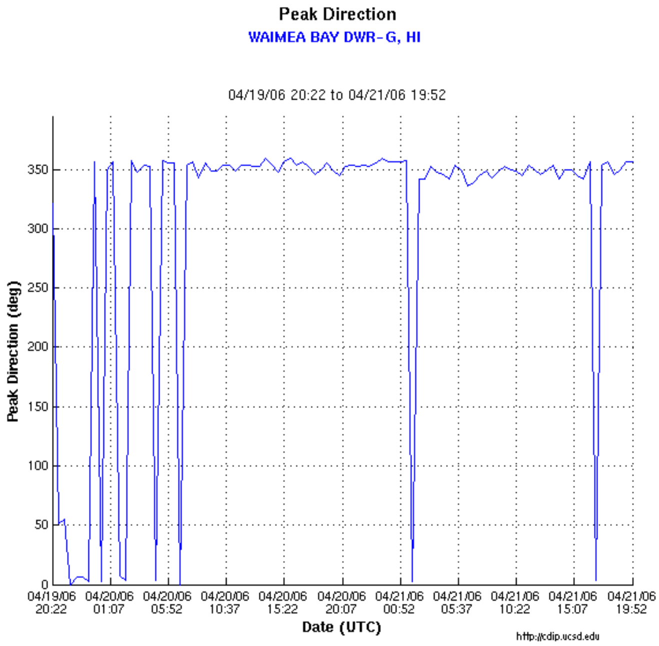

figure 40

From figure 40 it is shown how the dominant wave direction at the offshore wave buoy 5.6 km offshore is 350°, while it is 327° at the location of the ADCP 540 m offshore the Waimea Bay entry. As reference the shore normal of this part of the coastline is facing approximately 300 °

4.1.5 Selecting the MIKE21 BW input time-series.

Due to extensive model run-times it was decided only to apply the MIKE21 BW model to 30 minutes of field data at the time. Instead of trying to simulate the entire 48 swell event focus has been made on modeling only few discrete "slices".

As mentioned earlier a potential problem with the model setup is that linear wave conditions at the boundary are not fully satisfied. The least non-linear conditions (considering Ur) occur during Wednesday and the most non-linear conditions occur Thursday morning.

In order to qualitatively assist model calibration, a digital camcorder has been used to film a limited number of 5-30 min video-clips of the wave action in Waimea bay during the 48-hour deployment.

Due to limited camcorder battery life, only a few video clips where taken each day and only some of these video clips contains easily recognizable occurrences such as the sudden arrival of a wave much larger than the rest and also observable wave reflection.

Based on the considerations above, the two following 30-minute periods of the field data has been selected for being modeled in MIKE21 BW:

- 16.15-16.45 Wednesday April 19. 2006
- 9.25 -9.55 Thursday April 20. 2006

The two time-series represents respectively the least non-linear and most non-linear wave conditions during the field campaign and both contain video footage well suitable for visual comparison.

An overview of the two input time series acquired from the ADCP is given below:

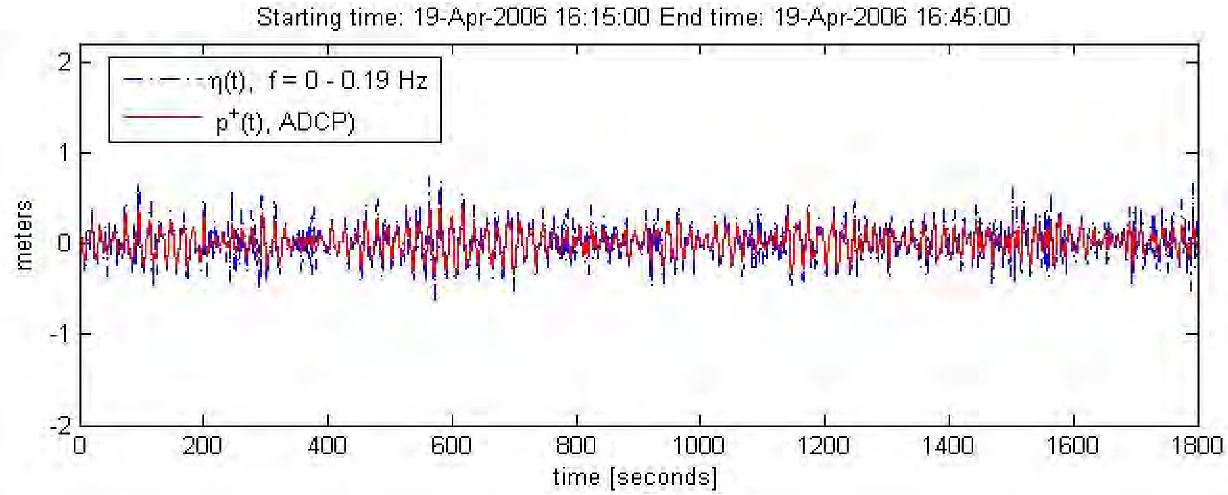

figure 41

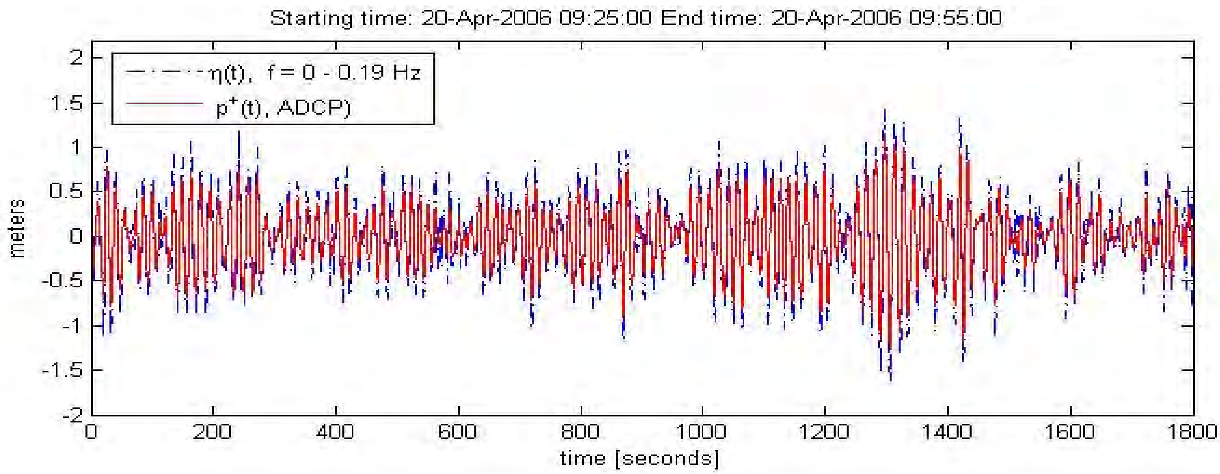

figure 42

The power spectra generated for these time-series are presented in figure 43 using:

$$E_n = \frac{1}{4}\left(a_n{}^2 + b_n{}^2\right)\cdot \Delta f^{-1} \tag{31.}$$

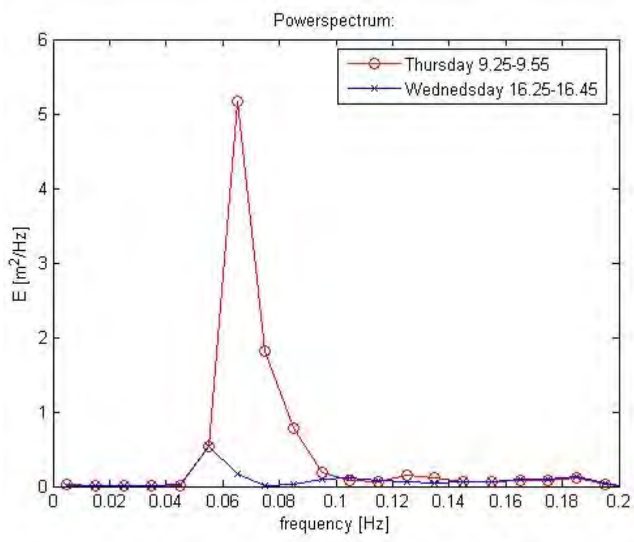

figure 43

From the spectral energy an expression for the significant wave height can be obtained using:

$$H_{m0} = 4 \cdot \sqrt{M_0} = 4 \cdot \sqrt{2 \cdot \sum_{n=1}^{N} E_n} = \frac{4}{\sqrt{2}} \cdot \sqrt{\sum_{n=1}^{N} \left(a_n^{\ 2} + b_n^{\ 2}\right)} \qquad (32.)$$

The average wave direction for the two time series is obtained from scatter-plots of the horizontal velocities:

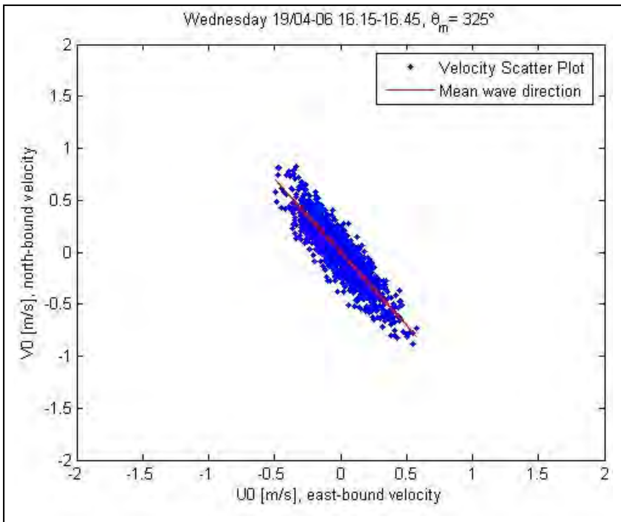

figure 44

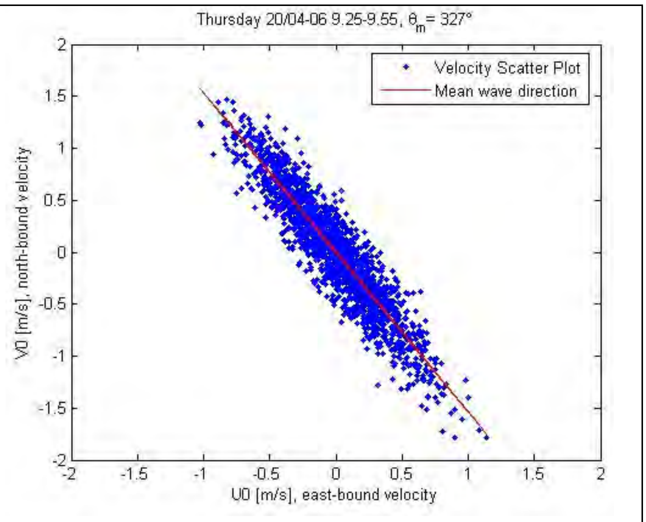

figure 45

From figure 41 and figure 42 the mean wave height H_m, the significant wave height H_{sig} and the maximum wave height H_{max} are obtained from the time-series using the zero-upcrossing method.

Finally a schematic overview of all the calculated parameters is presented in table 3.

Date	H_m	H_{sig}	H_{max}	T_p	H_{m0}	Wave dir.	Ur (H_{max})
19/04-06 16.15-16:45	0.48 m	0.73 m	1.10 m	18.2 sec	0.64 m	325°	7.4
20/04-06 9.25-9:55	1.14 m	1.79 m	3.06 m	15.4 sec	1.57 m	327°	14.5

table 3

As mentioned earlier there is a significant difference between the 2 selected time-series, while in spite of them being only 17 hours apart and belonging to the same swell event. While the wave direction is almost the same there is a tremendous difference in wave height and spectral energy and also a notable difference in wave peak period. From calculating the Ursell parameter using T_p and H_{max} (h = 21m) it is also confirmed (from previous discussion) that there is a significant difference in non-linearity between these time-series both used as offshore boundary condition in the model.

4.2 The Model Setup

4.2.1 Choosing the domain size

The first concern when setting up the MIKE21 BW model is on what grid size (*dx, dy*) and time-step *dt* that should be used given the wave conditions at the offshore boundary and the expected coastal dynamical processes that is expected to occur within the computational domain.

As the computational domain will include both wave breaking and a moving shoreline, the spatial resolution of the wavelength of the most energetic wave should be 20-40 grid-points *(Dhi Software 2004)*. Using a grid spacing of 2 m the spatial resolution requirement is assessed for the two selected time-series:

Date	**T_p**	**h_{min} (Resolution: 40 point)**	**h_{min} (Resolution: 20 point)**
Time series 1: 19/04-06 16.15-16:45	18.2 sec	2.0 m	0.5 m
Time series 2: 20/04-06 9.25-9:55	15.4 sec	2.8 m	0.7 m

table 4

From table 4 it is observed that due to the long period nature of the dominant waves in the model, minimum wavelength resolution requirements (20 points) is satisfied into the swash zone at a water depth of 0.5-0.7 m. As the shallowest measuring station (AQDP 2) is positioned at a water depth of 7.4 m, it is assumed that slacking on the resolution requirement in the inner swash zone won't have a notable impact on the model predictions at any of the measuring stations.

The time step *dt* should be selected so that the minimum wave period occurring in the model should be resolved by 25-35 time steps, while still at all locations satisfying the requirement given by the Courant number:

$$Cr_{\max} = c_{\max} \cdot \frac{dt}{dx} < 1 \tag{33.}$$

where

$$c_{\max} = \frac{g \cdot T}{2 \cdot \pi} \cdot \tanh(kh_{\max})$$

The minimum wave period that can be resolved correctly at locations where instruments are deployed, is at AQDP 2, where T_{min} = 3.13 sec as governed by the Mike21 BW *kh*-limitation. Selecting a *dt* of 0.1 sec will thus allow for a 31 step resolution of the minimum wave period while keeping the maximum Courant number (at the offshore boundary) at less than 0.72.

Next to be decided is how large a geographical area to include in the computational domain.
The most common approach in MIKE21 BW is to generate waves is by internal generation along a defined line inside the model. All open boundaries (such as open ocean) are closed using walls of artificial land and the wave action in front of these walls are damped by placing a sponge layer in front of each one. As a result no artificial reflection from the boundaries will be generated, which in that case could seriously distort the wave action inside the model, but in return the waves close to the boundary will dissipate and diffract into the sponge layer making the model predictions in the close proximity non-physical.
As a result care must be taken to make the model domain large enough so that the area of interest (Waimea Bay) is located far enough away from the boundaries in order not to experience any of these undesirable effects. On the other hand the size of the model domain should be kept within reasonable limits in order not to make computational run-times within realistic limits (max 30 hours).

Domain 1

Domain size: 700 x 941 = 658.700 grid point

In the first attempt to set up the computational domain it was decided that the domain should be rotated 30 degrees making the shore-normal of the bay perpendicular to the wave generation line located along the "left" side of the domain. The domain is set to have a height corresponding to approximately 3 times the width of the Waimea Bay entry assuming that this height is sufficient to avoid non-physical effects from the upper and lower boundary. The width of the domain is selected so the landward boundary is wide enough (approximately 1 bay length) not to cause artificial reflection from the right side back wall, as water close to the shoreline to some extent will propagate into the beach-slope giving rise to unrealistic reflection if the landward boundary is too close.
The left side boundary is set well offshore of the location of the ADCP allowing for a sufficiently wide sponge layer an in attempt to avoid non-physical processes occurring close to the boundary will have any harmful effects to the wave processes along the generation line.
In this model approach it has been emphasized that the wave generation line should run through the location of the ADCP enforcing that the wave conditions at this distance from the bay are exactly, what was originally measured by the instrument. As earlier mentioned the instrument is placed in 21 m of water so all water depths deeper than this is set to 21 m in model bathymetry.

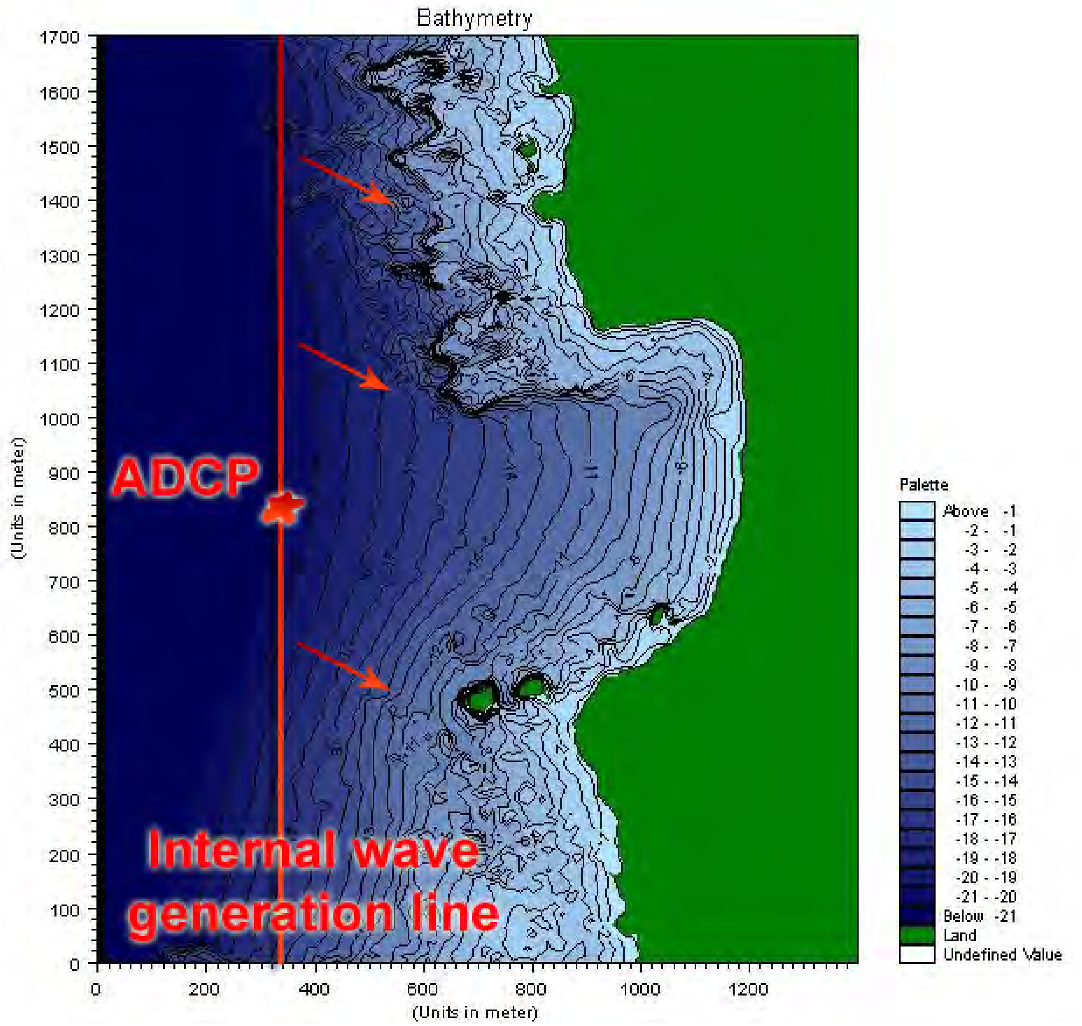

figure 46

However from figure 46 it is noticed how the bathymetry in the top and (especially) in the bottom of the domain is shallower than 21 m and must be altered in order to satisfy the requirement of uniform water depth along the generation line. It is fully understood that such alteration of the bathymetry could to some extend affect the accuracy of the model predictions inside Waimea Bay. But as it was of interest to carry out the simulation with the ADCP location placed on the generation line, this domain setup has been kept and thereby avoids eventual transformations in the wave train while it passes flat bottom if the generation line was placed further offshore.

Domain 2.

Domain size: 1169 x 1201 = 1.403.969 grid point

As mentioned earlier the alteration in the bathymetry could pose distortions to model results. So could the eventually too close proximity of the upper and lower boundary and the energy dissipating effects (due to time extrapolation of the Boussinesq cross-terms) due to the angled wave propagation.

As a result a second and much larger domain has been generated that due to its orientation does not need a unidirectional input at the generation line and by enforcing a deepwater limit of 21 m, no alteration of the near shore bathymetry is necessary. However the computational time for this model is more than double than when using "Domain 1". As a result Domain 2 has only been applied to time series 2 (Thursday) as verification of the model results obtained using Domain 1.

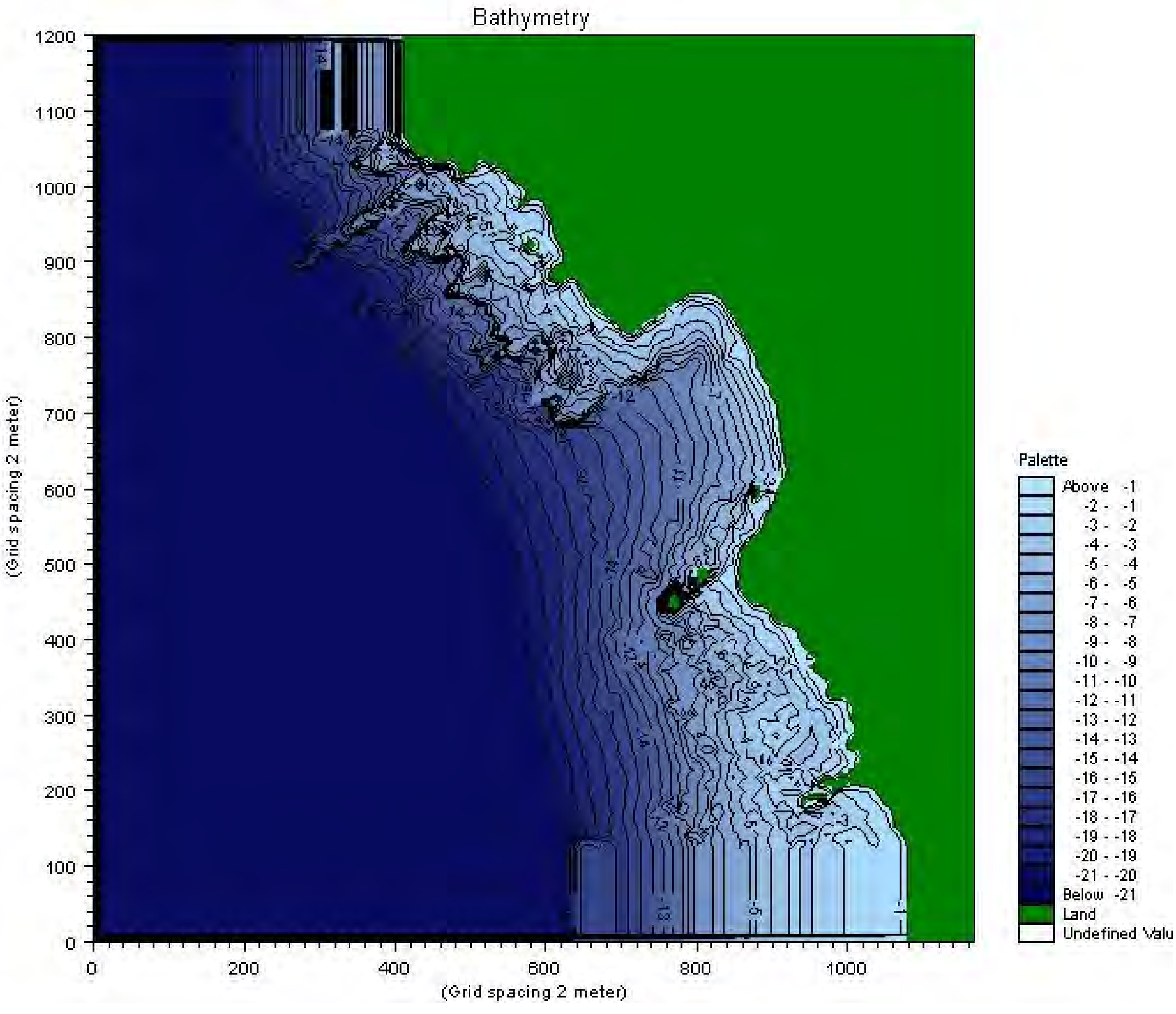

Figure 47

4.2.2 Generating the bathymetry

The bathymetry for Waimea Bay was surveyed in year 2000 by airplane-mounted LIDAR and is collected from the shoreline to 1 km offshore at 3-5 m spacing. Topographic data are collected from the shoreline to 0.5 km inland at 1 m spacing. The depth precision is given to +/- 10 cm *(JALBTCE web page)*. A problem with the LIDAR data is that it cannot resolve the bathymetry in areas of high turbidity such as the shore-break and wave induced turbidity around steep cliffs and rocky outcrops. Secondly many of the small rocky outcrops along especially the south end of the bay is only resolved partially and some does not even appear due to insufficient overlapping between the bathymetry and topography surveys. As a result, great care had to be taken in order to perform a correct interpolation of the unresolved "shadow" areas and also make sure that the rocky outcrops are represented correctly in the model bathymetry.

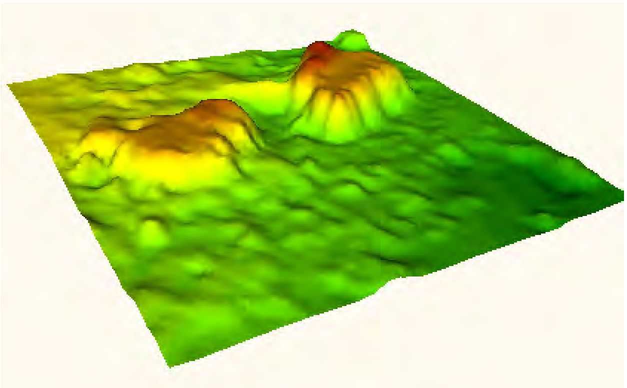

figure 48 – Satisfactory representation

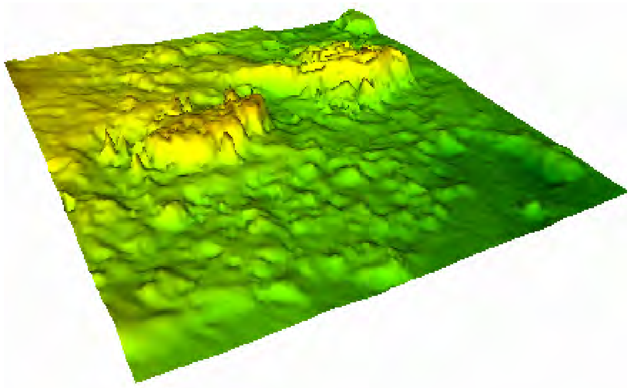

figure 49 – Insufficiently accurate representation

figure 48 and figure 49 represents two different attempts to resolve the two rocky outcrops at the south entrance of the bay and poses an example of what problems were occurred when trying to have features like these represented correctly in the model domain.

figure 50

figure 51

In this study it was not accomplished to setup an interpolation scheme in the MIKE Zero's imbedded Bathymetry editor that could resolve these features sufficiently correctly. Instead the "nearest neighbor" interpolation method was used in the open sourced program "Generic Mapping Tools" (GMT) to carry out the interpolation scheme and generate a new equidistant bathymetric dataset that could be imported into the MIKE Bathymetry Editor. Subsequently these coastal features appearing in the model were compared with photos and to some extend manually smoothened and adjusted in order to obtain the most realistic representation.

Another concern was caused by the fact that while the bathymetry was surveyed in 2000, the topography was surveyed in 2003. In addition, from a water depth of 0-3 meters in front of the Waimea bay beach, no bathymetry data is available most likely due to high turbidity in this region during the survey campaign in 2000 (see figure 55). The missing bathymetry points correspond to a 20-25 wide band that extend along the entire width of the bay.

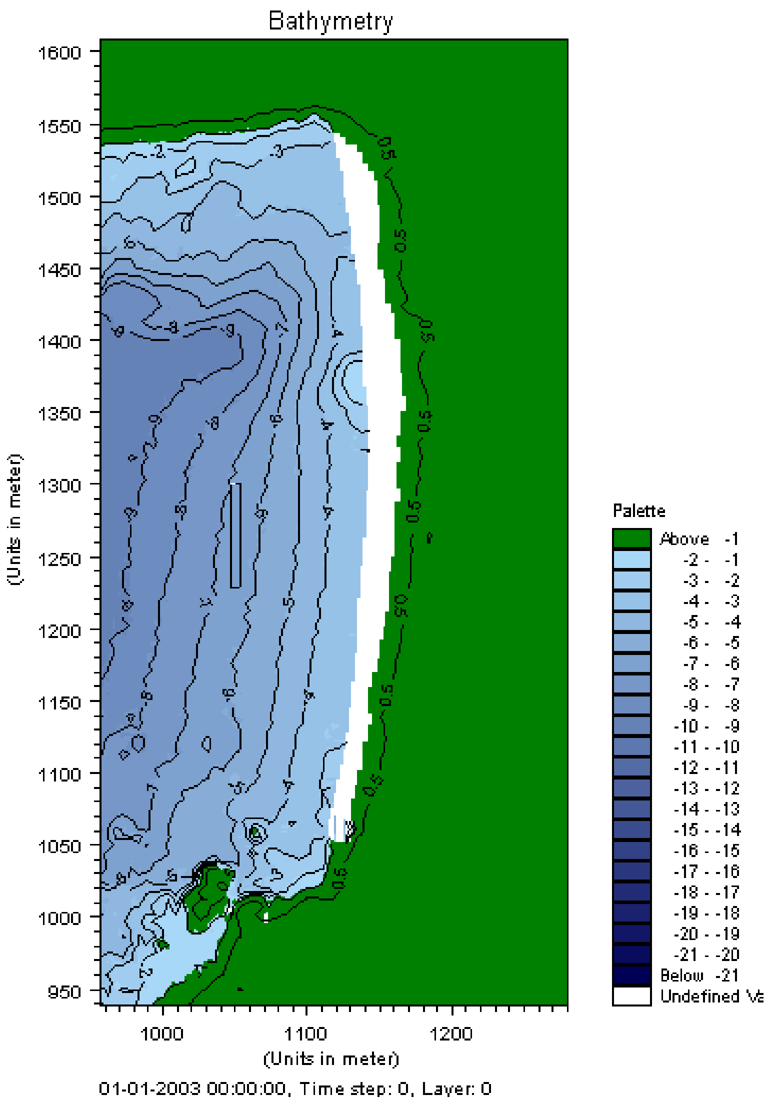

figure 52

However as the bathymetry in this unresolved area is assumed to be fairly uniformly sloping, it was decided to resolve this gap by linear interpolation.

But from visual inspection it was soon discovered that the data gap between the topography and bathymetry data and the following interpolation resulted in a large rock in the south end of the bay to be entirely excluded from the generated bathymetry (compare figure 53 and figure 54). However even though the rock is notable in size its overall contribution to the wave transformations in the bay must considered to be insignificant (see figure 55).

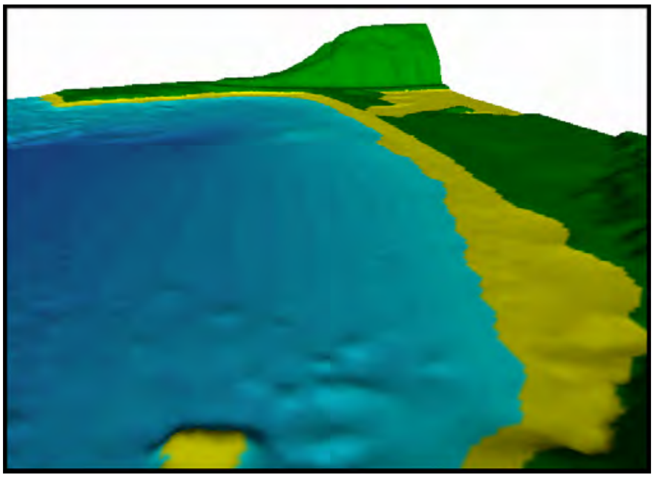

figure 53

figure 54

As a result no action has been taken just for the purpose of manually surveying and including this feature in the model bathymetry.

figure 55

4.2.3 The sponge layer

The sponge layer has to be capable of absorbing even the most energetic wave from each of the two time-series that is to be used in the Waimea bay model. As a general guideline good absorbing characteristics has been obtained with a sponge layer L/2 wide, where L is the wavelength.

In order to make sure the sponge layer performs sufficiently, a flat-bottomed channel-simulation has been carried out using a water depth of 21 m.

A fully reflecting wall has been placed in the right side of the channel and an absorbing sponge layer has been placed behind the internal wave generation line in the other end of the channel.

The width of the sponge layer has been determined based on the spectral wave peak period of 18.2 sec from the Wednesday time-series corresponding to a wavelength of 250 m at h=21 m.

Hence the width of the sponge is set to 125 m (63 grid points) corresponding to the half-length. The sponge layers is assessed for the two monochromatic input wave conditions based on the peak period T_p and maximum wave height H_{max} occurring in the two time series:

Wave ínput 1:

T = 18.2 sec, H= 1.10 m

Wave input 2

T=15.4 sec, H = 3.06 m

The length of the channel has been set to 1000 m and the grid spacing and time stepping are the same as for the Waimea Bay model runs (*dx* =2 m, *dt*=0.01).

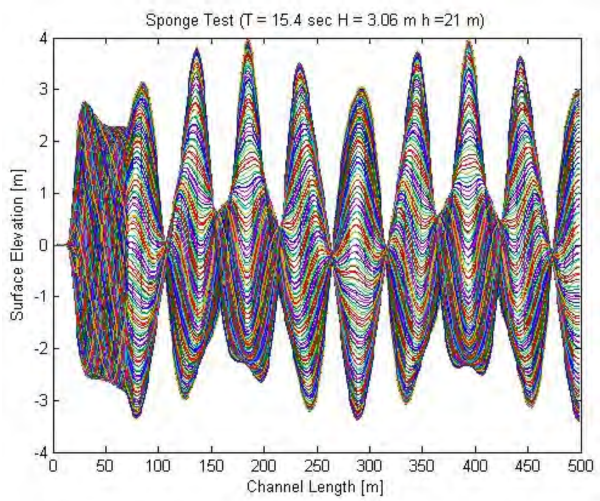

figure 56

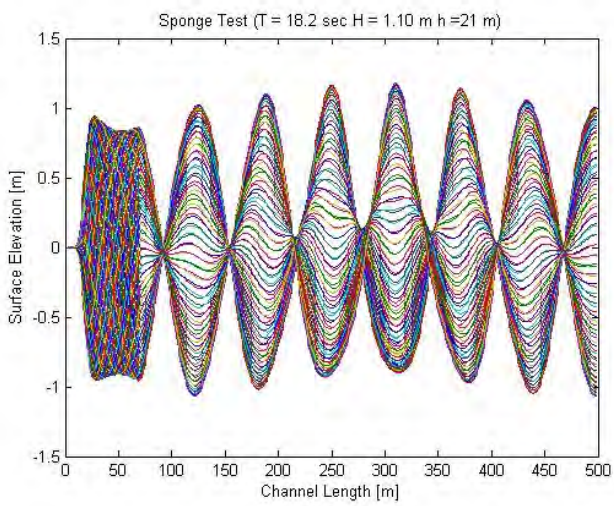

figure 57

From figure 56 and figure 57 it is observed how the standing wave plots suggests a successfully damping and dissipation of wave action at the offshore boundary by the sponge for both test cases (no accumulation of wave energy).

However the asymmetrical shape of the envelope plots confirms the expectation of non-linearity as discussed in section 4.1.5. In order to justify this assumption a new simulation was carried out with same wave conditions as in figure 56 but with a water depth of 150 m. The time-step *dt* had to be lowered to 0.05 sec in order to keep the Courant number below 1.

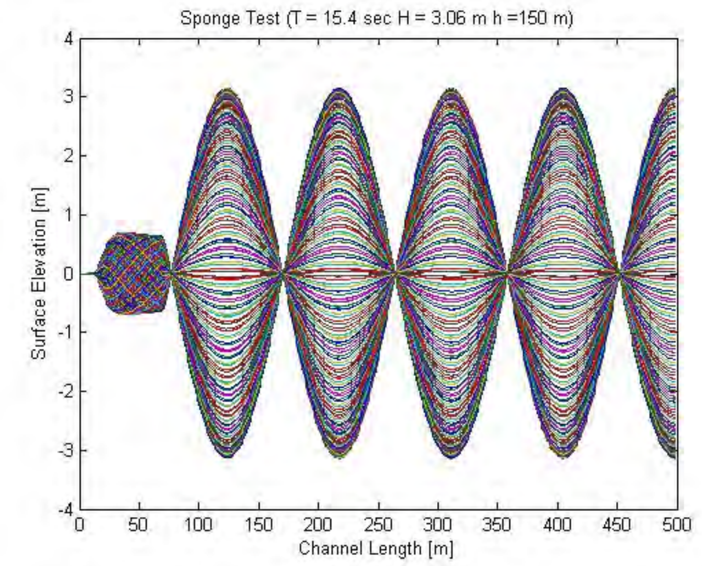

figure 58

In this case it is observed how linear conditions are obtained for the deep water case (Ur=0.12) and that the sponge layer is still working effectively even though its thickness in this simulation only corresponds to about 1/3 wavelength. The conclusion of this section is that a sponge layer with the width of L/2 is sufficient for these two wave time-series that unfortunately are not entirely linear at the model offshore boundary. Thus the width of the sponge layers used in these simulations will be 125 m (63 grid points) wide. In order to assure stabile model conditions inside the sponge a uniform bathymetry over its cross-section is induced so that the last point outside the sponge is kept constant along its cross-section (see figure 59):

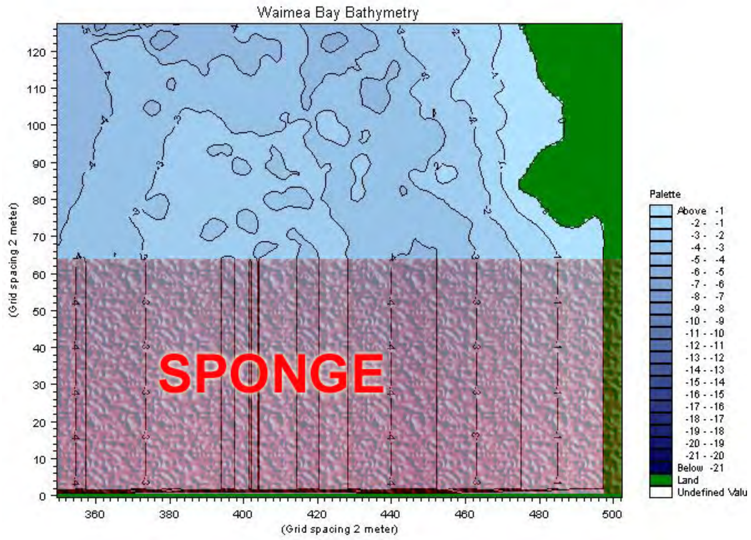

figure 59

4.2.4 Further discussion of the non-linear boundary conditions.

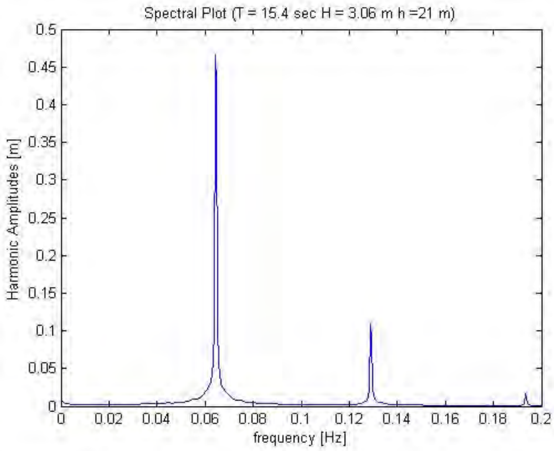

figure 60

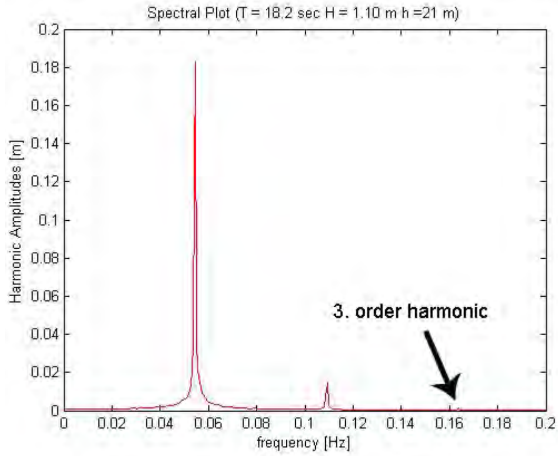

figure 61

In order to look more closely on the non-linear behavior of the input wave conditions at the offshore boundary, a new channel simulation has been conducted using the same wave input as for the sponge test, but with damping at both boundaries hence generating a free propagating wave on a flat bottom. In figure 60 and figure 61 it is observed how a free second order harmonic and even a tiny 3rd order harmonic are released in the flume as a result of the introduction of a linear wave into the non-linear environment. The small "curtain" appearing off each spectral peak and is caused by the problem in using the FFT-method (Fast Fourier Transform) to resolve a finite time-series *(Smith 1999)*.

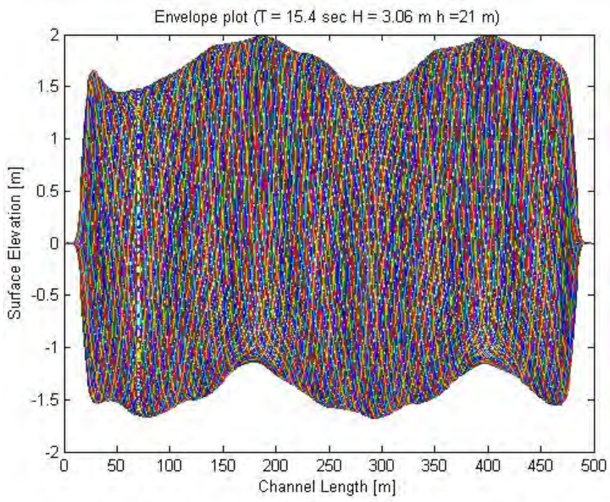

figure 62

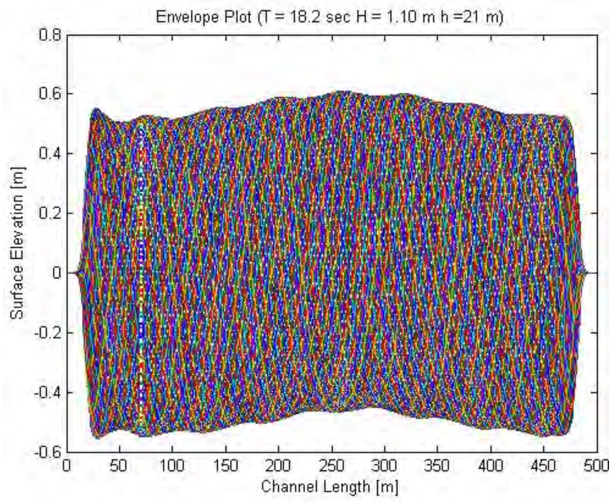

figure 63

From the time-domain plots in figure 62 and figure 63 it is clear how the higher order contributions affect the propagating wave train. It can be seen that it is mainly the influence of the 3rd order harmonic that causes the spatially varying wave height in the channel.

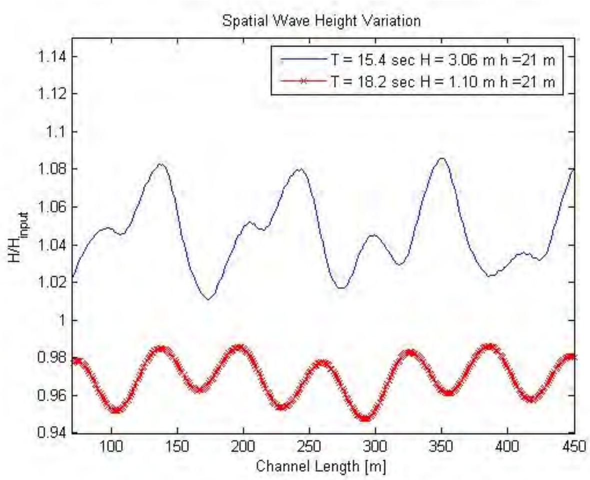

figure 64

When plotting the spatial wave height distribution over the flat-bottomed channel it can be observed how the wave-height is fluctuating with as much as 8%. It should be recalled that these test cases corresponds to the most extreme occurring incident waves occurring Wednesday and Thursday and as the non-linearities decreases for smaller wave height it is expected that the overall wave height inaccuracies in the Waimea Bay simulation due to this phenomenon should be expected to be significantly smaller than observed in figure 64.

4.2.5 Filter layer

As numerical instabilities will occur in the swash zone in areas where the surface roller cannot be resolved, a filter layer is applied to the Waimea Bay model. Due to the complex distribution of wave breaking occurring in the model, the filter layer is applied from a water depth of 3 meters at the steep cliffs and 1 m and the beach slope of Waimea bay. It is acknowledged that in areas where the filter had to be extended out to 3 m, artificially induced wave damping will occur over a significant area affecting the reliability of the model predictions in these areas. It can only be hoped that this would only insignificantly affect the overall model predictions inside the bay.

From previous good experience in the preliminary study a filter coefficient of 0.5 is used. Inside the bay from a water depth of 1.0-1.5 m, the filter coefficient is undergoing a smooth transition to 0 using linear interpolation.

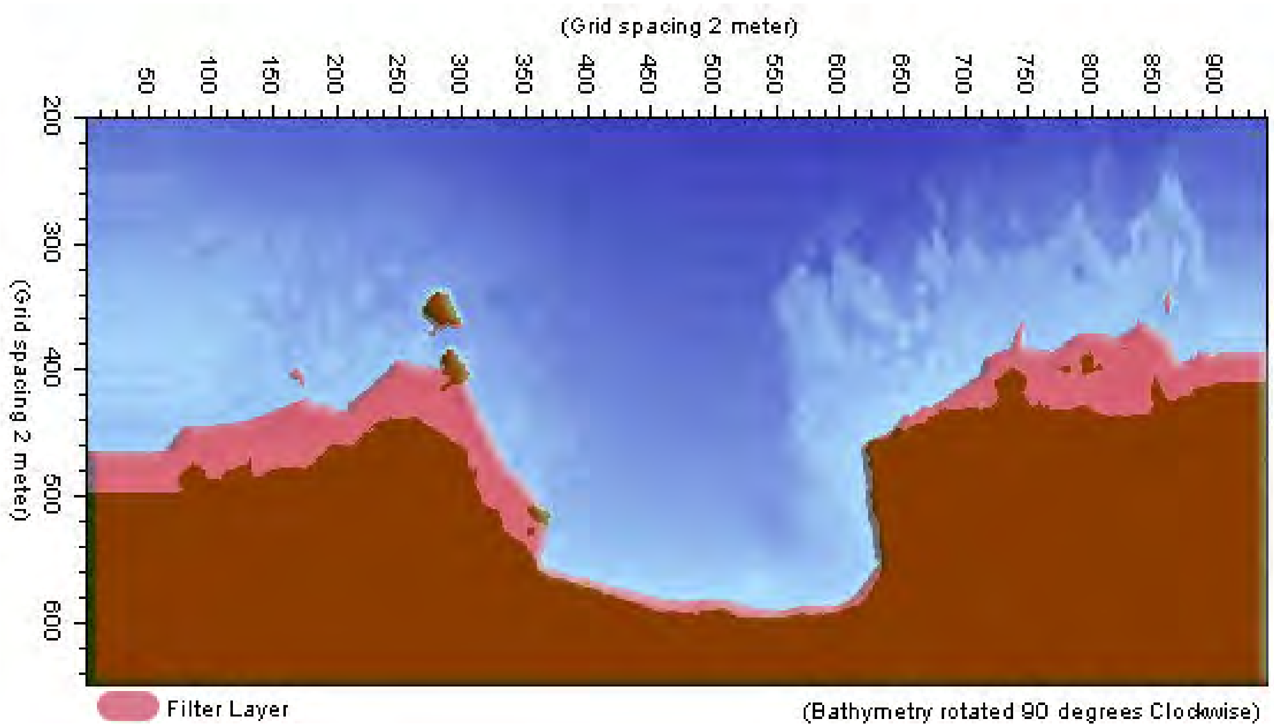

figure 65

4.2.6 Porosity layer

Porosity layers are usually applied to simulate partial reflection from rubble mound breakwaters but are in this study in some simulations applied to simulate partial reflection from the steep cliffs in the domain. The porosity layer is applied by substituting the “porous structure” with a porosity layer setting the water depth at this location to equal the water depth in front of the structure. A more detailed description is given where Porosity is applied.

4.2.7 Additional parameters

Due to the large number of adjustment options provided in MIKE21 BW, the huge model run-times and the limited opportunity to assess the value of every single one, a number of parameters have been kept unchanged throughout this study. This concerns the moving shoreline and wave breaking parameters. This decision to keep these unchanged is based on the experiences in the preliminary study that suggests that an alteration of these values would not notably change model results.

The parameters are:

Moving shore	**Wave breaking**
Slot depth: -21 Slot width: 0.2 Slot smoothing parameter: 100 Slot friction coefficient: 0.2	Roller form factor: 2 (plunging breakers) Type of roller celerity: Type 3 Roller celerity factor: 1.3 Initial breaking angle: 20 Final breaking angle: 10 Half-time for cut-off roller: 3

Additionally the time extrapolation factor is kept at 0.8, which is the heights possible value assuring a stable model simulation.

The last model parameter to be mentioned is the bottom friction factor defined by the Chezy number C. As it is not possible to determine an accurately uniform value for Waimea Bay, a number of different values have been tested in the simulations in order to obtain the most correct representative value.

4.3 Simulation Results:

4.3.1 The first attempt.

Simulation info: Simulation 1	
Wave-input: *Time-series 2* Incident wave direction: 327° Bottom friction: C=32 Bathymetry: Domain 1 Porosity map: none	

For the first model run the times-series from Thursday morning is used as offshore boundary condition. Being the most energetic wave input it was considered suitable for the initial simulation, as it would set the upper bar for eventual model instabilities (Blow-ups) that could occur during simulation.

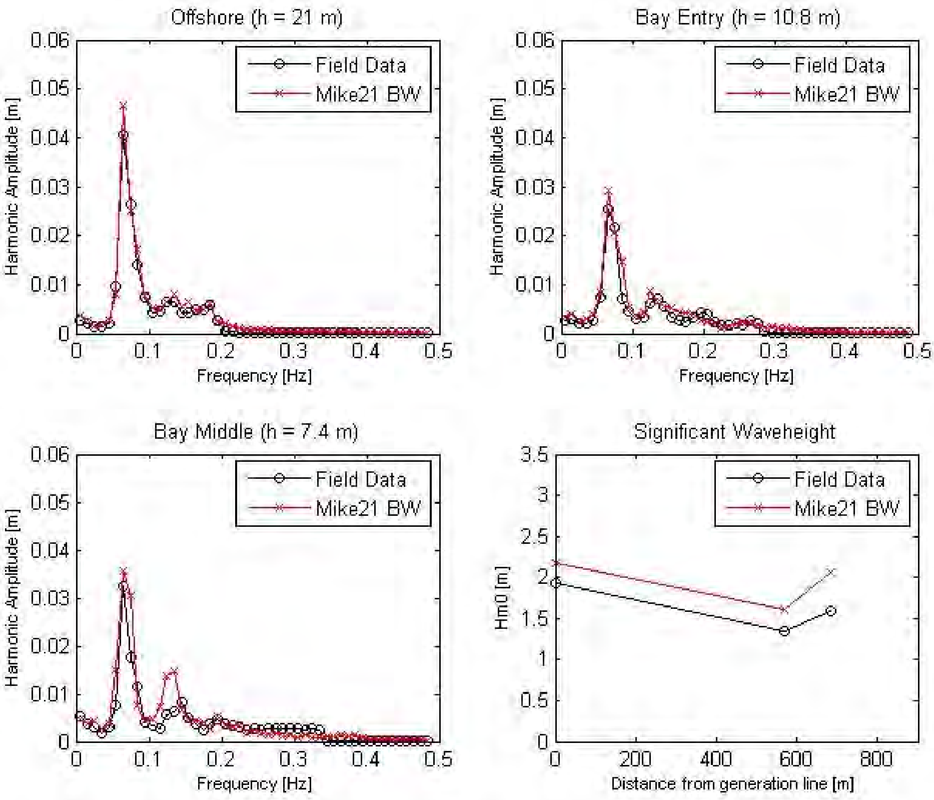

figure 66

Hm0			
H_{m0}	Field Data	Mike21 BW	Diff. [%]
Offshore	1.93 m	2.18 m	13 %
Bay Entry	1.35 m	1.60 m	19 %
Bay Middle	1.59 m	2.06 m	30 %

table 5

Additionally, the larger waves in this time-series will induce a much more pronounced surf zone in the domain that to some extend can be compared in time and space to recorded video from within the same timeframe. Also during this energetic time-series, processes such as wave reflection from the landward boundaries are much easier visually detectable from the model results.

In figure 66 the surface elevation time-series from three field stations are decomposed into their harmonic components and presented in frequency space where they are compared in to model results at these exact locations. Based on these spectra, H_{m0} has been calculated and compared.
The zero-upcrossing method has been applied to extract H_m and H_{sig} from the surface elevation time-series. Also the mean, minimum and maximum velocities have been extracted from the U- and V-velocity time-series. As Mike21 BW outputs the depth-integrated values P and Q, these have been divided with their corresponding water depths (e.g. U (t) =P (t)/(h+η(t)) to provide the correct representation for comparison with the field measurements given in depth averaged values. The U and V time-series from the field measurements have been rotated 30 degrees (clock-wise) to match the axis orientation in the domain.

Mean Wave height			
H_m	Field Data	Mike21 BW	Diff. [%]
Offshore	1.22 m	1.38 m	13 %
Bay Entry	0.84 m	0.99 m	17.1 %
Bay Middle	0.94 m	1.29 m	27.1 %

table 6

Sig. Wave height			
H_{sig}	Field Data	Mike21 BW	Diff. [%]
Offshore	1.84 m	2.05 m	11 %
Bay Entry	1.30 m	1.55 m	19 %
Bay Middle	1.48 m	2.02 m	36 %

table 7

Velocities offshore						
	U_{max}	U_{min}	U_{mean}	V_{max}	V_{min}	V_{mean}
Field Data	1.07 m/s	-0.87 m/s	-0.01 m/s	0.50 m/s	0.69 m/s	0.00 m/s
Mike21 BW	0.92 m/s	-1.07 m/s	-0.05 m/s	-1.10 m/s	-0.38 m/s	0.01 m/s

table 8

The offshore location

In figure 66 it is observed that the spectral peak at the location of the ADCP (offshore) is clearly overestimated by the model. The result is an overestimation of the corresponding H_{m0}. Also an offshore overestimation of H_m and H_{sig} (presented in table 6and table 7) is clearly noticed.
The most likely explanation for this is that the overestimated model wave height is caused by wave reflection. Especially from the steep cliffs and rocky outcrops around the entry of the bay.

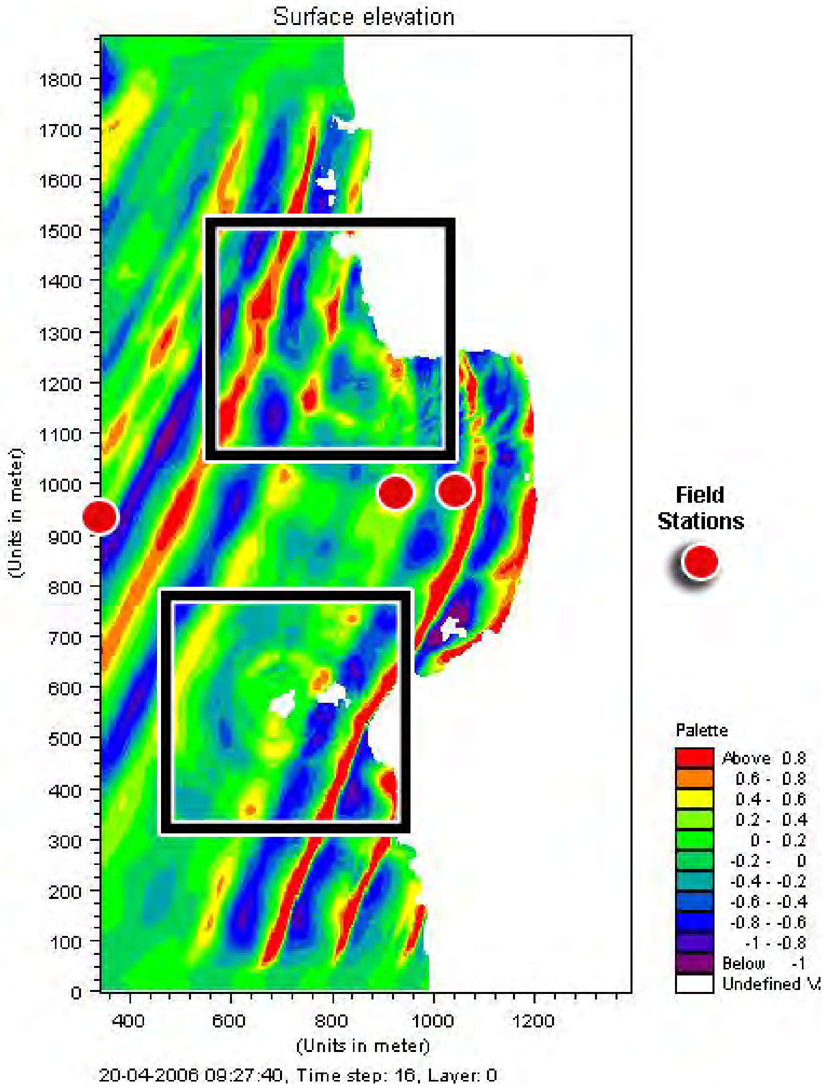

figure 67

In figure 67 it is observed how extensive wave reflection occurs from the cliffs of the northern bay entry and the two rocky outcrops outside the south end of the bay entry producing scattered waves that unquestionably affects the model output in both the offshore station and in the bay entry.

The first question that arises is if the models prediction of the magnitude of this reflection is correct. This also yields the question if the input surface elevation time-series measured by the ADCP in fact can be treated as a purely incident wave input or if the signal also contains a significant contribution from reflected waves traveling in an adverse direction (not necessarily the direct opposite direction) of the incident wave train. If significant wave reflection indeed does occur during the field campaign, it is not straightforward to tell if the surface elevation data collected in a particular point is magnified or inhibited by this phenomenon. It entirely depends if the point is close to a node or half-node in the system (e.g. recall figure 58).

In order to look deeper into this matter, a comparison between the measured and calculated depth-integrated velocities must be taken into consideration.

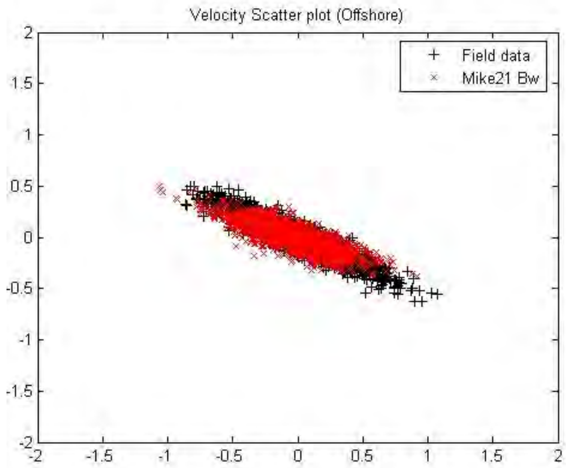

figure 68

From comparison of the offshore velocity scatter plots in figure 68 there seems to be a good agreement between filed measurement and model predictions and no apparent cross-directional velocity components are visible suggesting that the most dominant contribution to the signal from reflected waves occurs in the adverse direction of the wave direction. If this assumption is to be related to figure 67 it would be suggested that the dominant reflection registered in Station 1 mainly occurs from the two rocky outcrops outside south end of the bay as well as from the cliffs along the south entry of the bay itself.

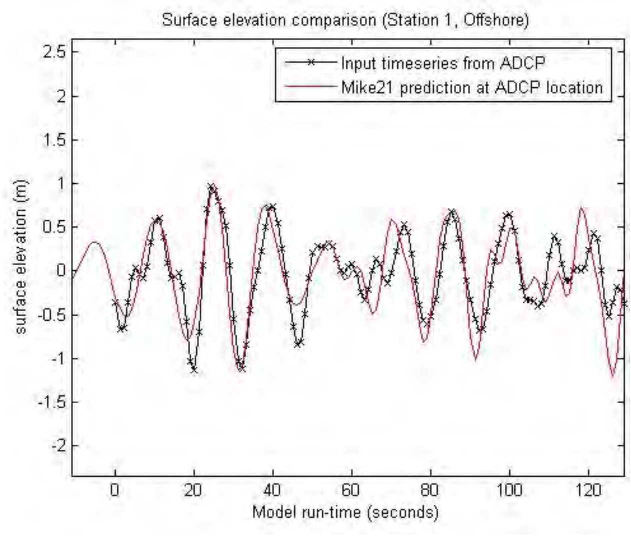

figure 69

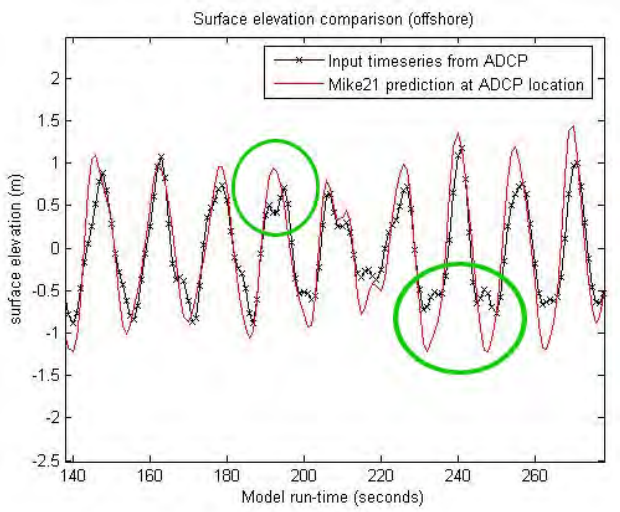

figure 70

By performing a time-series comparison in Station 1, the influence of reflection at this location is quite evident. In figure 69 it is observed how the first few waves are well predicted.

But in figure 70 it is observed how deviations stats to occur as the input time series shows indications of wave reflection as small "bumps" in the wave troughs and small sudden "drops" in the wave crests, which is not in the same manner represented in the model time-series. This initially suggests that the model at this location does not predict wave reflection that is actually occurring in the bay. However from figure 67 it is confirmed that the model does predict reflected waves to be propagating in the direction of Station 1 so it could also just be that it is the phase shift between the reflected and incident wave that is not correctly predicted. From figure 70 it could be suggested that the model predicts the reflected wave train to be in phase with the incident wave train resulting in wave height amplification instead of a reduction.

However the only thing that can be concluded at this point is that significant reflection occurs in both the model domain and apparently also in the physical domain and that the wave signal in Station 1 in the model is sensitive to this reflection. It will be left to the following model runs to attempt to resolve this question in further detail.

The bay Entry

From figure 66 it is observed how the spectral peak is well predicted by the model at the bay entry location (STATION 2). It is also noticed how the wave conditions at this location has become more non-linear due to the shallower water depth, as a more pronounced 2nd order harmonic amplitude is now clearly visible in the spectrum. However it is also noticed that the model slightly overestimates the magnitude of the 2nd order harmonic. The overall result is a small overestimation in H_{m0}, H_m and H_{sig}.

Velocities Bay Entry						
	U_{max}	U_{min}	U_{mean}	V_{max}	V_{min}	V_{mean}
Field Data	1.05 m/s	-0.88 m/s	-0.02 m/s	0.33 m/s	-0.33 m/s	0.01 m/s
Mike21 BW	1.02 m/s	-1.10 m/s	-0.01 m/s	0.46 m/s	-0.44 m/s	0.01 m/s

table 9

When comparing the velocity amplitudes presented in **table 9** it is observed how a good agreement exists between model results and field data for U_{min} and U_{max} while the model overestimates V_{min} and V_{max} with a factor 2. This suggests that the model overestimates the amount of wave reflection occurring at the southern entrance of the bay (recall figure 67), where the incident waves "bounces off" the northern and southern cliff sending a reflected wave traveling along the cross-section of the bay entrance*.

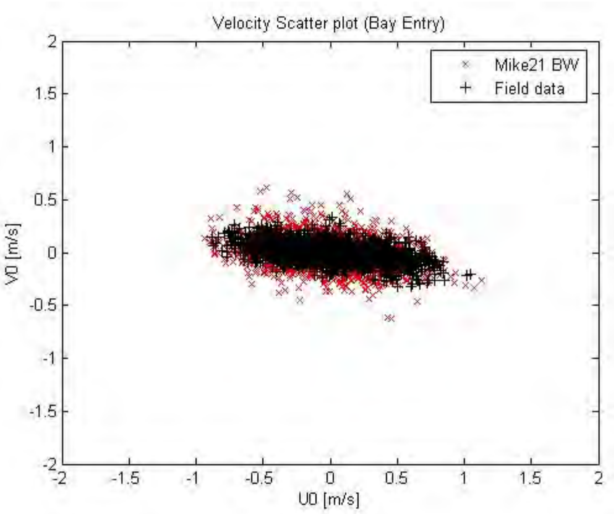

figure 71

In the velocity scatter plot from the bay entry location (figure 71), the directional agreement between model and field data is general in good agreement. It is noticed how the waves have now refracted almost 30 degrees since leaving the wave generation line and are now traveling almost in-line with the shore normal. However in the model predictions occasional minor deviations from this narrow band direction can be noticed, which most likely are caused by the previously mentioned reflected waves traveling cross-directional of the primary wave direction. It is noticed that this phenomenon does not show up in the field data.

* Due to the bays orientation in the model, U is parallel to the shore normal.

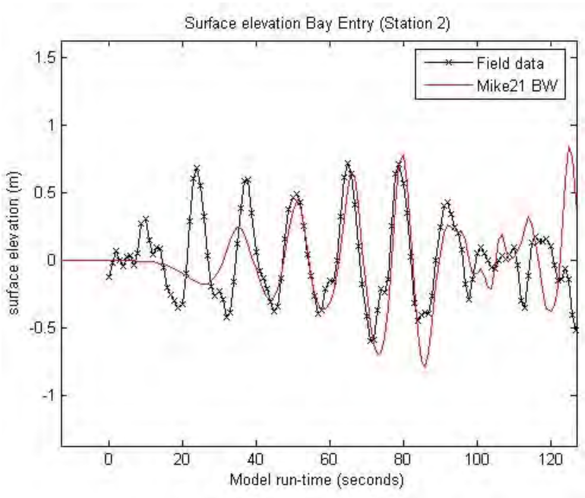

figure 72

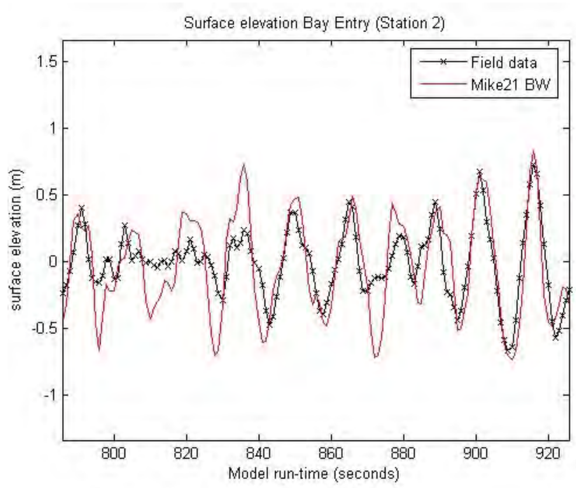

figure 73

In figure 72 it is illustrated how the first 3 waves (the initial forerunner excluded) that reach station 2 in the bay entry are in very good agreement with field measurements. But subsequently the agreement starts to deteriorate. While the agreement between the two time-series always remains fair, it is clearly visible that something is distorting the model predicted signal sometimes causing an overestimated crest or through (or vice versa) and occasionally even producing a wave that does not seem to be in any coherence with field measurements.

The fact that the time-series agreement is good for about 40 seconds after the first wave passes station 2 and then deteriorates strongly suggests that the way in which the waves are subsequently being dissipated and/or reflected at the landward boundaries are not represented correctly with the initial model setup.

Velocities Bay Middle						
	U_{max}	U_{min}	U_{mean}	V_{max}	V_{min}	V_{mean}
Field Data	1.35 m/s	-1.26 m/s	-0.03 m/s	0.46 m/s	-0.58 m/s	-0.06 m/s
Mike21 BW	1.40 m/s	-1.58 m/s	0.01 m/s	1.56 m/s	-0.91 m/s	-0.01 m/s

table 10

The Bay Middle

In figure 66 it is apparent how the non-linearity of the wave signal at this location is even stronger (compared to the bay entry) as now also small 3rd order harmonic amplitudes has become visible in the wave spectra. Unfortunately the model significantly overestimates the higher order harmonics resulting in overestimating of H_{m0}, H_m and H_{sig} of 28-36%. But from the comparison of velocity amplitudes in table 10 it is again clear that while U_{max} and U_{min} are in order of magnitude with field measurements, V_{max} and V_{min} are overestimated with as much as a factor 2-3.

Again these results strongly suggests that the model clearly overestimates the wave reflection occurring at the southern end of the bay, which results in the clearly defined waves traveling along the bay cross-section.

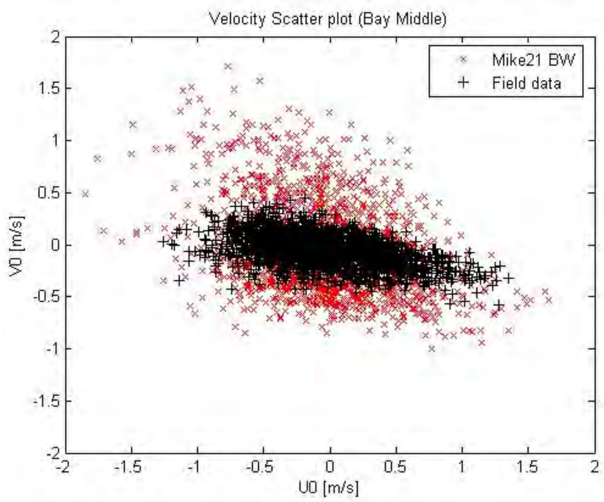

figure 74

From figure 74 it is observed how there exist a strong mismatch between field data and model results, and it is very clear that the significant cross-sectional wave motion occurring in the model (generating extensive directional spreading in the scatter plot) is not physically represented in the field data, where the direction is very narrow banded and almost inline with the shore normal.

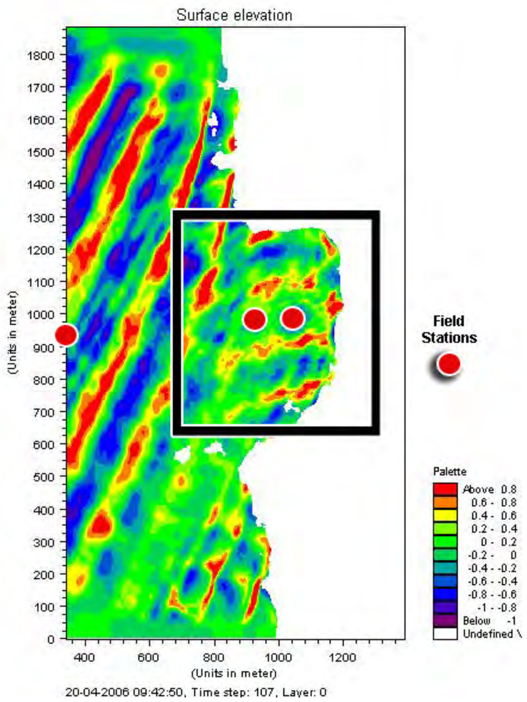

figure 75

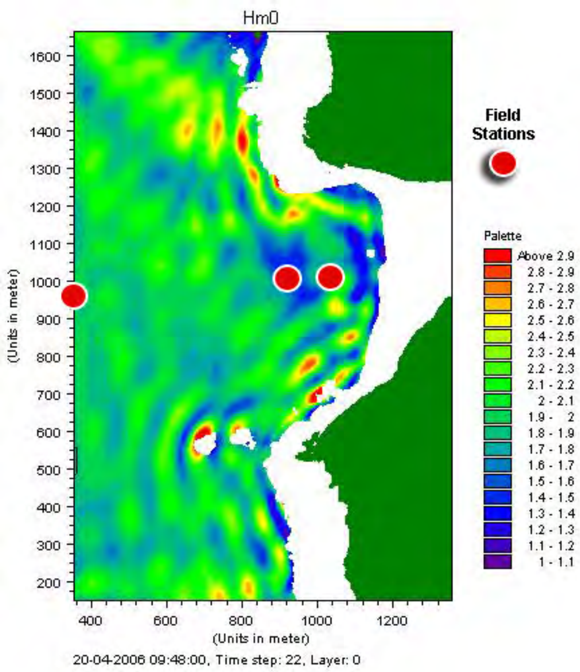

figure 76

The cross-sectional wave propagation is illustrated in figure 75, where a notable fraction of the incident wave energy is reflected from the southern cliff walls of the bay and right into the direction of the two instruments at station 2 and 3.

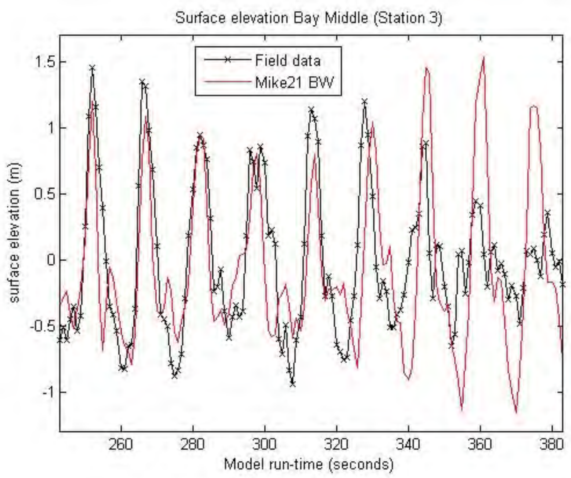

figure 77

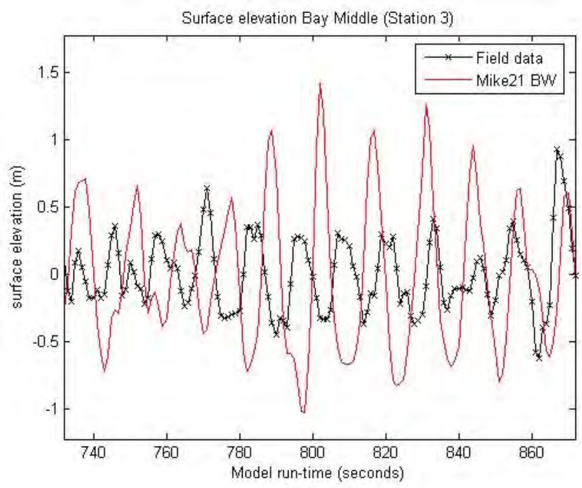

figure 78

Finally from the time-series comparison in figure 77 and figure 78 it is observed, how the coherence is heavily distorted by this phenomenon and frequently no apparent coherence seems to exist at all.

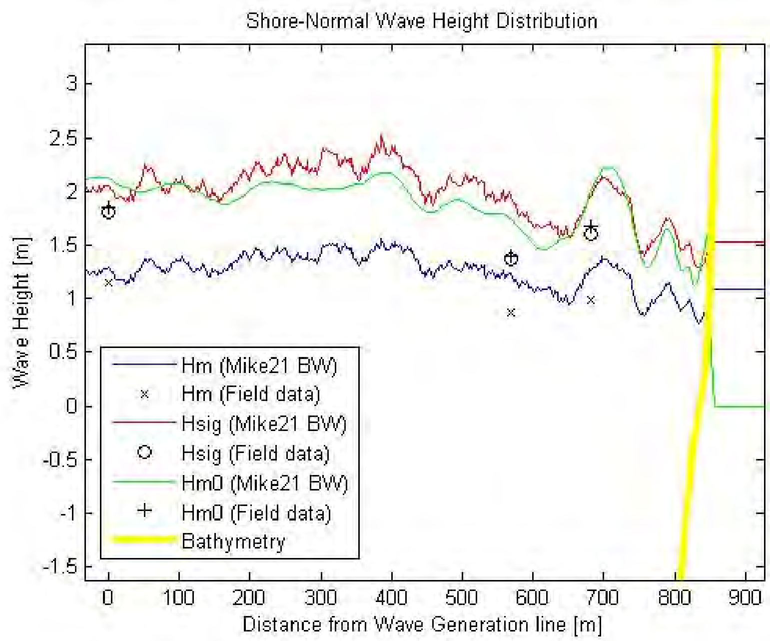

figure 79

From the spatial plot of H_{m0} in figure 76 it is seen how a good indication of the presence of wave reflection is apparent, being visually distinguishable as the strongly oscillating wave height patterns running perpendicular to the land boundary at a number of areas in the domain. As expected a pronounced standing wave pattern is located off the south side of the bay, but also a similar pattern is noticed running parallel to shore normal of the Waimea beach indicating significant reflection also occurring from the beach profile itself. In figure 79 a shore normal standing wave pattern inside Waimea Bay is clearly distinguishable. Again at this stage it is hard from only two measurement stations inside the bay to determine if this standing wave pattern is in fact occurring during the field campaign. The only thing that can be concluded at this stage is that the cross-sectional wave motion in the bay is overestimated with the current model setup (recall figure 71 and figure 74).

Remarks to simulation 1:

The total model run is 18000 time-steps However with the current setting the simulation blows up after 14300 time steps due to extraordinary cross-sectional wave action inside the bay. After lots of unsuccessful attempts to make the model run stable for its full duration, a stabile setting was found by decreasing both the Time-extrapolation factor to 0.5, the roller form factor to 1.5 and extending the sponge layer inside the bay to a water depth of 3 m (instead of just 1 m). However these changes only contribute to a damped solution of the former and the resulting simulation is considered a much poorer representation of the actual physical processes occurring in the domain. As a result it was considered more correct to compare the first 14300 time steps of the original simulation with the corresponding field results and from there clarify the problems that spawned the following attempt to improve model results.

4.3.2 Introducing porosity layer

Simulation info: simulation 2	
Wave-input: *Time-series 2* Incident wave direction: 327° Bottom friction: C=35 Bathymetry: Domain 1 Porosity map: porosity map 1 (cliffs + rocky outcrops)	

In this simulation a porosity layer has been applied along all the steep cliffs in the domain and the rocky outcrops along the southern entry of the bay. By introducing porosity layers along these parts of the landward boundary a reduced reflection at these locations is enforced, in an attempt to improve model predictions.

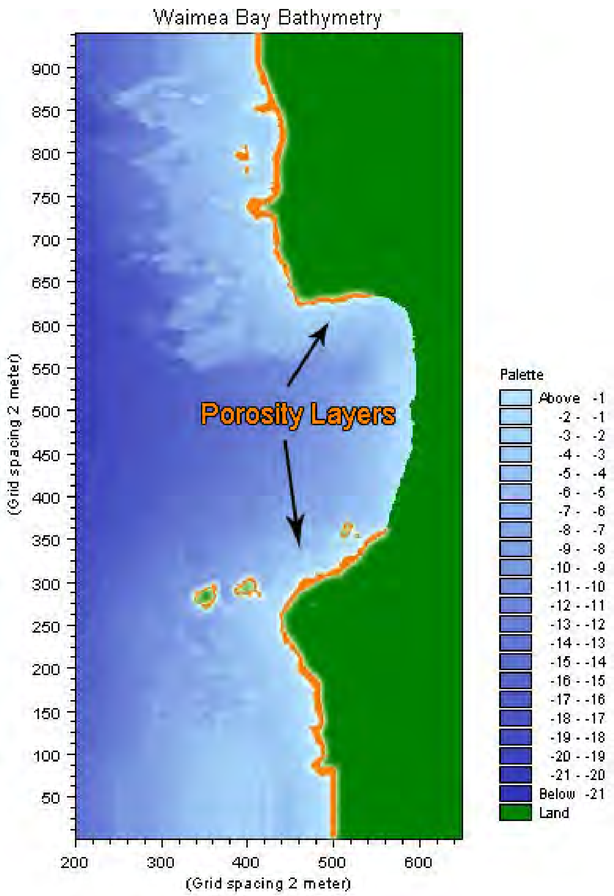

figure 80

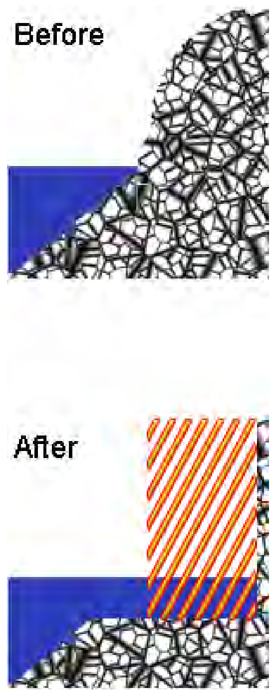

figure 81

The porosity layers were designed as suggested in *(DHI Software 2004)* being 6-8 grid points wide (12-16 m) corresponding to approximately L/4 with wave period T_p in a water depth of 1 m which in this setup was considered the "toe" of the structure The reflection coefficient was set to 0.8

assuming a “smooth impermeable slope”. An illustration of the selected porosity layer setup is given in figure 81.

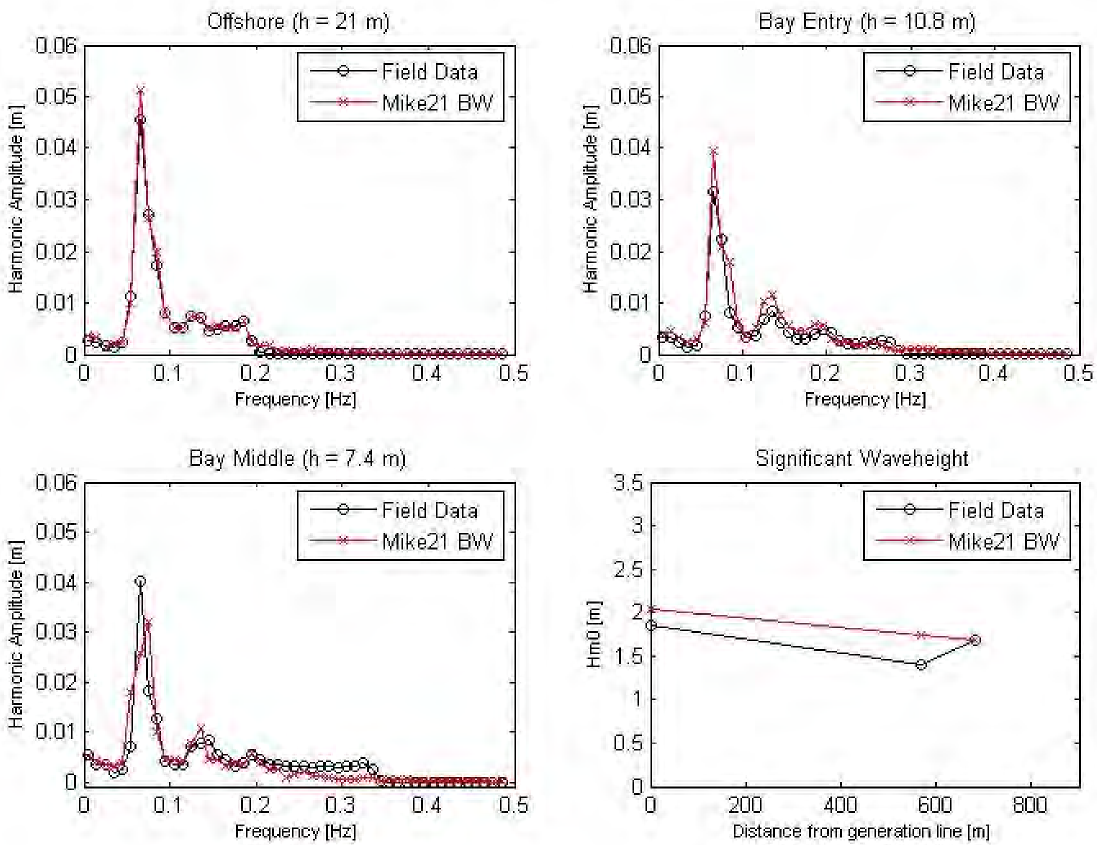

figure 82

Hm0			
H_{m0}	Field Data	Mike21 BW	Diff. [%]
Offshore	1.85 m	2.03 m	9.7 %
Bay Entry	1.39 m	1.74 m	25 %
Bay Middle	1.68 m	1.68 m	0 %

figure 83

From figure 82 it is observed how the implementation of the porosity layer provides a desired decrease in the spectral peak offshore and also significantly improves the prediction of the higher order harmonics in the bay middle. However on the contrary it is now observed that the amplitude of the spectral peak frequency in the bay middle (correctly represented in simulation 1) has decreased. At the same time the spectral peak and its 2nd order harmonic in the bay entry have been increased compared to simulation 1.

Mean Wave height			
H_m	Field Data	Mike21 BW	Diff. [%]
Offshore	1.15 m	1.30 m	13 %
Bay Entry	0.89 m	1.10 m	24 %
Bay Middle	1.00 m	1.07 m	7 %

table 11

Sig. Wave height			
H_{sig}	Field Data	Mike21 BW	Diff. [%]
Offshore	1.80 m	1.95 m	8.3 %
Bay Entry	1.37 m	1.73 m	26%
Bay Middle	1.61 m	1.72 m	7%

table 12

Again in table 11 and table 12 (based on the zero-upcrossing time-series analysis) it is observed how prediction of the wave conditions offshore and in the bay middle has been significantly improved by applying the porosity layer. However again it is noticed that the predicted wave height in the bay entry has increased compared to Simulation 1, where no porosity layer was applied.

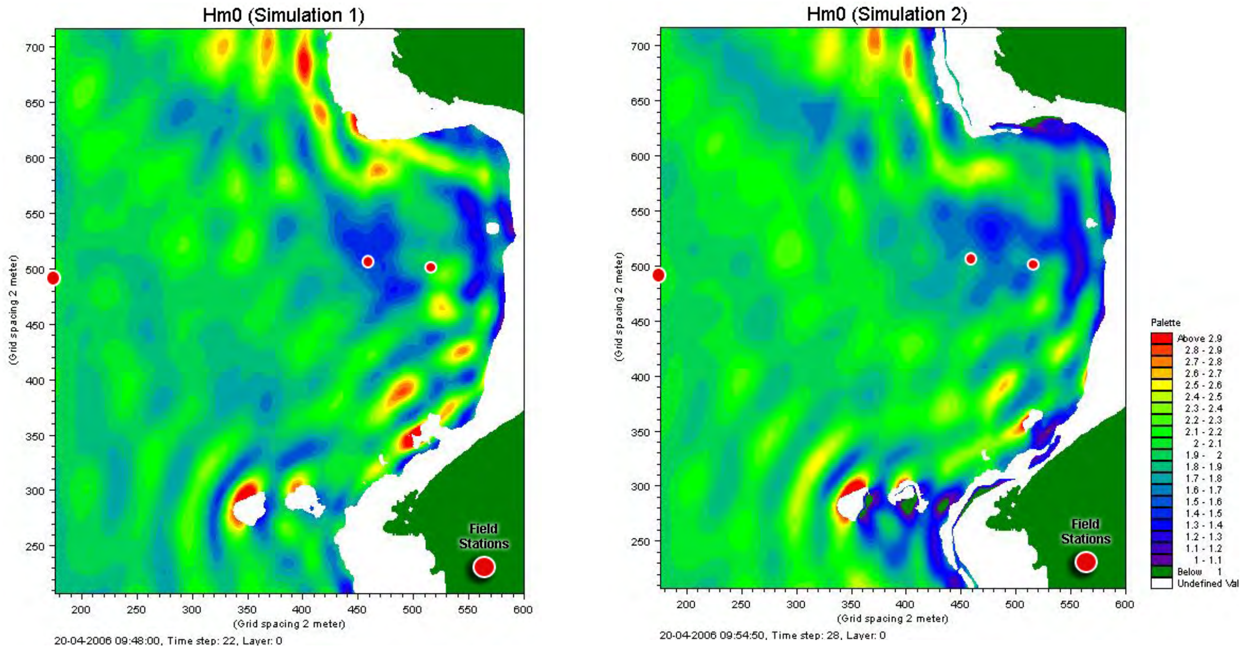

figure 84

From the H_{m0} plot in figure 84 it is observed how the assumed standing wave patterns are far from as apparent as for simulation 1 (figure 76) and thus the porosity map seems successful in damping the reflection from the steep cliffs and rocky outcrops. However, clearly notable standing wave patterns are still noticed from especially the south corner of the bay rocky outcrops but also along the beach in the bottom of Waimea bay.

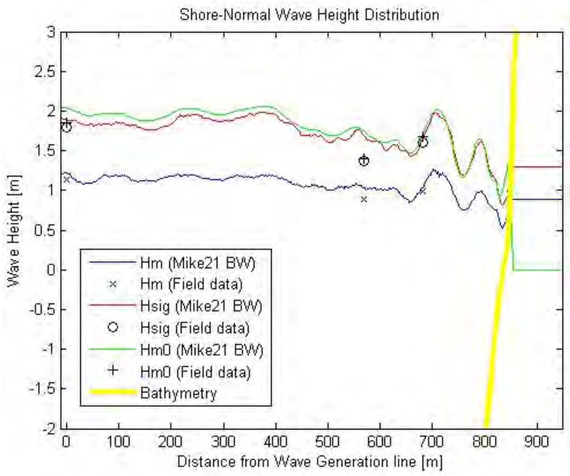

figure 85

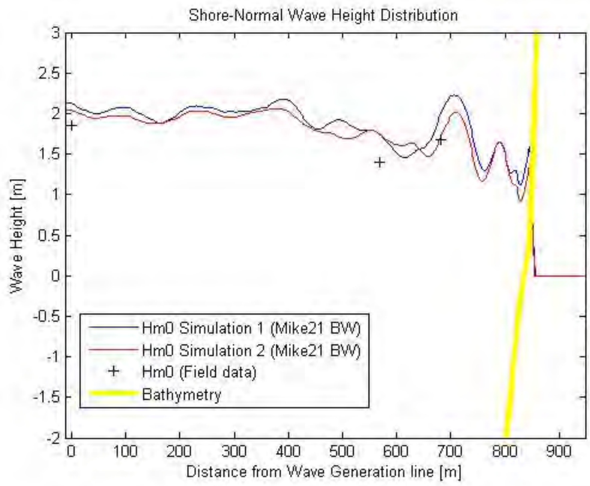

figure 86

When plotting the in-line wave height distribution along the shore-normal it is observed how the implementation of the porosity map to some extent have damped the standing wave pattern inside the bay compared to simulation 1. However it is observed how especially Station 3 is located in an area with very large wave height gradients making it evident that a correct prediction of the magnitude and 2D-distribution of wave reflection occurring in the bay is very important to the accuracy of model predictions at this location.

Velocities offshore						
	U_{max}	U_{min}	U_{mean}	V_{max}	V_{min}	V_{mean}
Field Data	1.07 m/s	-0.87 m/s	-0.01 m/s	0.50 m/s	-0.62 m/s	0.00 m/s
Mike21 BW	0.81 m/s	-1.12 m/s	-0.03 m/s	-0.59 m/s	-0.44 m/s	0.01 m/s

table 13

Velocities Bay Entry						
	U_{max}	U_{min}	U_{mean}	V_{max}	V_{min}	V_{mean}
Field Data	1.05 m/s	-0.88 m/s	-0.02 m/s	0.33 m/s	-0.33 m/s	0.01 m/s
Mike21 BW	1.22 m/s	-1.10 m/s	-0.01 m/s	0.51 m/s	-0.52 m/s	0 m/s

table 14

Velocities Bay Middle						
	U_{max}	U_{min}	U_{mean}	V_{max}	V_{min}	V_{mean}
Field Data	1.35 m/s	-1.26 m/s	-0.03 m/s	0.46 m/s	-0.58 m/s	-0.06 m/s
Mike21 BW	1.64 m/s	-1.78 m/s	-0.01 m/s	1.27 m/s	-0.80 m/s	-0.01 m/s

table 15

From table 13, table 14 and table 15 it is noticed that the mean and peak velocity values are rather unchanged compared to simulation 1 with the exception of the cross-sectional peak velocities that have decreased significantly compared to simulation 1 and are now in much better agreement with field data.

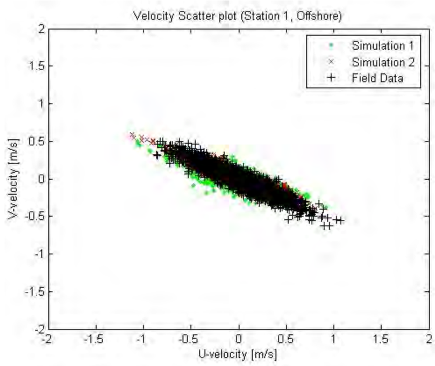

figure 87

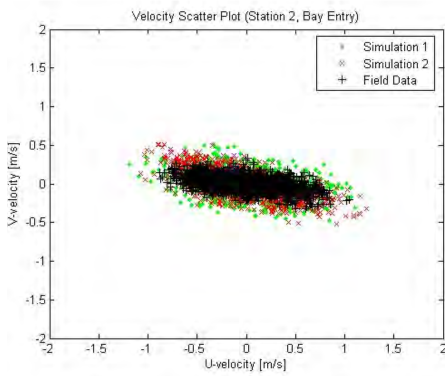

figure 88

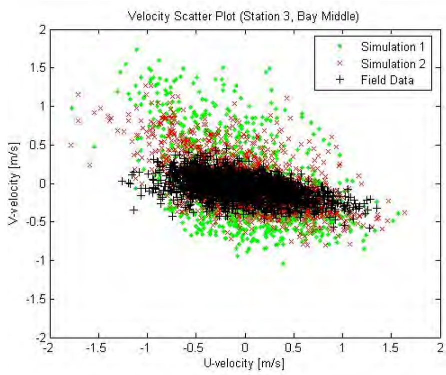

figure 89

When considering the scatter plots from these two locations it is obvious that introducing a porosity layer in the model domain has made a significant improvement in resolving the cross-sectional reflection in the bay middle as observed in figure 89. However some cross-sectional oscillation is still noticed from waves reflected from the southern end of the bay and it is possible that this could be eliminated if a more absorbing porosity layer were applied in along the south side of the bay that appears to be the source of this reflection affecting the velocity prediction in Station 3.

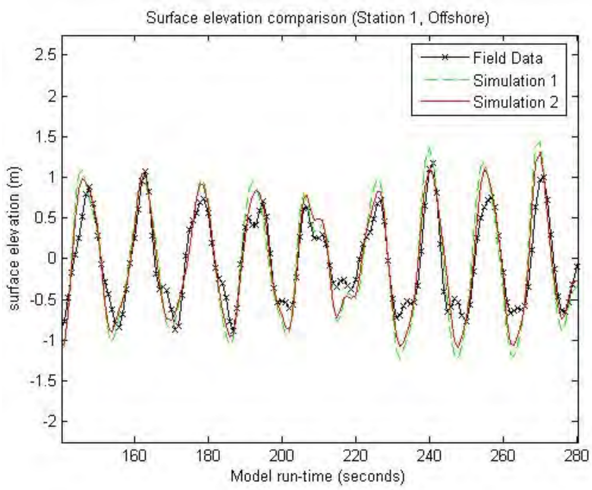

figure 90

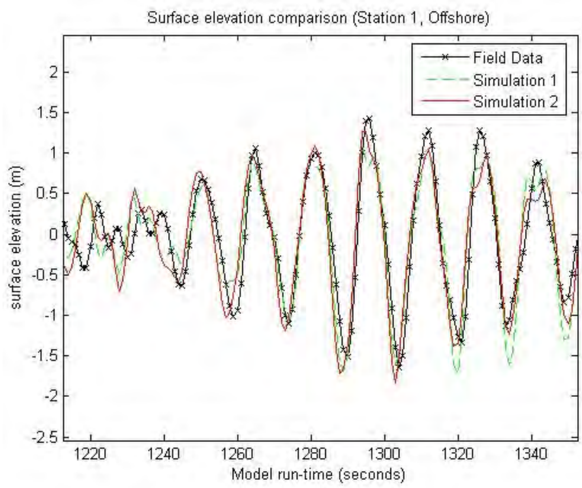

figure 91

When comparing the times-series from Simulation 1 and 2 at the offshore location a slightly better agreement has been obtained by introducing a porosity map. However major features in the field data time series (such as assumable reflected waves appearing as “trough bumps” in figure 90) is still not well represented by the model predictions. *But what is very interesting is that the locations where the “trough bumps” are not predicted, the adjacent wave crests are usually overestimated with the same order of magnitude. This could suggest that the lack of coherence is caused by a small phase mismatch between the incident wave and the predicted reflected wave.*

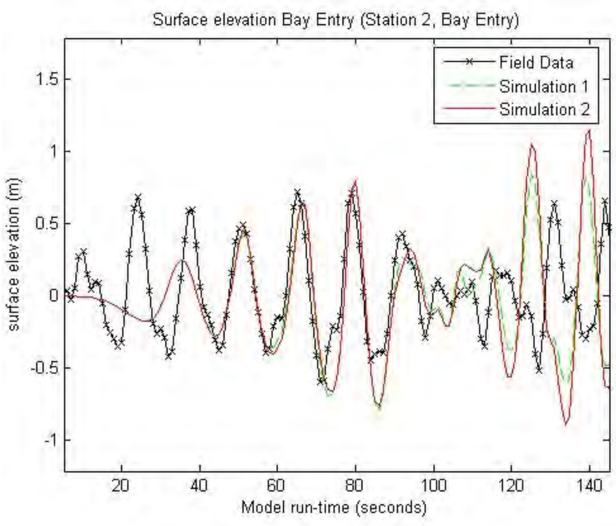

figure 92

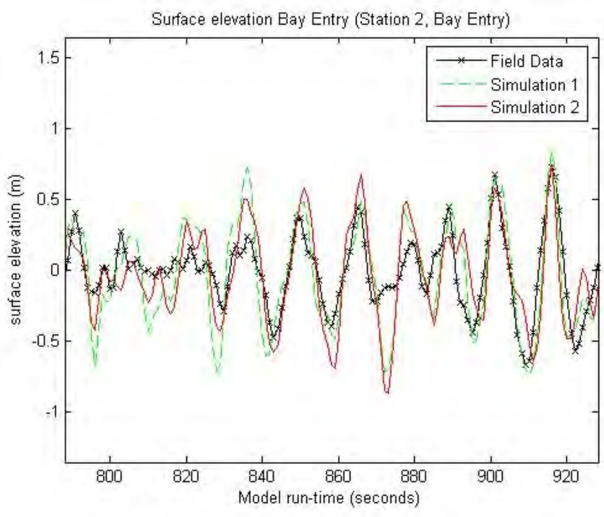

figure 93

At station 2 in the bay entry it is noticed that in spite of the implementation of the porosity map there is still occasional difficulties with representing the reflection at this point correctly.

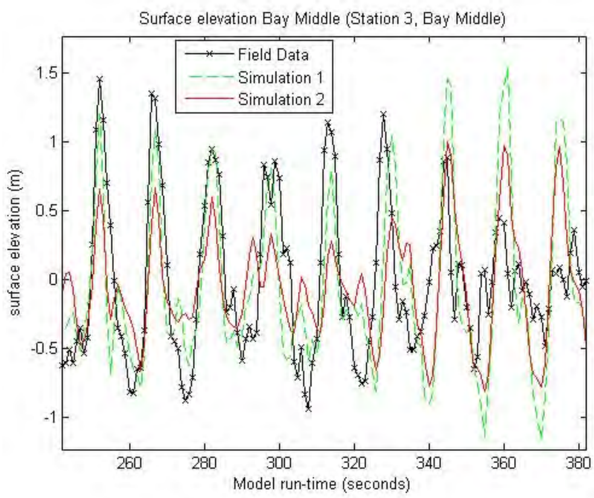

figure 94

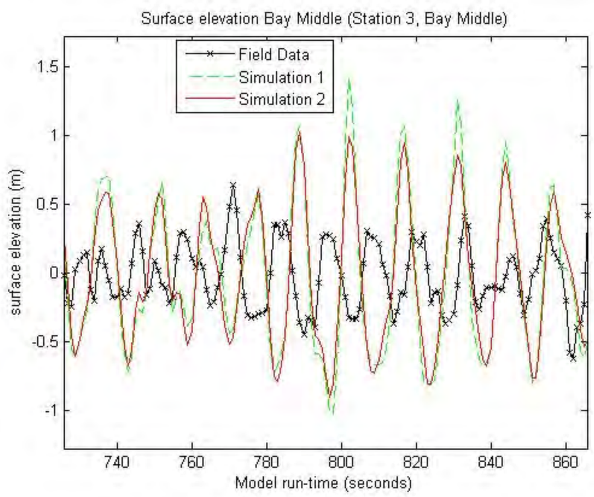

figure 95

Also at station 3 in the Bay middle it is clear how the implementation of the porosity layer has lead to improved wave height prediction at some locations (in the time series) and inaccurate predictions elsewhere. But in spite of not being convincingly clear from figure 94 and figure 95, a much better integral wave prediction is obtained in the bay middle by applying the porosity map. However it is concluded that the difficulties with resolving the bay reflection correctly might not be as easily solved by simply just introducing porosity map.

4.3.3 Extracting the reflected wave

Simulation info: Simulation 3	
Wave-input: *Time-series 2* (extracted incident wave) Incident wave direction: 327° Bottom friction: C=32 Bathymetry: Domain 1 Porosity map: porosity map 1	

As mentioned previously it is suspected that the wave signal given by the ADCP and used as input wave condition might contain a significant contribution from reflected waves off the landward boundary. In an attempt to account for this matter a simple method by *(Kubota et al. 1989)* has been applied on "time series 2" to extract the incident wave from the total surface elevation signal using the velocity time series *U0* and *V0* from this location. The principle is based on the 1D-assumption that the total wave signal can be considered a superposition of an incident and reflected wave train traveling in the direct opposite direction of each other. Hence:

$$\eta = \eta_I + \eta_R \tag{34.}$$

$$u = u_I - u_R \tag{35.}$$

Due to the 1D-formulation *u* is here the projection of U0 and V0 on the primary wave directionϕ. Hence:

$$u = U0 \cdot \sin(360^\circ - \phi) - V0 \cdot \cos(360^\circ - \phi) \tag{36.}$$

Further more it is assumed that the surface elevation can be sufficiently represented by a finite number of free harmonics, thus:

$$\eta_I = \sum_{i=1}^{N} A_i \cos(\omega_i t + \varepsilon_i) \tag{37.}$$

$$\eta_R = \sum_{i=1}^{N} B_i \cos(\omega_i t + \varepsilon_i^*) \tag{38.}$$

From these expressions the corresponding u-velocities are calculated from linear wave theory:

$$u_I = \sum_{i=1}^{N} H_i A_i \cos(\omega_i t + \varepsilon_i) \tag{39.}$$

$$u_R = \sum_{i=1}^{N} H_i B_i \cos(\omega_i t + \varepsilon_i^*) \tag{40.}$$

Where

$$H_i = \frac{\omega_i \cosh k_i (h+z)}{\sinh k_i h} \tag{41.}$$

Using Fourier analysis the following expression is obtained for u:

$$u = \sum_{i=1}^{N} \left(C_i \cos \omega_i t + D_i \sin \omega_i t \right) \tag{42.}$$

Where C_i and D_i are the Fourier coefficients.

Inserting (29), (30) and (32) into (25) you get:

$$\sum_{i=1}^{N} H_i A_i \cos(\omega_i t + \varepsilon_i) - \sum_{i=1}^{N} H_i B_i \cos\left(\omega_i t + \varepsilon_i^*\right) = \sum_{i=1}^{N} \left(C_i \cos \omega_i t + D_i \sin \omega_i t \right) \tag{43.}$$

Recalling that each wave can be treated as free, both sides are divided through with H_i and by inserting (27) and (28) you obtain:

$$\eta_I - \eta_R = \sum_{i=1}^{N} \frac{1}{H_i} \left(C_i \cos \omega_i t + D_i \sin \omega_i t \right) \tag{44.}$$

Finally by applying (24) you obtain:

$$\eta_I = \frac{1}{2} \cdot \left\{ \eta + \sum_{i=1}^{N} \frac{1}{H_i} \cdot \left(C_i \cdot \cos(\omega_i \cdot t) + D_i \cdot \cos(\omega_i \cdot t) \right) \right\} \tag{45.}$$

From this equation the incident wave train can be extracted from the ADCP wave signal.

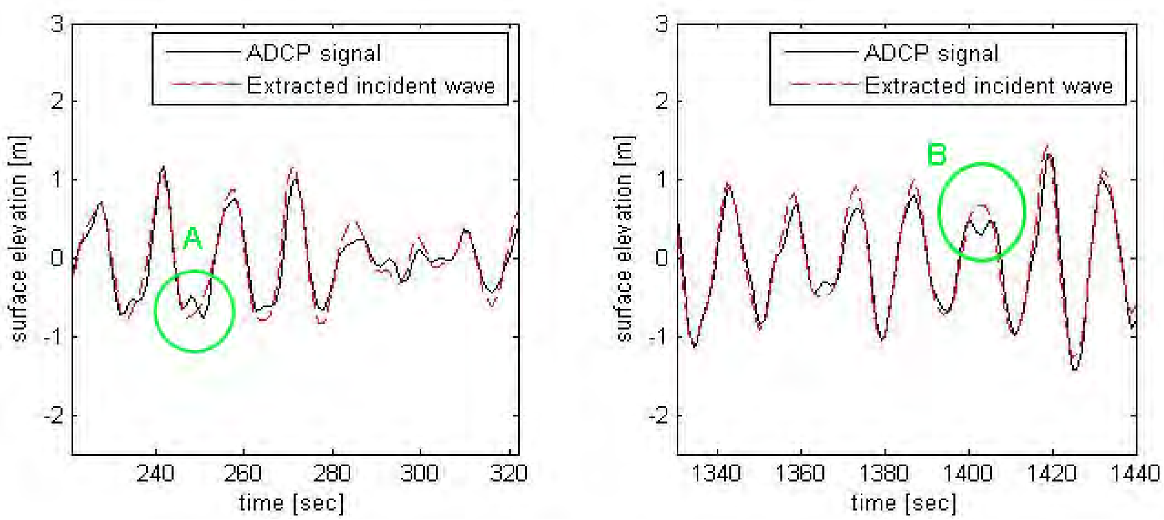

figure 96

By comparing the two time-series it does appear that this method is quite successful in filtering out suspected contributions from a reflected wave train observed in “A” and “B”.

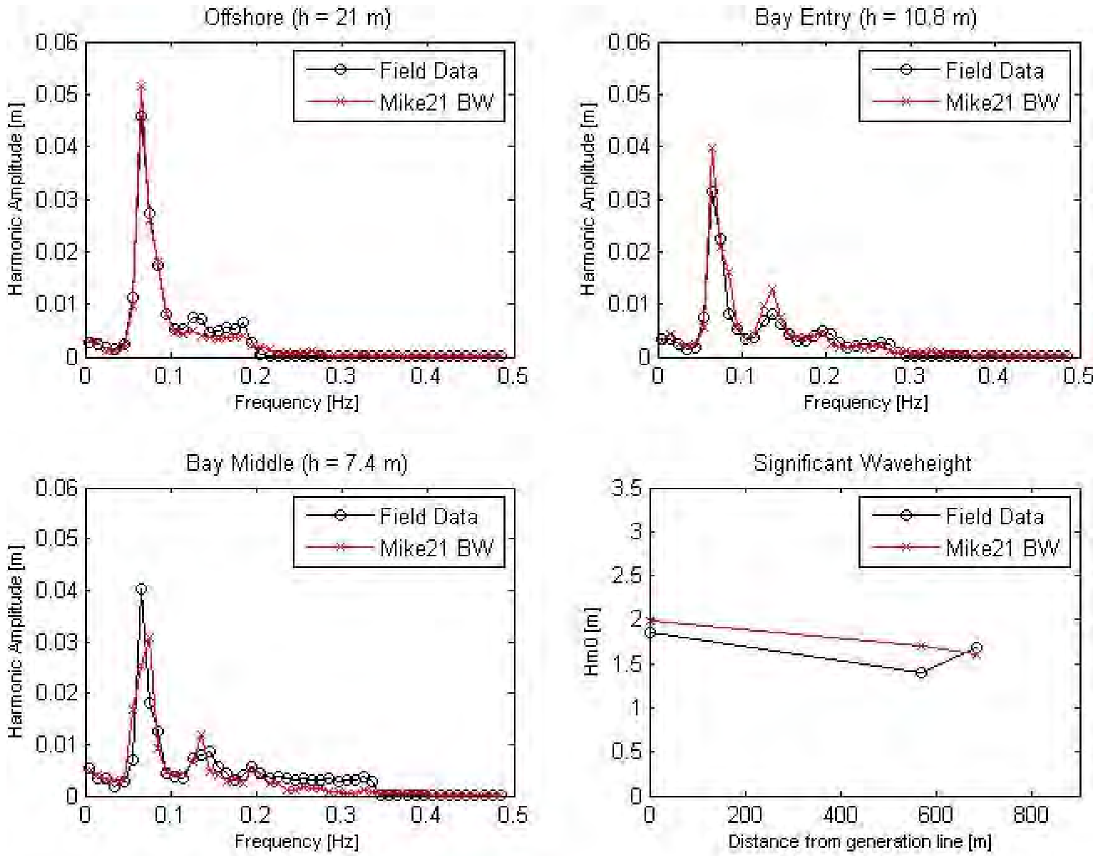

figure 97

Hm0			
H_{m0}	Field Data	Mike21 BW	Diff. [%]
Offshore	1.85 m	2.00 m	8 %
Bay Entry	1.39 m	1.70 m	22 %
Bay Middle	1.68 m	1.60 m	5 %

table 16

Mean Wave height			
H_m	Field Data	Mike21 BW	Diff. [%]
Offshore	1.15 m	1.25 m	9%
Bay Entry	0.89 m	1.10 m	23%
Bay Middle	1.00 m	1.01 m	1 %

table 17

Sig. Wave height			
H_{sig}	Field Data	Mike21 BW	Diff. [%]
Offshore	1.80 m	1.96 m	9%
Bay Entry	1.37 m	1.71 m	20%
Bay Middle	1.61 m	1.66 m	3%

table 18

It is noticed that using the produced "incident" time-series as offshore wave input lead to small improvement in the prediction of H_{m0}, H_m and H_{sig}.

However the spectral peak at station 3 is still not correctly represented and the 2nd order harmonics for station 2 and 3 are still overestimated. Also it does not solve the problem of what causes the model predictions in station 2 to be clearly exaggerated.

Velocities offshore						
	U_{max}	U_{min}	U_{mean}	V_{max}	V_{min}	V_{mean}
Field Data	1.07 m/s	-0.87 m/s	-0.01 m/s	0.50 m/s	-0.62 m/s	0.00 m/s
Mike21 BW	0.74 m/s	-0.90 m/s	-0.03 m/s	0.47 m/s	-0.46 m/s	0.01 m/s

table 19

Velocities Bay Entry						
	U_{max}	U_{min}	U_{mean}	V_{max}	V_{min}	V_{mean}
Field Data	1.05 m/s	-0.88 m/s	-0.02 m/s	0.33 m/s	-0.33 m/s	0.01 m/s
Mike21 BW	1.00 m/s	-0.00	0.00 m/s	0.42 m/s	-0.49 m/s	0.00 m/s

table 20

Velocities Bay Middle						
	U_{max}	U_{min}	U_{mean}	V_{max}	V_{min}	V_{mean}
Field Data	1.35 m/s	-1.26 m/s	-0.03 m/s	0.46 m/s	-0.58 m/s	-0.06 m/s
Mike21 BW	1.25 m/s	-1.40 m/s	0.02 m/s	1.19 m/s	-0.62 m/s	0.00 m/s

table 21

From the tables above a small improvement of the velocity magnitudes at Station 2 and 3 is obtained, while the model performance for the offshore prediction is rather unchanged.

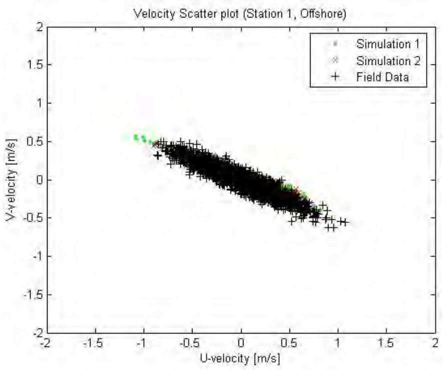

figure 98

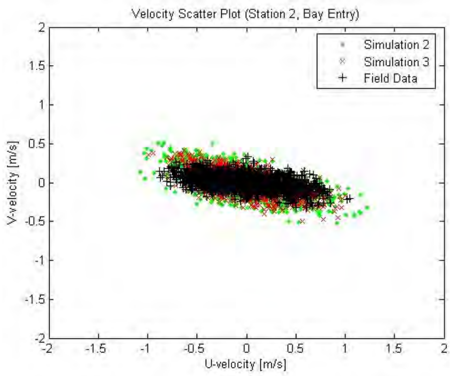

figure 99

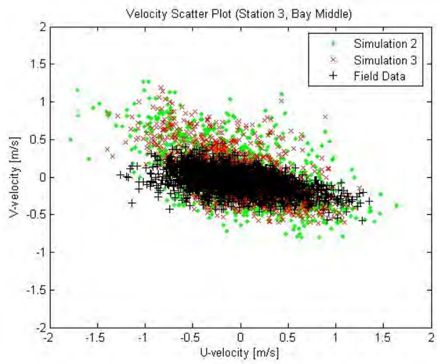

figure 100

In the velocity scatter plots the same trend is evident as a slightly improved agreement with field data.

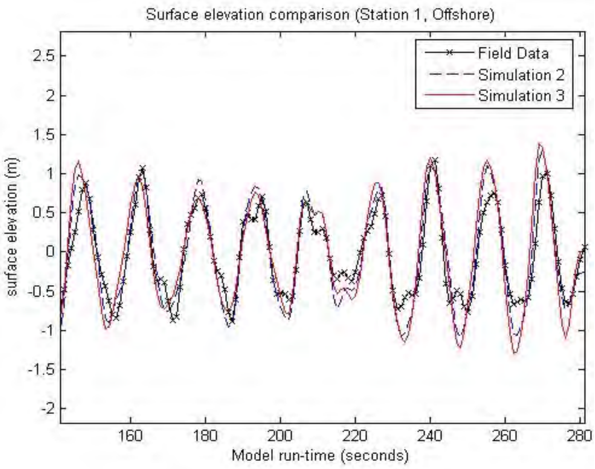

figure 101

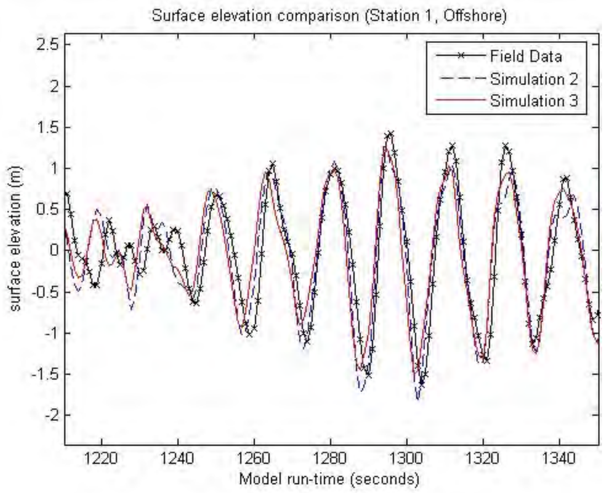

figure 102

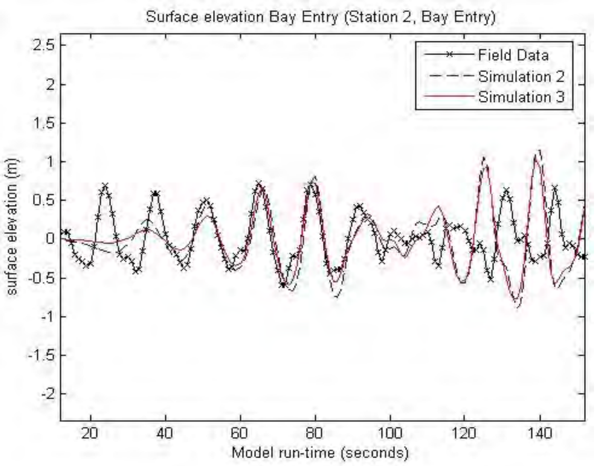

figure 103

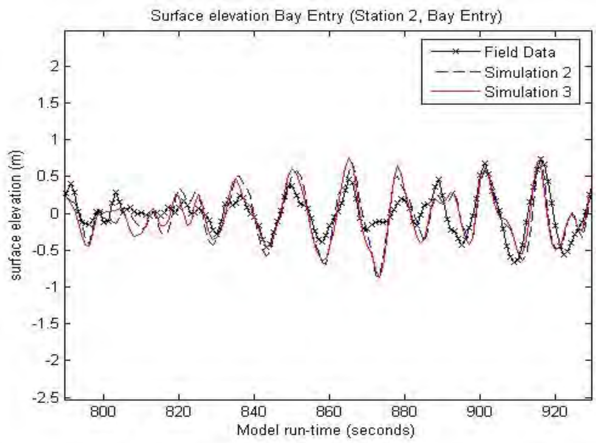

figure 104

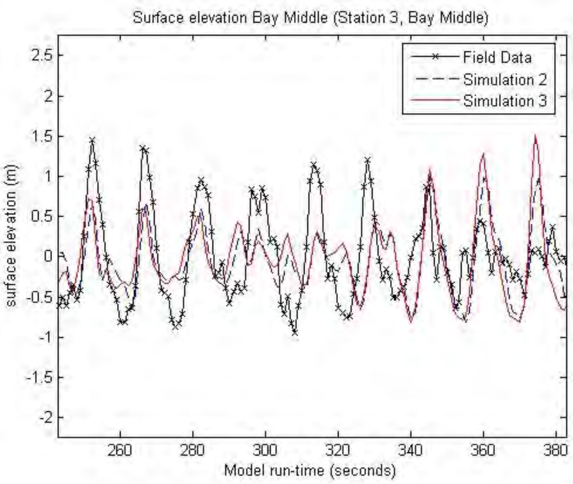

figure 105

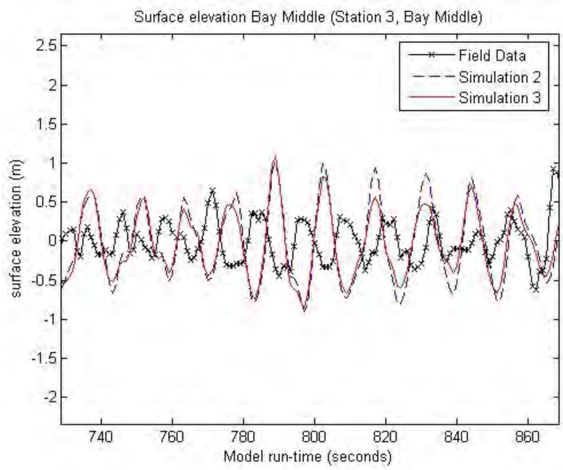

figure 106

For all the time series plots for Simulation 3 it can be observed that the influence of extracting the incident wave is only small. Most significantly is the fact that the resultant incident wave is less energetic in terms of wave amplitude compared to the “raw input” and as a result it leads to a general decrease in predicted wave height at all 3 field stations.

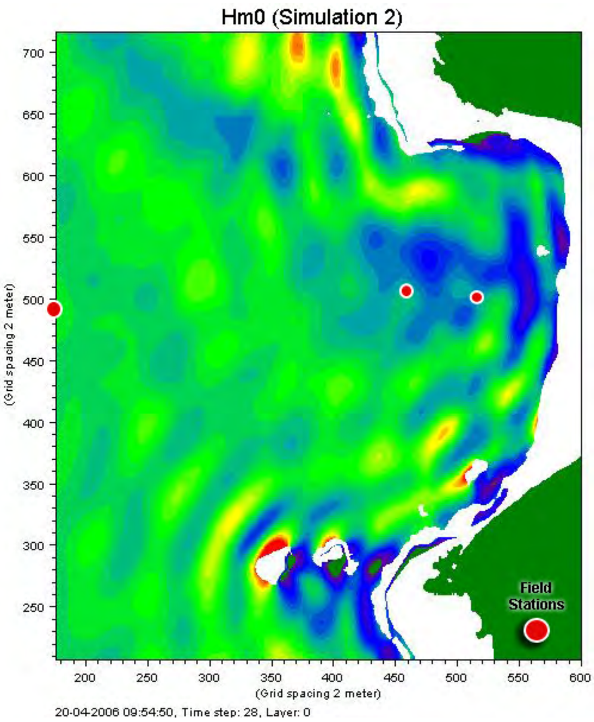

figure 107

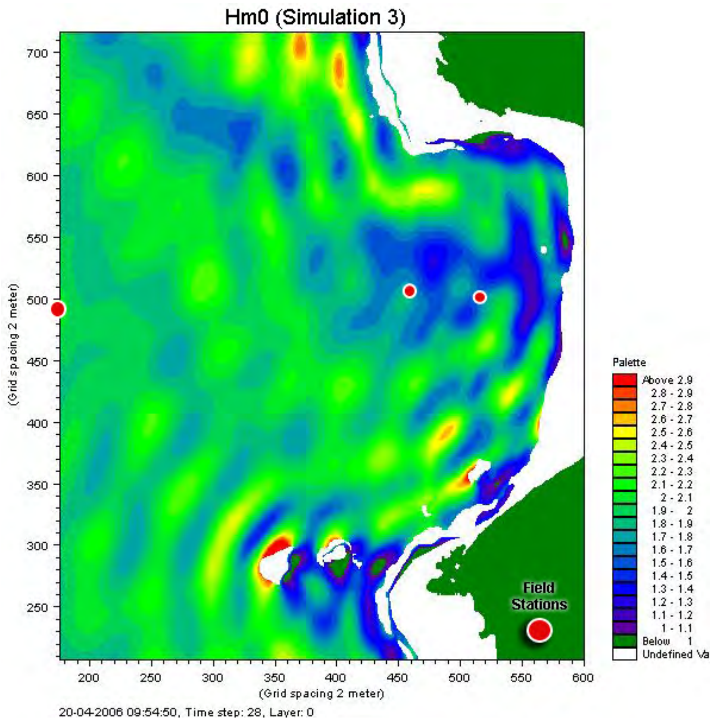

figure 108

However from a comparison of H_{m0}-plots it is observed that changing the wave input condition only has a small influence on the wave transformation processes inside the bay.

The conclusion of this simulation is that even though providing slightly better model estimates, extracting (and removing) the reflected wave train from the input wave conditions is not crucial in solving the problems with resolving the wave reflection occurring inside the bay.

4.3.4 Increasing bottom friction

Simulation info: simulation 4	
Wave-input: *Time-series 2* Incident wave direction: 327° Bottom friction: C=25 Bathymetry: Domain 1 Porosity map: none	

This simulation is identical to "simulation 2" with the exception that the bottom friction in the model has been increased (lower Chezy nr.). While it hardly ever was assumed that changing the bottom friction alone could lead to significantly improved results, it was found necessary to investigate and quantify the effect of a change in bottom friction on how it affected the models predictions of velocities and surface elevation in the domain.

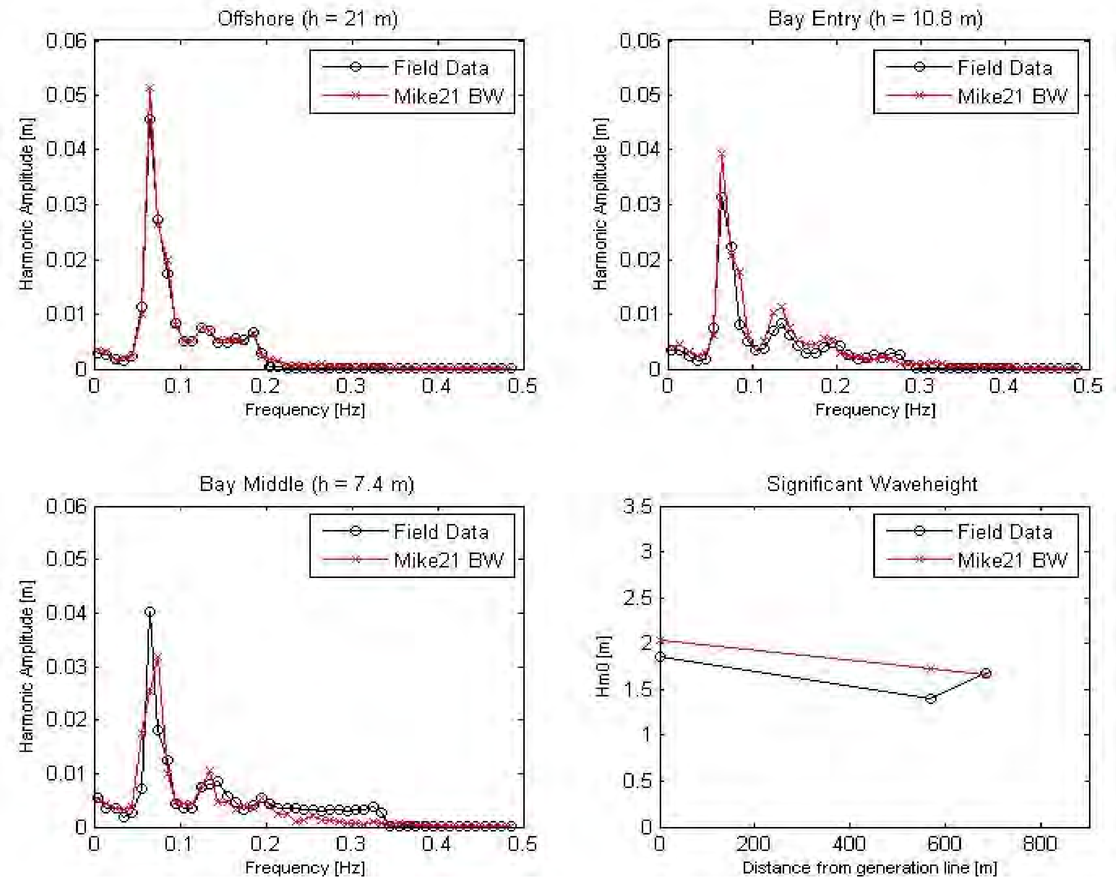

figure 109

Hm0			
$\mathbf{H_{m0}}$	Field Data	Mike21 BW	Diff. [%]
Offshore	1.85 m	2.03 m	10 %
Bay Entry	1.40 m	1.72 m	23 %
Bay Middle	1.68 m	1.65 m	2 %

table 22

Mean Wave height			
H_m	Field Data	Mike21 BW	Diff. [%]
Offshore	1.15 m	1.29 m	12%
Bay Entry	0.89 m	1.10 m	24%
Bay Middle	1.00 m	1.05 m	5%

table 23

Sig. Wave height			
H_{sig}	Field Data	Mike21 BW	Diff. [%]
Offshore	1.80 m	1.94 m	8%
Bay Entry	1.37 m	1.72 m	26%
Bay Middle	1.61 m	1.69 m	5%

table 24

From the spectral plots in figure 109 it is observed that they are almost identical to those in simulation 1 (figure 66) only insignificantly smaller in magnitude due to the increased energy dissipating due to the increased bottom roughness. As a result H_{m0}, H_m and H_{sig} are slightly smaller than in Simulation 1, which leads to a slight improvement of model results.

Velocities offshore						
	U_{max}	U_{min}	U_{mean}	V_{max}	V_{min}	V_{mean}
Field Data	1.07 m/s	-0.87 m/s	-0.01 m/s	0.50 m/s	-0.62 m/s	0.00 m/s
Mike21 BW	0.82 m/s	-1.12 m/s	-0.03 m/s	0.59 m/s	-0.42 m/s	0.01 m/s

table 25

Velocities Bay Entry						
	U_{max}	U_{min}	U_{mean}	V_{max}	V_{min}	V_{mean}
Field Data	1.05 m/s	-0.88 m/s	-0.02 m/s	0.33 m/s	-0.33 m/s	0.01 m/s
Mike21 BW	1.12 m/s	-0.96 m/s	-0.01 m/s	0.46 m/s	-0.47 m/s	0.00 m/s

table 26

Velocities Bay Middle						
	U_{max}	U_{min}	U_{mean}	V_{max}	V_{min}	V_{mean}
Field Data	1.35 m/s	-1.26 m/s	-0.03 m/s	0.46 m/s	-0.58 m/s	-0.06 m/s
Mike21 BW	1.43 m/s	-1.55 m/s	0.01 m/s	1.14 m/s	-0.70 m/s	0.00 m/s

table 27

It is also noticed that the velocity amplitudes are slightly smaller in magnitude compared to Simulation 2. However it is clear that an increase in bottom friction does not help in improving the inaccurate model prediction in Station 2.

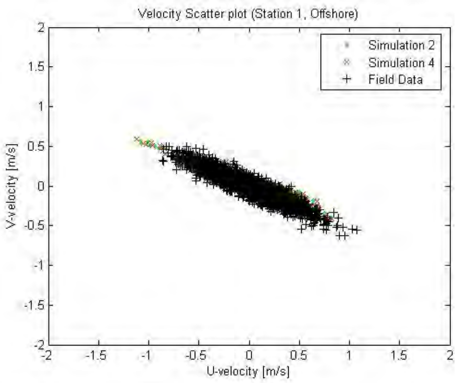

figure 110

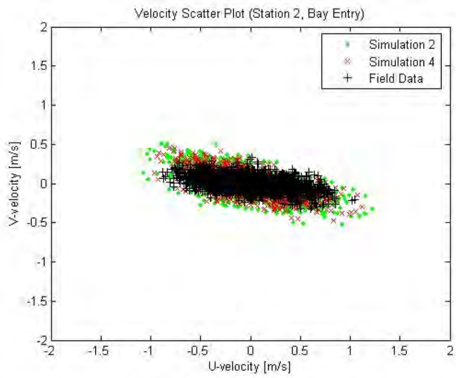

figure 111

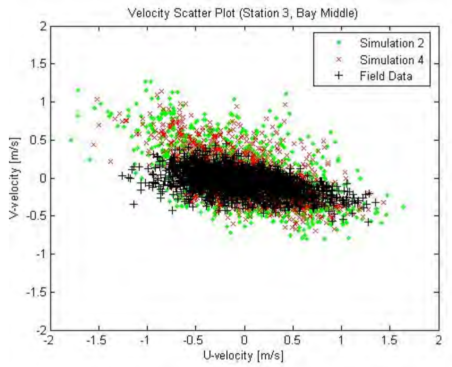

figure 112

Again the velocity scatter plots confirm the sight improvement in velocity prediction for Station 3 in the bay middle and to a lesser degree also for Station 2 in the bay entry. The offshore velocity prediction remains rather unaffected.

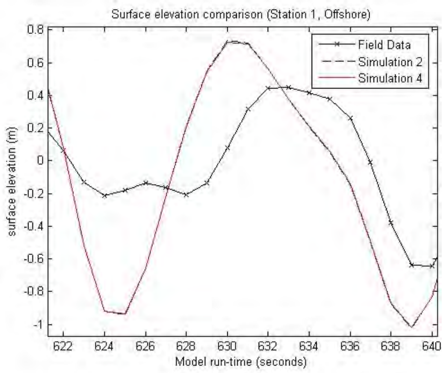

figure 113

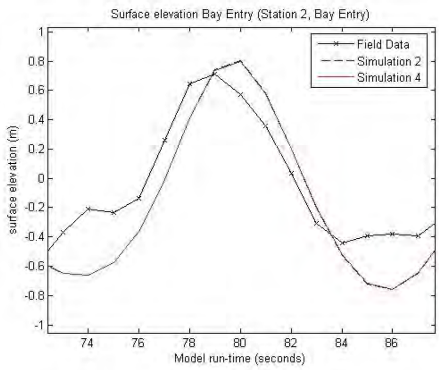

figure 114

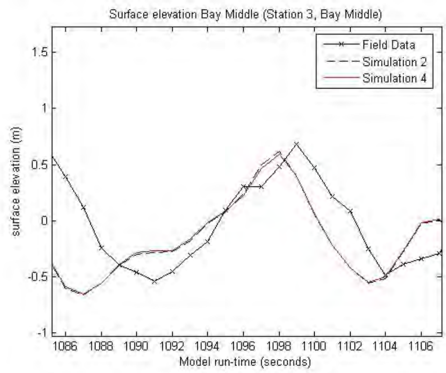

figure 115

However, when examining the time-series plots it is evident that changing the bottom friction virtually has no effect on the models wave height prediction for the selected station locations. The most obvious explanation for this is that the wave driven current values are very small and almost insignificant, thus not affecting the wave height at these locations as e.g. was the case in the rip current simulation in the preliminary study.

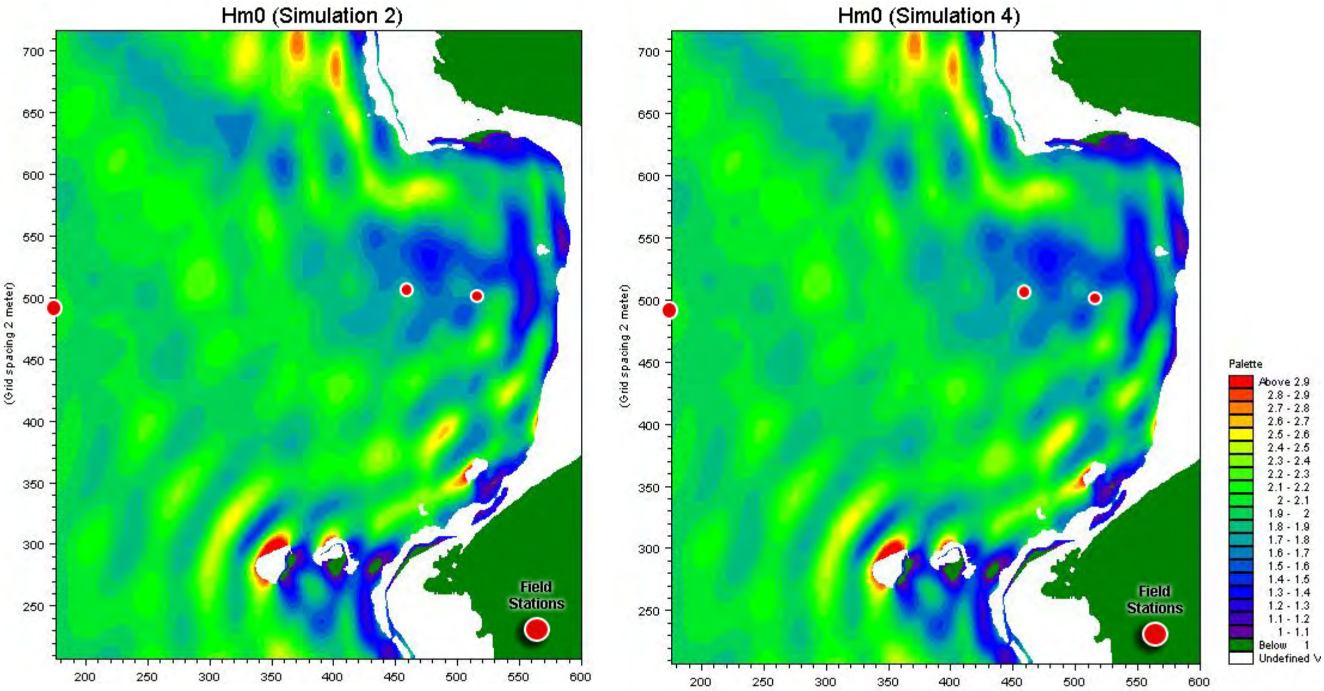

Also from a comparison of Hm0 plots it is observed that changing the bottom friction has almost no effect on the wave transformation processes occurring in the bay.

4.3.5 Enlarging the domain

Simulation info: simulation 5	
Wave-input: *Time-series 2* Incident wave direction: 0 ° (327°) Bottom friction: C=35 Bathymetry: Domain 2 Porosity map: porosity map 1	

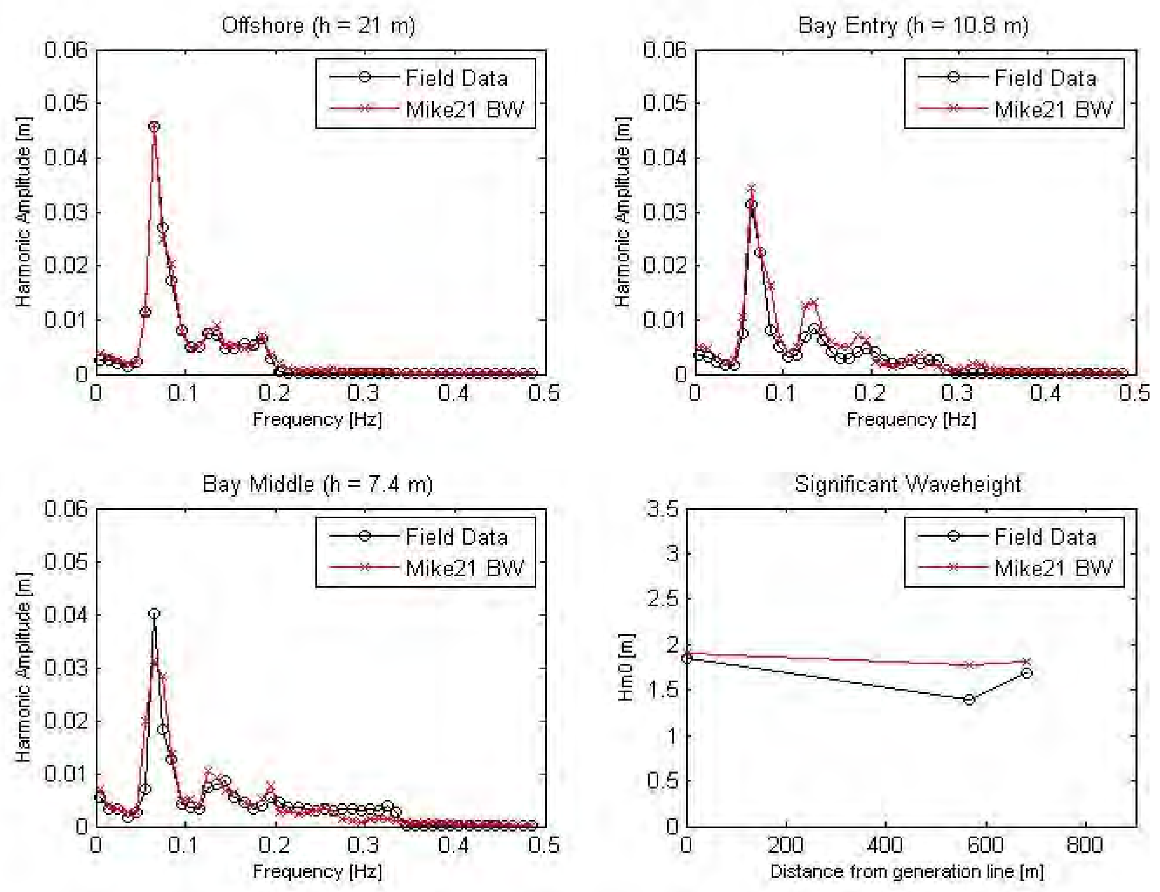

figure 116

Hm0			
H_{m0}	Field Data	Mike21 BW	Diff. [%]
Offshore	1.85 m	1.90 m	3%
Bay Entry	1.40 m	1.78 m	27%
Bay Middle	1.68 m	1.81 m	8%

table 28

Mean Wave height			
H_m	Field Data	Mike21 BW	Diff. [%]
Offshore	1.15 m	1.18 m	3%
Bay Entry	0.89 m	1.10 m	24%
Bay Middle	1.00 m	1.11 m	11%

table 29

Sig. Wave height			
H_{sig}	Field Data	Mike21 BW	Diff. [%]
Offshore	1.80 m	1.83 m	2%
Bay Entry	1.37 m	1.75 m	28%
Bay Middle	1.61 m	1.78 m	11%

table 30

From the spectral plots and the wave tables it is noticed that the wave height predictions at Station 1 has improved and is now in very good agreement with field data. But at the same time it is noticed that the larger domain and the domain-perpendicular wave propagation does not improve results inside the bay where the wave height in Station 2 is still significantly overestimated the spectral peak in Station 3 is still underestimated.

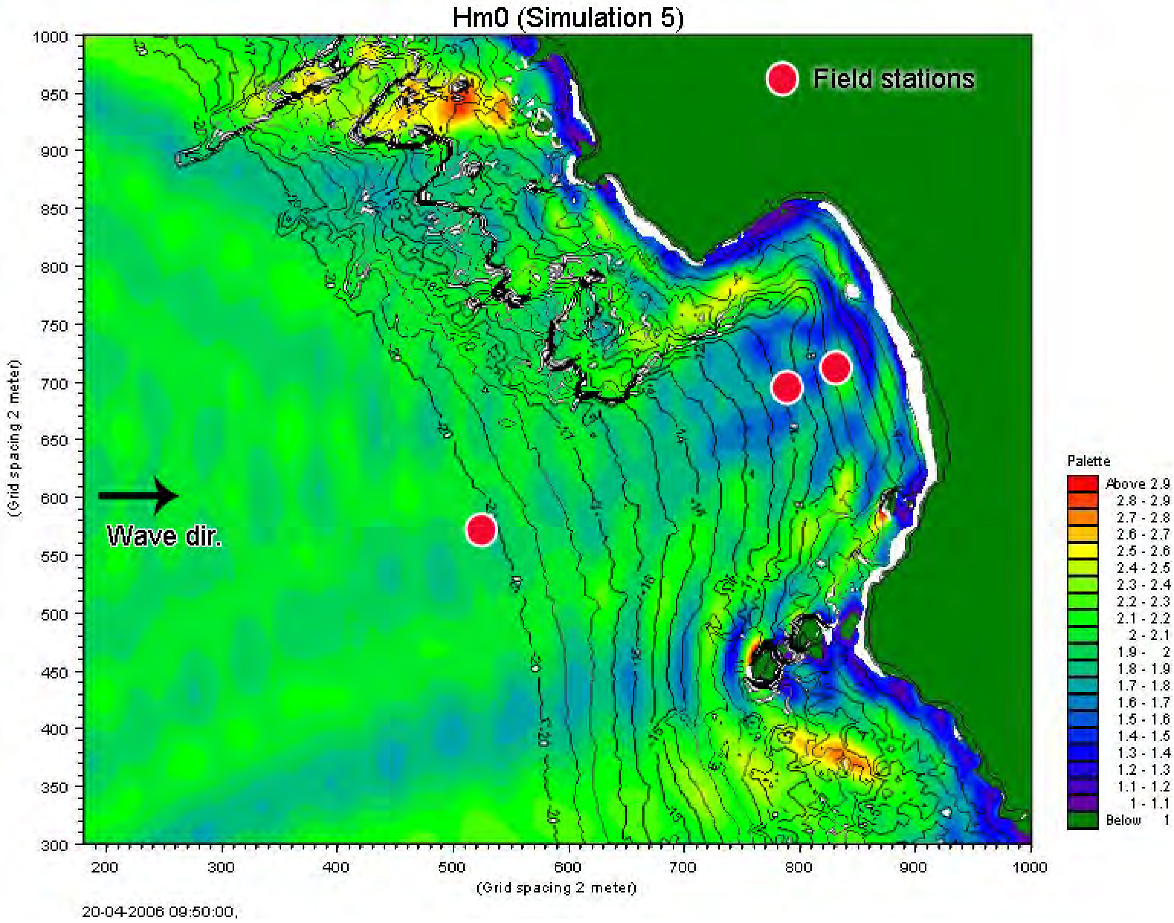

figure 117

From the Hm0-plot in figure 117 it is observed how the accurate wave height prediction in Station 1 might me a coincidence as the significant wave height offshore fluctuates between 1.83 m and 2.15 m in spite of the uniform conditions and flat bottom. From the Hm0-plot it looks like the spatial variation in wave height is greatly influenced by extensive reflection from especially the southern end of Waimea bay and the two large rocky outcrops in front of the southern entrance. But also from figure 64 it should be recalled that due to the weakly non-linearity of “time-series 2” (used as wave-input) the interaction between the (assumed free) primary and 2nd order harmonic will alone generate a spatially fluctuating wave height of up to 8%.

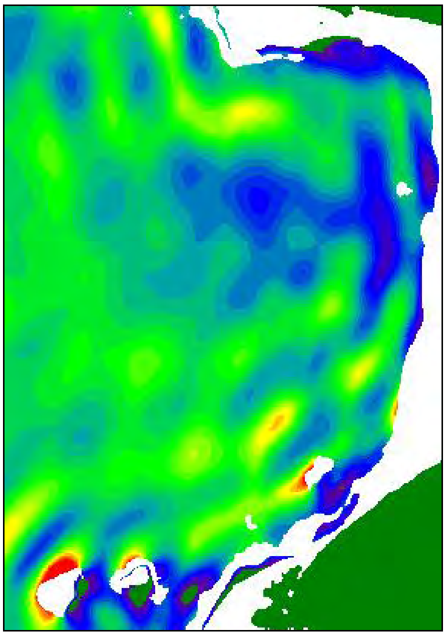

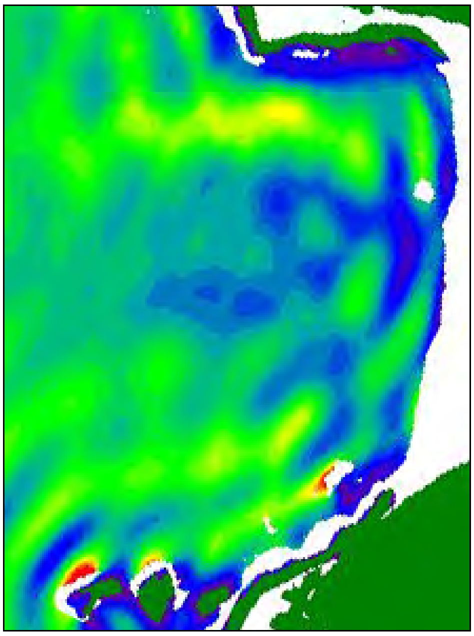

figure 118 – Bay Close-up, Simulation 2 **figure 119 – Bay Close-up, Simulation 5**

From Hm0 comparison with simulation 2, it is observed that no significant change in predicted wave height has occurred by applying Domain 2. The small deviations between the two plots are considered to be mostly due to small inconsistencies in the applied porosity layers that each had to be applied manually

Velocities offshore						
	U_{max}	U_{min}	U_{mean}	V_{max}	V_{min}	V_{mean}
Field Data	1.07 m/s	-0.87 m/s	-0.01 m/s	0.50 m/s	-0.62 m/s	0.00 m/s
Mike21 BW	0.86 m/s	-0.92 m/s	0.00 m/s	0.39 m/s	-0.39 m/s	0.00 m/s

table 31

Velocities Bay Entry						
	U_{max}	U_{min}	U_{mean}	V_{max}	V_{min}	V_{mean}
Field Data	1.05 m/s	-0.88 m/s	-0.02 m/s	0.33 m/s	-0.33 m/s	0.01 m/s
Mike21 BW	1.01 m/s	-0.90 m/s	0.00 m/s	0.59 m/s	-0.56 m/s	-0.01 m/s

table 32

Velocities Bay Middle						
	U_{max}	U_{min}	U_{mean}	V_{max}	V_{min}	V_{mean}
Field Data	1.35 m/s	-1.26 m/s	-0.03 m/s	0.46 m/s	-0.58 m/s	-0.06 m/s
Mike21 BW	1.17 m/s	-1.44 m/s	0.01 m/s	0.78 m/s	-1.02 m/s	-0.02 m/s

table 33

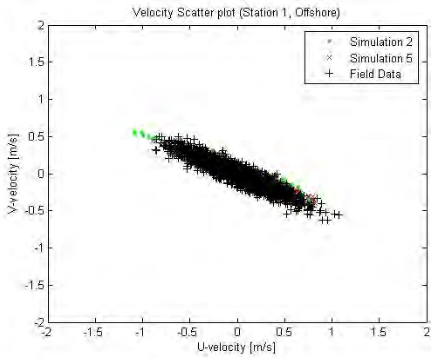

figure 120

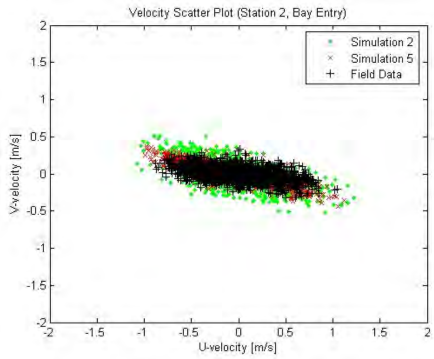

figure 121

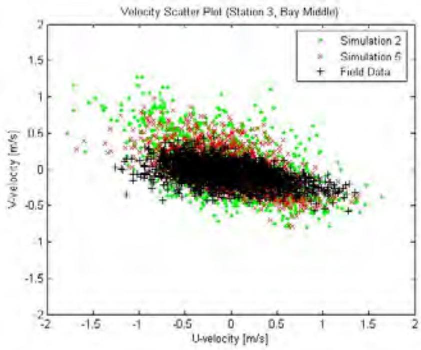

figure 122

As no significant difference in the wave field is noticed it is not a surprise that the velocity magnitudes and the directional agreement are unchanged for this simulation.

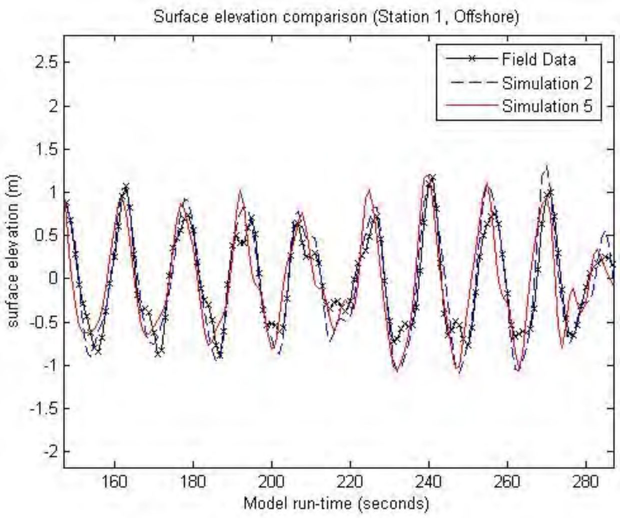

figure 123

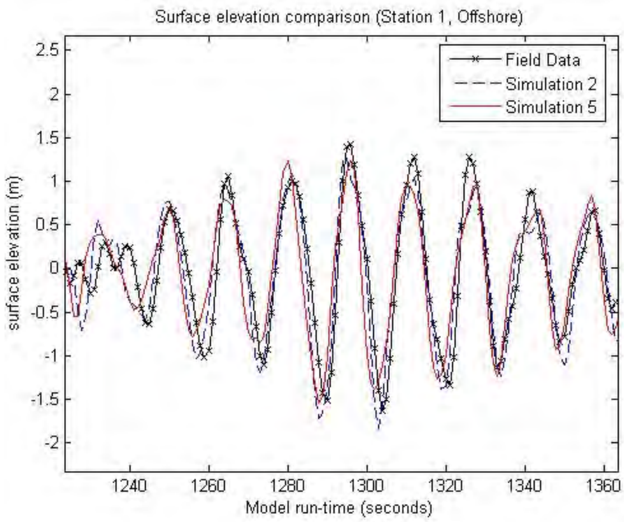

figure 124

In the time-series comparison for Station 1 it is observed how the wave amplitudes are in slightly better agreement using domain 2, but still it is noticed that features such as occasional “bumps” in the crest and trough are predicted more consistently in this simulation.

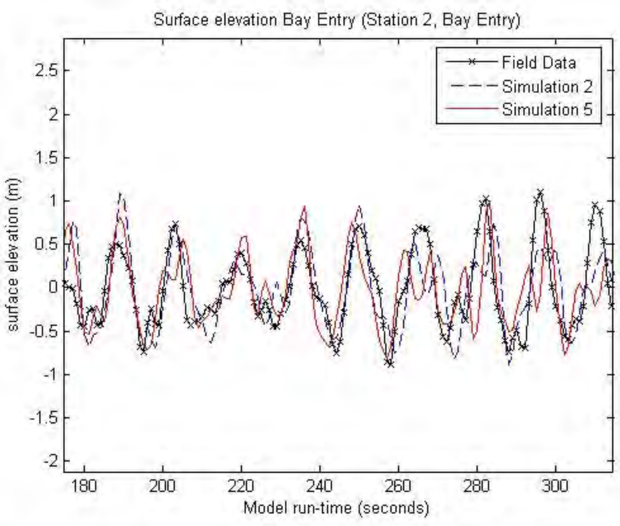

Figure 125

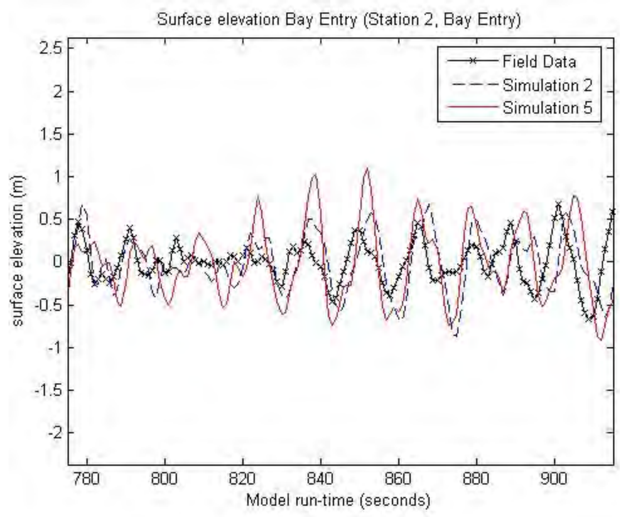

Figure 126

At Station 2 at the bay entry it is again observed how the time-series from Simulation 2 and 5 are almost identical. However at some locations, small variations are noticed mostly just as a variation in wave amplitude but these variations are mainly considered to be due to small inconsistencies between the two porosity maps.

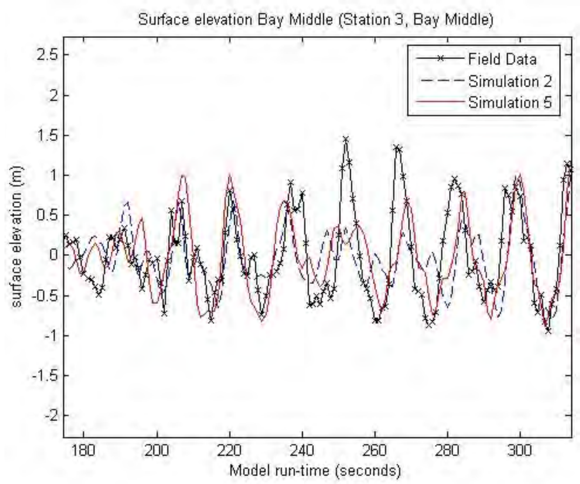

Figure 127

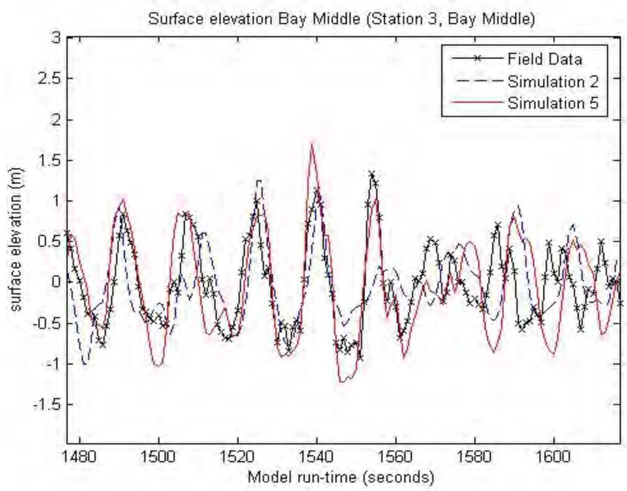

Figure 128

At Station 3 in the bay middle the same trend is observed as for Station 2.

Based on Simulation 5 it has been observed that even though a better wave height estimation is obtained using Domain 2, it does not in any significant way change the models prediction of the wave height distribution inside the bay, nor does it improve the overall correlation with field data (in Station 2 and 3). It is acknowledged that running the model on domain 2 has the potential of assuring more reliable results because the area of interest (the bay) is further away from the boundaries and also because of the fact that no artificial damping of the Boussinesq cross-terms will be experienced since the dominant wave propagation occur perpendicular to the domain. However on the other hand a 30-minute simulation using Domain 2 takes 35 hours to complete compared to "only" 11 hours using domain 1.

And as the two model predictions provides virtually the same predictions it has been decided that Domain 1 is a sufficiently reliable platform for the model simulations in this study.

4.3.6 Altering the wave direction

Simulation info: simulation 6	
Wave-input: *Time-series 2* Incident wave direction: 330° Bottom friction: C=32 Bathymetry: Domain 1 Porosity map: porosity map 1	

As mentioned previously the dominant wave direction at the offshore boundary is determined from the velocity measurements gathered in Station 1 by the ADCP. The instrument generates its directional output using its imbedded compass. However, it was informed by laboratory staff that this compass could only be expected an accuracy margin within +/- 2-3 degrees. As a result a simulation with an incident wave direction of 330° in order to assess the models response sensitivity to this change.

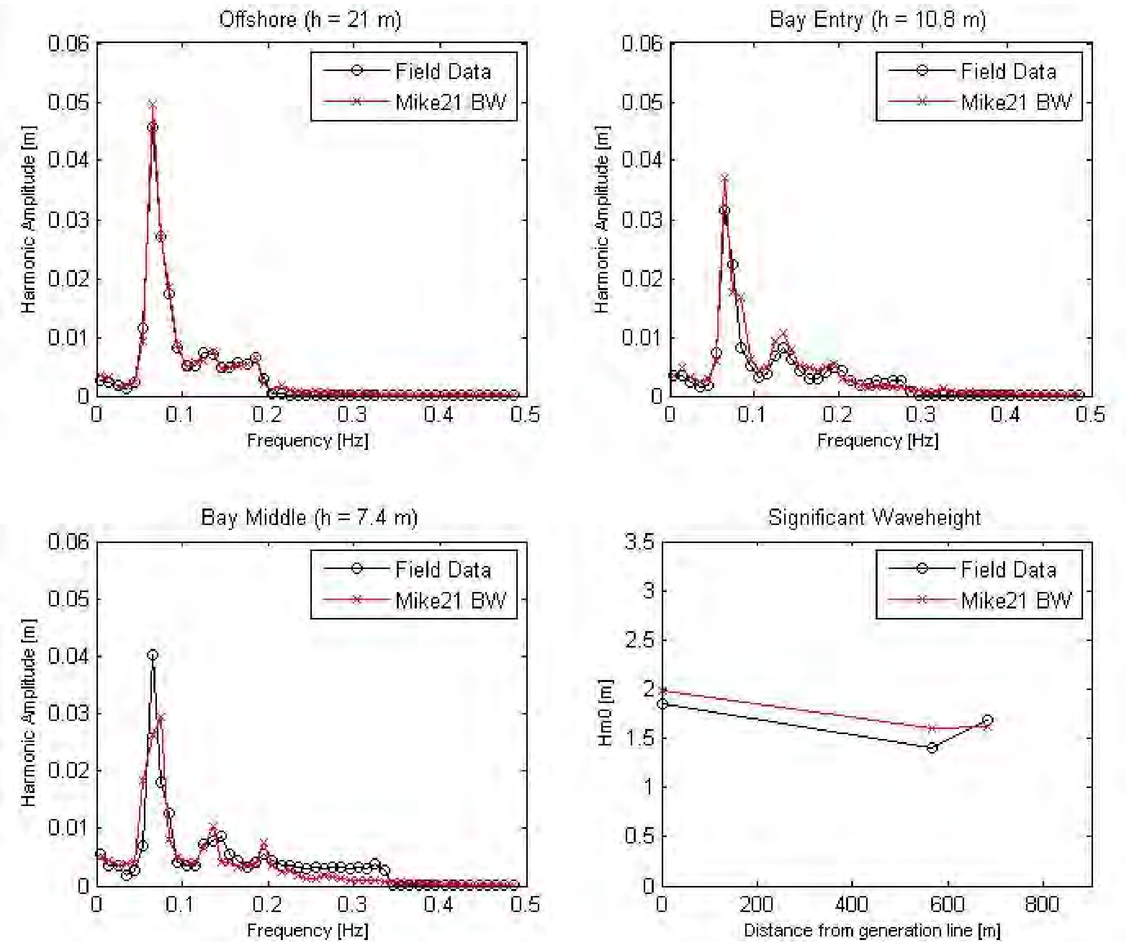

figure 129

Hm0			
H_{m0}	Field Data	Mike21 BW	Diff. [%]
Offshore	1.85 m	1.99 m	8%
Bay Entry	1.40 m	1.60 m	14%
Bay Middle	1.68 m	1.62 m	4%

table 34

Mean Wave height			
H_m	Field Data	Mike21 BW	Diff. [%]
Offshore	1.15 m	1.27 m	10%
Bay Entry	0.89 m	1.00 m	12%
Bay Middle	1.00 m	1.07 m	7%

table 35

Sig. Wave height			
H_{sig}	Field Data	Mike21 BW	Diff. [%]
Offshore	1.80 m	1.94 m	8%
Bay Entry	1.37 m	1.59 m	16%
Bay Middle	1.61 m	1.68 m	4%

table 36

The most noticeable observation from the wave tables and spectral plots is that the change in incident wave angle significantly increased the accuracy of the models wave prediction in Station 2, while the agreement in Station 1 and 3 remains almost unchanged.

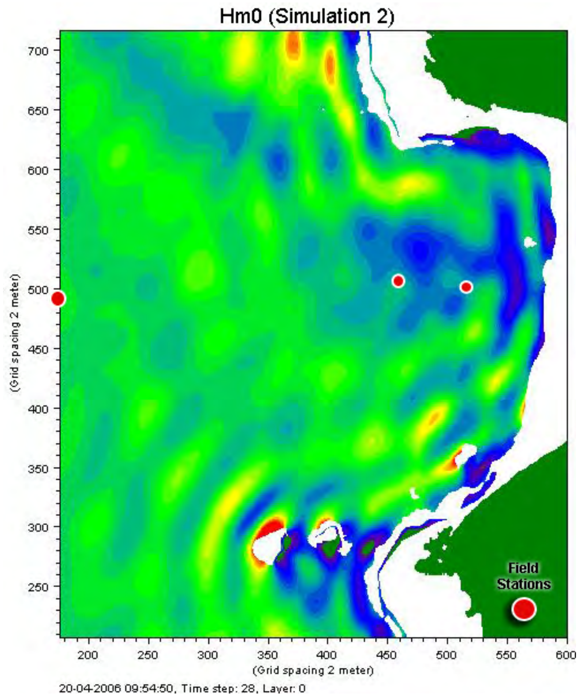

figure 130

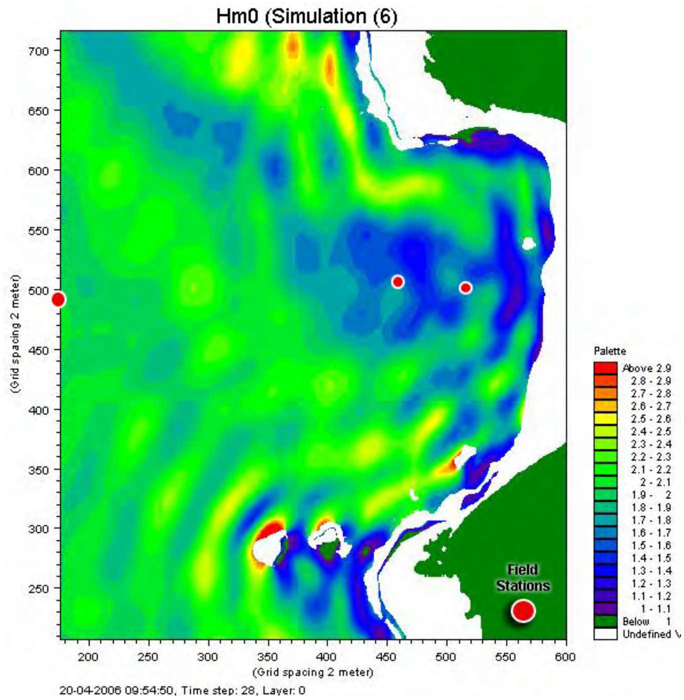

figure 131

The explanation for this is found by comparing the Hm0 plot with the one from Simulation 2. As recalled the only difference between these two simulations is an incident wave angle of 3°. As experienced in all previous simulations, Station 2 seems to be located on the ridge of a sheltered area (a “shadow zone”) that on average does not experience wave heights as large the rest of the respective cross-section in the bay.

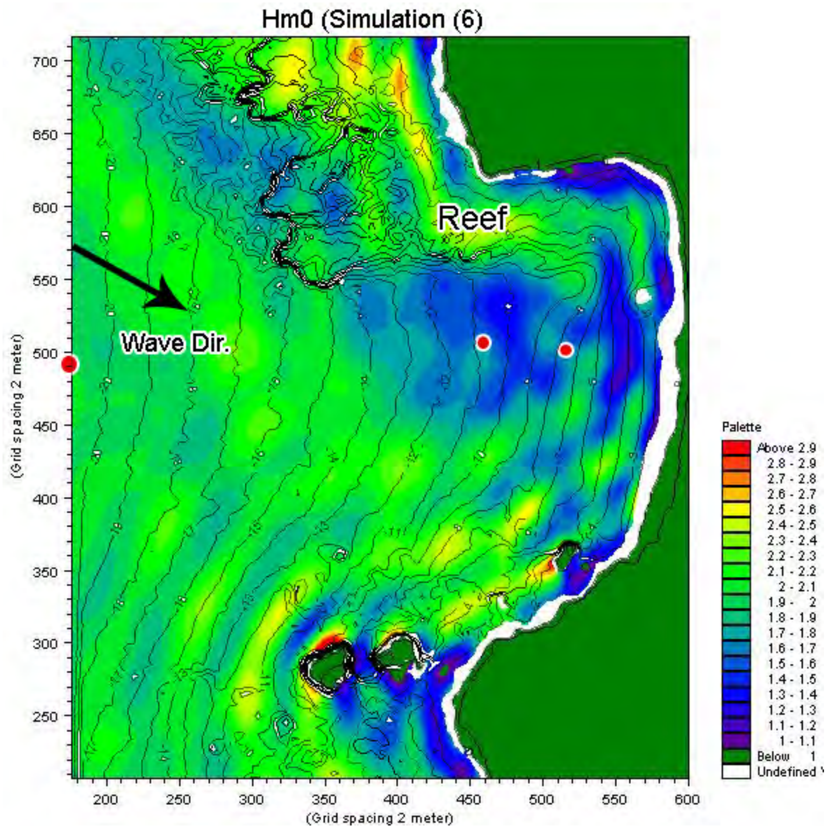

figure 132

As noticed in figure 132 the incident waves will experience significant refraction immediate offshore of the north end of the bay due to the presence of the reef, where the waves will wrap around, shoal and break leaving the immediate area of Station 2 much more sheltered. The south entrance of the bay lies fair unprotected at this wave direction and the waves arriving here will not have undergone much refraction since their generation at the offshore boundary. The result is a small sheltered zone at the bay entrance just leeward of the reef where the wave heights in general are smaller. And as Station 2 apparently is located in the rim of this zone, even a small change in incident wave direction (3°) can have a tremendous effect on the predicted wave heights in this point. During times of small to medium sized swell action (such as “time-series 2” Thursday morning) the reef also known as “Pinball's” provides a popular spot for surfing. During these occasions the zone just leeward of the reef does provide a “safe” passage for surfers when paddling out into the surf spot located at the bay entry, as the waves in this zone are usually smaller and are not breaking. So the models prediction of this sheltered zone does seem realistic estimated from visual observations.

Waimea bay south end – Thursday AM, April 20. 2006

Waimea bay north end – Thursday AM, April 20. 2006

However due to the severely limited amount of instruments inside the bay (2!) it is not possible in this study scientifically to document and verify the existence of this “sheltered” zone as predicted by the model.

Velocities offshore						
	U_{max}	U_{min}	U_{mean}	V_{max}	V_{min}	V_{mean}
Field Data	1.07 m/s	-0.87 m/s	-0.01 m/s	0.50 m/s	-0.62 m/s	0.00 m/s
Mike21 BW	0.88 m/s	-1.06 m/s	-0.02 m/s	0.60 m/s	-0.45 m/s	0.00 m/s

table 37

Velocities Bay Entry						
	U_{max}	U_{min}	U_{mean}	V_{max}	V_{min}	V_{mean}
Field Data	1.05 m/s	-0.88 m/s	-0.02 m/s	0.33 m/s	-0.33 m/s	0.01 m/s
Mike21 BW	0.98 m/s	-0.93 m/s	-0.01 m/s	0.47 m/s	-0.42 m/s	0.00 m/s

table 38

Velocities Bay Middle						
	U_{max}	U_{min}	U_{mean}	V_{max}	V_{min}	V_{mean}
Field Data	1.35 m/s	-1.26 m/s	-0.03 m/s	0.46 m/s	-0.58 m/s	-0.06 m/s
Mike21 BW	1.52 m/s	-1.54 m/s	0.01 m/s	1.1 m/s	-0.85 m/s	-0.01 m/s

table 39

From table 37 it is observed how the change in velocity amplitudes are very small as would be expected for the small change in wave direction. The magnitude of U has decreased slightly and the magnitude of V has increased correspondingly simply due to the small change in the projection of the incoming wave velocity vector to the domain coordinate system.

At station 2 in the bay middle the velocity magnitude of both U and V has decreased, which is due to the simple fact that the wave action in this area (recall figure 131) is less than in Simulation2 and flowingly also the wave induced velocities.

Again the same trend is observed in Station 3 assumable due to a slight decrease in wave height at this location.

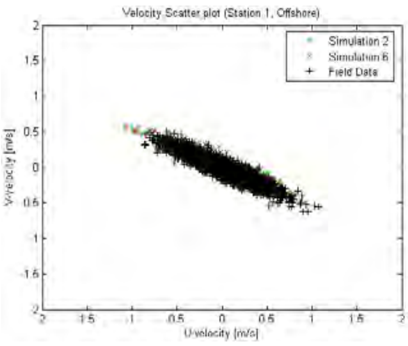

figure 133

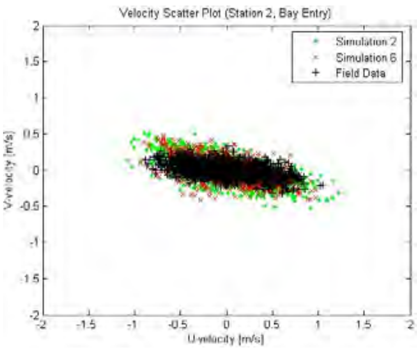

figure 134

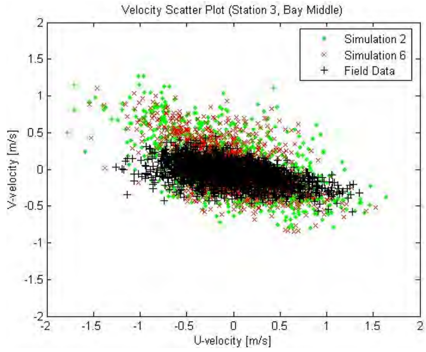

figure 135

As expected the direction scatter plots does not show any notable change in the directional velocity distribution due to the small change in incident wave direction. In comparison it is remarkable how an only 3-degree change in incident wave direction reduces deviation of model wave height predictions at Station 2 with 9-10% without causing any notable change in prediction accuracy for the two other Stations.

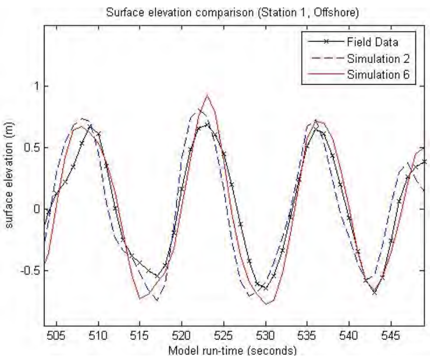

figure 136

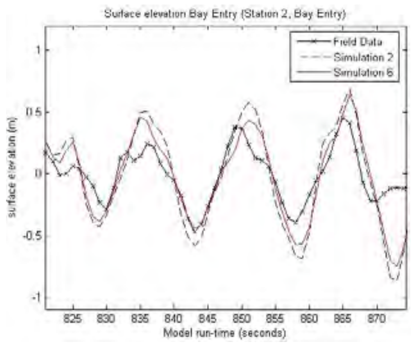

figure 137

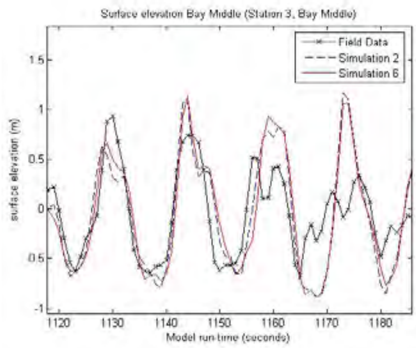

figure 138

As given by the average wave height properties the change in incident wave direction result in minor changes in wave height in Station 1 and 3 and a larger change in Station 2. When examining the time-series for the respective stations it is observed that while the adjusted incident wave direction improves model results in terms of wave magnitude, it does not change the nature of the waves occurring in the model domain. That is, the way incident and reflected waves are interaction (producing the net signal) at the 3 stations remains rather unchanged.

As illustrated in the comparison between figure 130 and figure 131 the general wave conditions does not change significantly by just changing the incident wave direction a few degrees. But the experiences made in Simulation 6 confirms that 2 instruments inside the bay is not much to sufficiently document the wave transformation processes occurring in a bay where both non-symmetrical refraction and 2 dimensional wave reflection consists key governing processes.

4.3.7 Wednesday time-series (excl. porosity layer)

Simulation info: simulation 7	
Wave-input: *Time-series 1* (Wednesday) Incident wave direction: 325° Bottom friction: C=32 Bathymetry: Domain 1 Porosity map: none	

Upon assessing the models ability do simulate the energetic wave conditions occurring in the bay Thursday morning it was decided to assess the model predictions for the much less wave conditions occurring Wednesday afternoon. The model setup for this simulation is identical to Simulation 1 which the exception of the change in wave input condition at the offshore boundary. Also the still water level has been raised 30 cm to account for the change in tidal elevation at this point in time.

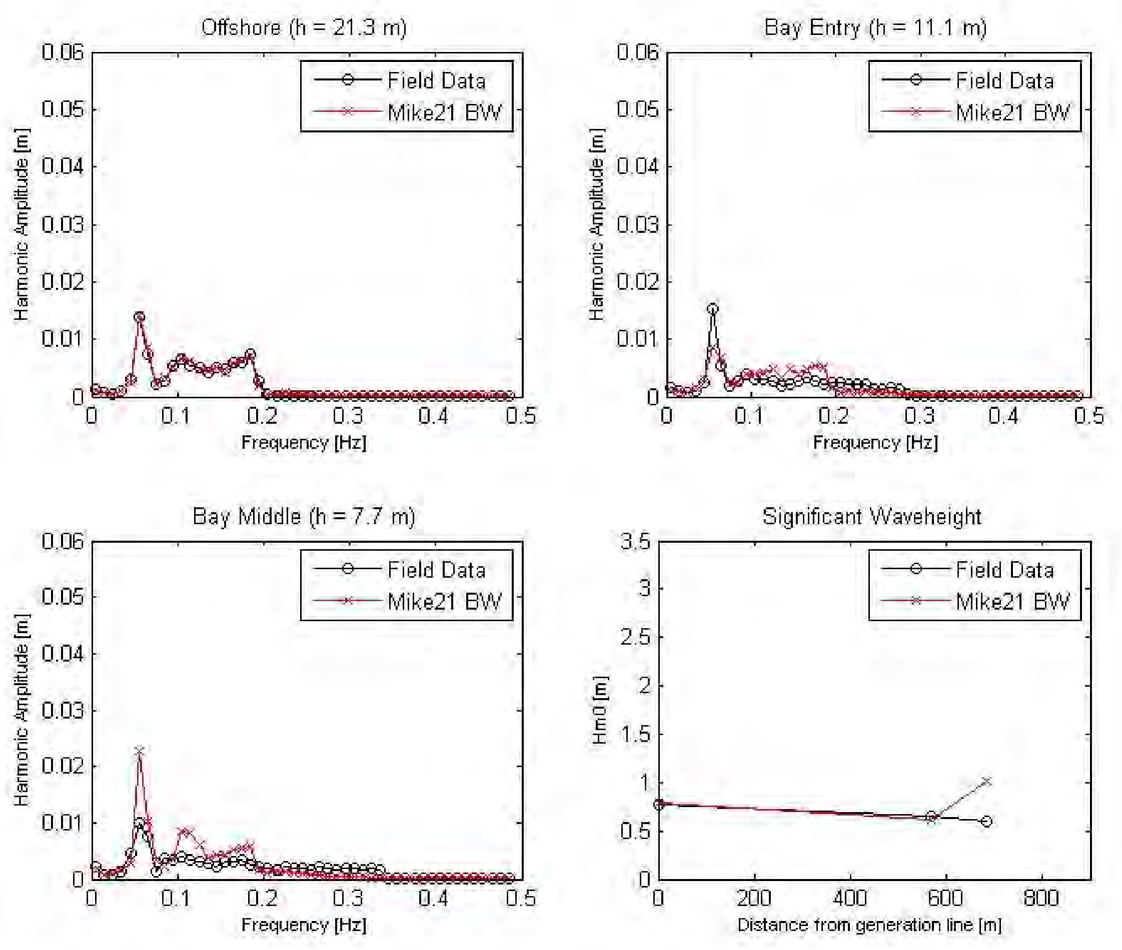

Figure 139

Hm0			
H_{m0}	Field Data	Mike21 BW	Diff. [%]
Offshore	0.77 m	0.80 m	4%
Bay Entry	0.64 m	0.61 m	5%
Bay Middle	0.60 m	1.02 m	70%

table 40

Mean Wave height			
H_m	Field Data	Mike21 BW	Diff. [%]
Offshore	0.48 m	0.50 m	4%
Bay Entry	0.36 m	0.39 m	8%
Bay Middle	0.35 m	0.65 m	84%

table 41

Sig. Wave height			
H_{sig}	Field Data	Mike21 BW	Diff. [%]
Offshore	0.73 m	0.73 m	0%
Bay Entry	0.59 m	0.59 m	0%
Bay Middle	0.55 m	1.01 m	84%

table 42

From the spectral plots and the wave height tables it is observed how there exists a virtually perfect agreement between field data and model predictions for this location. It is recalled how previous model simulations for the Thursday event (time-series 2) were often overestimating the wave height offshore. The explanation for the improved prediction capability for this simulation could be that the less energetic wave conditions in this simulation do not give rise to any significant contribution from wave reflection to the signal at Station 1. But the fact that the input for this simulation is more linear, and so does not cause the wave height to oscillate to the same degree due to its interaction with its forced free higher order harmonics (recall figure 140), could also have contributed to the improved model accuracy at this location. At the bay entry it is noticed that the model underestimates the spectral peak, while it slightly overestimates the higher order harmonics. It is noticed that the predicted spectral peak is only about half the magnitude of the field data value. However in spite of the notable disagreement in spectral amplitudes, there exists a very good agreement in terms of H_{m0}, H_m and H_{sig}. In the bay middle the spectral peak this time is overestimated by almost a factor 2. At the same time the higher order harmonics are significantly overestimated just as with the equivalent model setup in Simulation 1.

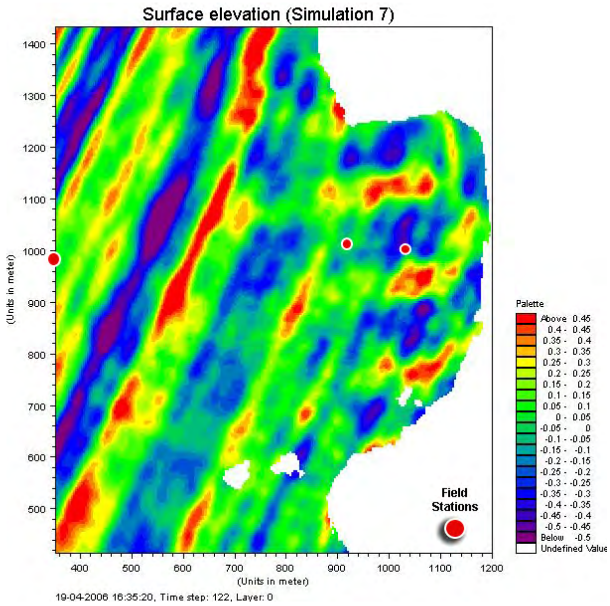

figure 141

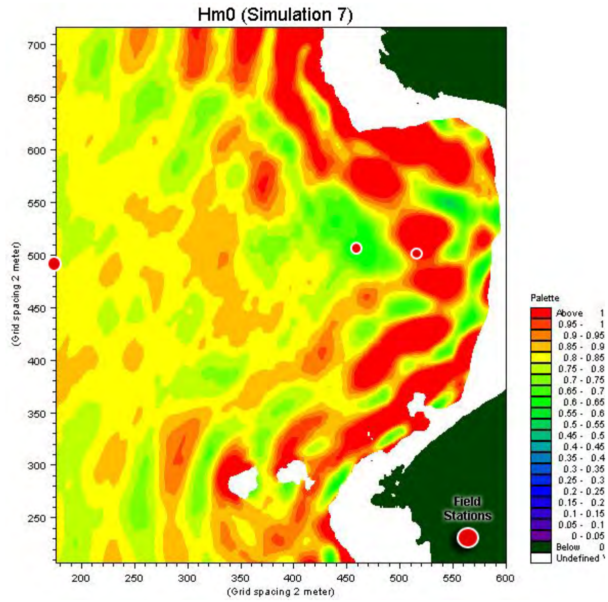

figure 142

From figure 141 it is observed how also for this Wednesday time-series there is a tremendous amount of cross-sectional wave propagation taking place in the model just as experienced in Simulation 1. Also from figure 142 it is observed how strong standing wave patterns are observed in front of basically every single land boundary. It was expected that even more reflection would occur inside the bay (both in the model and in the field) for time series 1 due to the longer wave peak period and the smaller wave amplitude. However as wave reflection becomes of even greater importance to the wave dynamical processes in the bay so does the models requirement to handle the reflection correctly.

Velocities offshore						
	U_{max}	U_{min}	U_{mean}	V_{max}	V_{min}	V_{mean}
Field Data	0.53 m/s	-0.47 m/s	0.01 m/s	0.31 m/s	-0.29 m/s	-0.01 m/s
Mike21 BW	0.38 m/s	-0.42 m/s	0 m/s	0.28 m/s	-0.24 m/s	0.01 m/s

Table 43

Velocities Bay Entry						
	U_{max}	U_{min}	U_{mean}	V_{max}	V_{min}	V_{mean}
Field Data	0.59 m/s	-0.48 m/s	0.01 m/s	0.15 m/s	-0.17 m/s	-0.01 m/s
Mike21 BW	0.47 m/s	-0.4 m/s	0.00 m/s	0.31 m/s	-0.27 m/s	0.00 m/s

Table 44

Velocities Bay Middle						
	U_{max}	U_{min}	U_{mean}	V_{max}	V_{min}	V_{mean}
Field Data	1.01 m/s	-0.85 m/s	0.00 m/s	0.26 m/s	-0.25 m/s	-0.01 m/s
Mike21 BW	0.61 m/s	-0.55 m/s	0.00 m/s	1.05 m/s	-0.77 m/s	-0.01 m/s

Table 45

Again it is noticed that the mean velocities are so small and insignificant that comparing them would not be sensible.

It is observed that the amplitudes of the offshore velocities are in general good agreement with field data. So are the U-amplitudes in the bay entry. The U-amplitudes in the bay middle are slightly underestimated by the model. However the cross-sectional velocities in the bay entry and the bay middle are significantly overestimated just as experienced in Simulation 1.

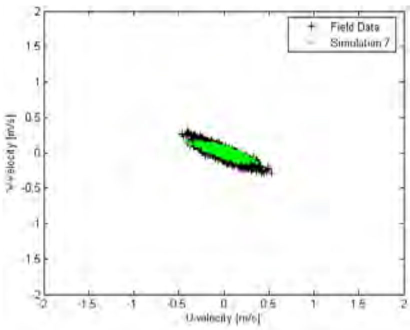

figure 143

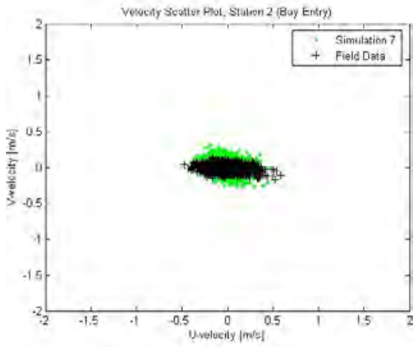

figure 144

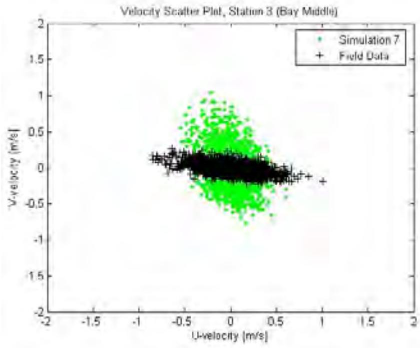

figure 145

From the velocity scatter plots it is seem how while there exists a good directional agreement at offshore at Station 1, it is observed how the model overestimates the cross-sectional velocities due to cross-sectional wave reflection. In the bay middle the significance of this phenomenon is all but extreme. Again it can be concluded that the model overestimation of wave reflection from the cliffs in the southern end of the bay also is of significant importance to wave conditions Wednesday afternoon.

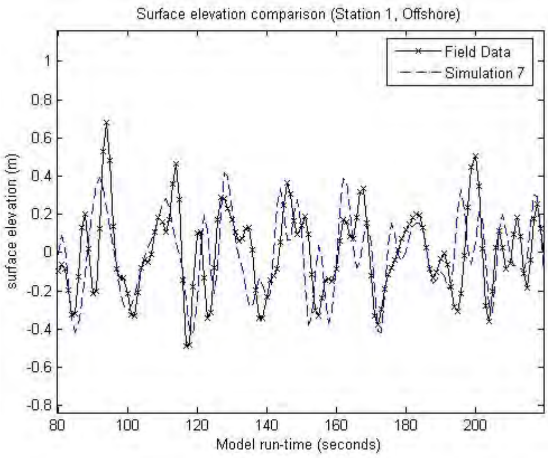

figure 146

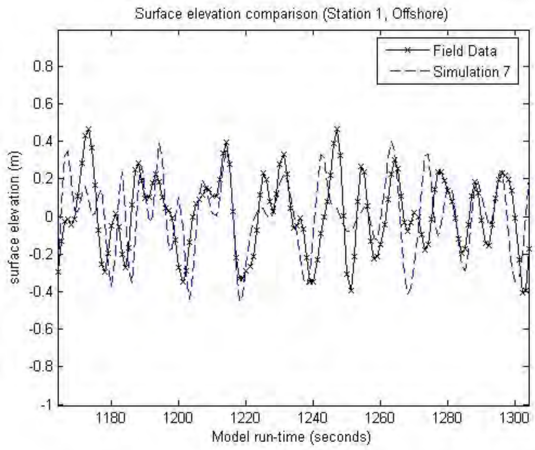

figure 147

When comparing the time-series at Station 1 it is observed that the previous assumption that no notable wave reflection is contributing to the wave signal at this location. However though this seems to distort the signal the wave height characteristics are still sufficiently maintained.

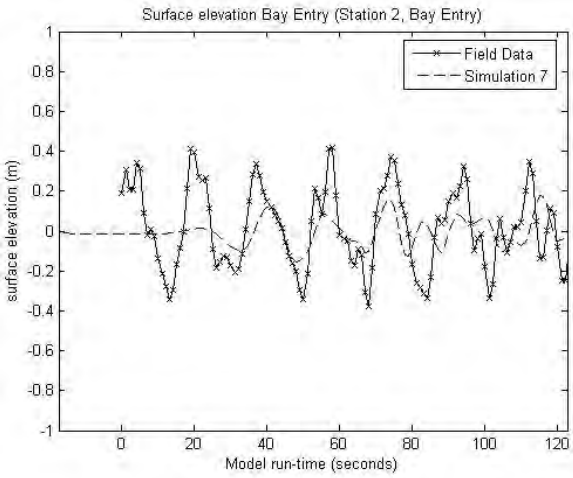

figure 148

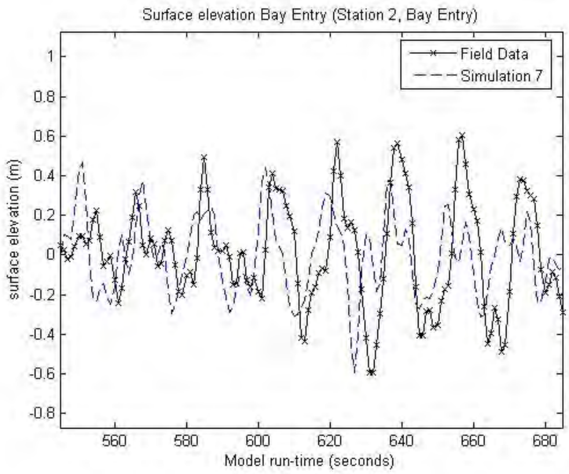

figure 149

When comparing the times-series in the bay middle it is observed how the simulated surface elevation in the beginning only is approximately half of what is given by the measured field data. However further into the time series the surface elevations are more in the same order of magnitude, though it is observed how the simulated time-series is strongly affected by the extensive reflection occurring in the model domain. This transition suggests that significant reflection occurs in the domain and that Station 2 in this system is located near an anti-node causing amplification in wave height. This could explain why the model underestimates the surface elevation for the first few waves, as the reflected waves have not yet reached the station.

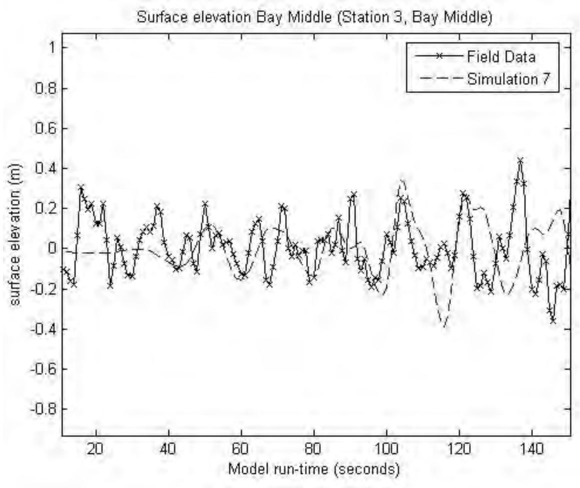

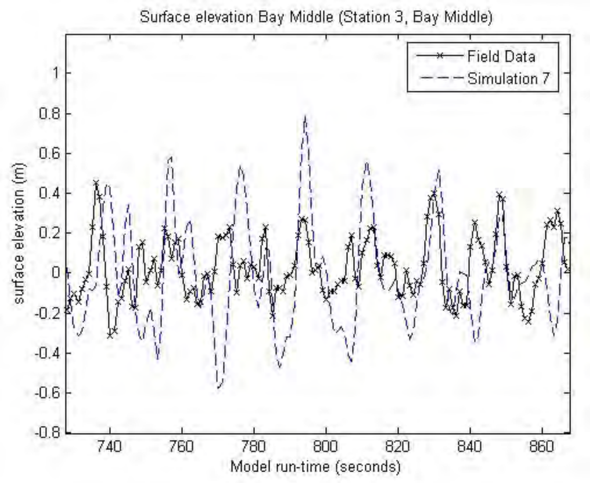

Figure 150

Figure 151

From the time-series comparison in the bay middle it is observed how the model predictions in the beginning are in good agreement with field data but soon after starts to overestimate the wave height at some locations due to an exaggerated predicted wave reflection especially from the southern end of the Bay.

4.3.8 Wednesday time-series (incl. porosity layer)

Simulation info: simulation 8	
Wave-input: *Time-series 1* (Wednesday) Incident wave direction: 325° Bottom friction: C=25 Bathymetry: Domain 1 Porosity map: 1	

From the experiences with cross-sectional wave reflection when modeling Thursday's wave-event, it was not a surprise that the same phenomenon would occur for when modeling the wave event from Wednesday. In order to account for this, the same porosity map as introduced in Simulation 2 is applied to this simulation in an attempt to improve model results.

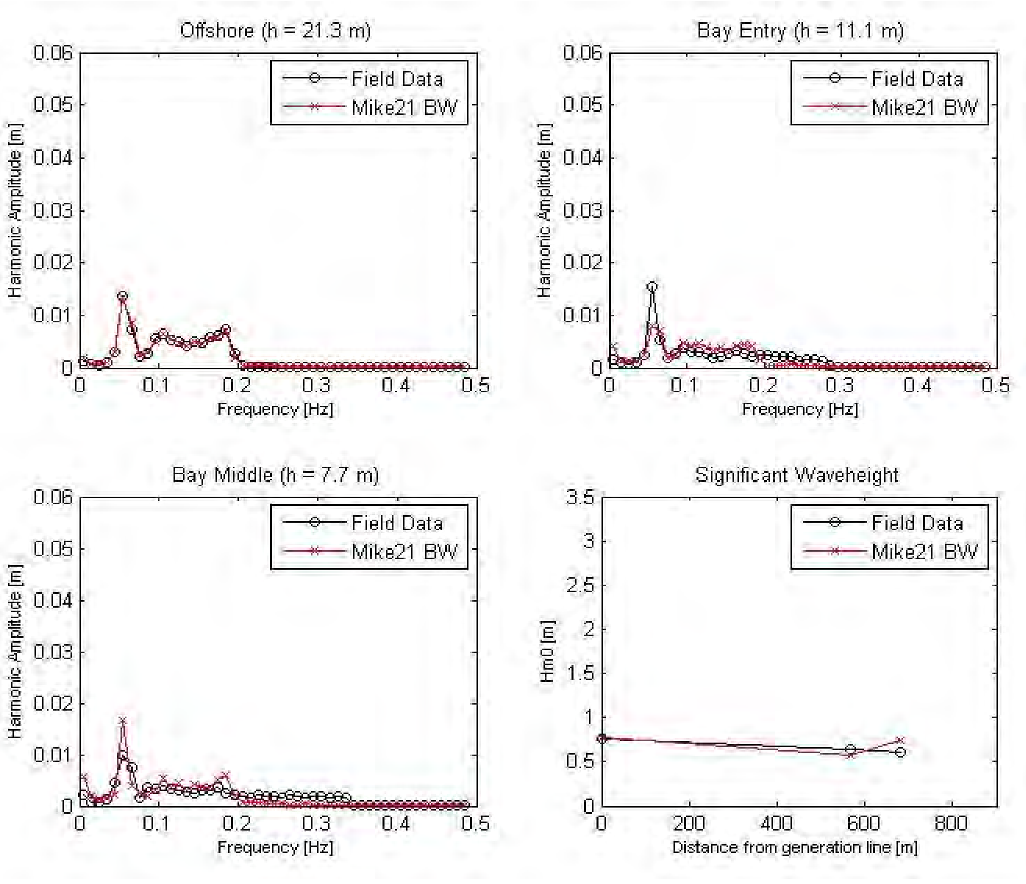

figure 152

Hm0			
H_{m0}	Field Data	Mike21 BW	Diff. [%]
Offshore	0.77 m	0.78 m	1%
Bay Entry	0.64 m	0.57 m	11%
Bay Middle	0.60 m	0.74 m	23%

table 46

Mean Wave height			
H_m	Field Data	Mike21 BW	Diff. [%]
Offshore	0.48 m	0.48 m	0%
Bay Entry	0.36 m	0.35 m	3%
Bay Middle	0.35 m	0.44 m	35%

table 47

Sig. Wave height			
H_{sig}	Field Data	Mike21 BW	Diff. [%]
Offshore	0.73 m	0.71	3%
Bay Entry	0.59 m	0.54	8%
Bay Middle	0.55 m	0.69	24%

table 48

From the spectral plots and the wave tables it is observed that a significant improvement to the model performance is obtained by implementing a porosity map along the cliffs and rocky outcrops. However from the spectral plots it is still observed that the spectral peak at Station 2 is underestimated while it is overestimated at Station 3.

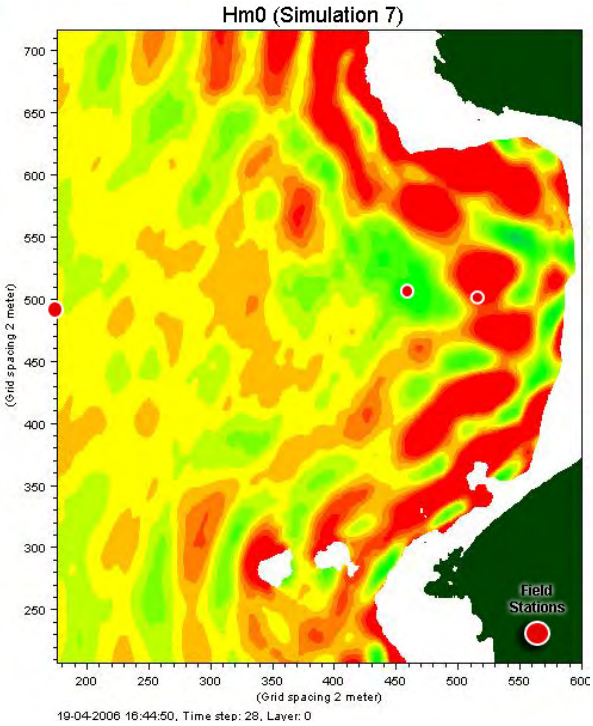

figure 153

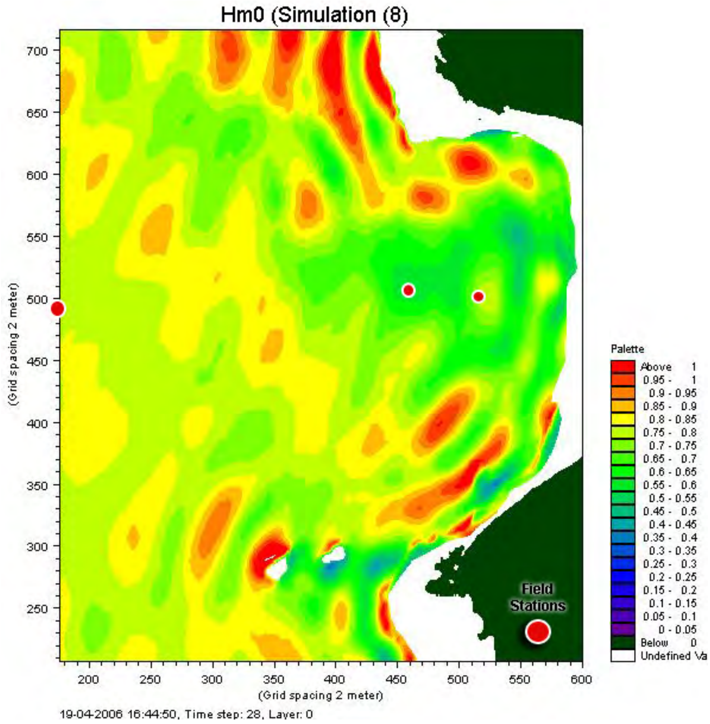

figure 154

Intuitively one would expect the wave heights at Station 3 to be larger compared to Station 2 due to shoaling. But previous simulations from Thursdays event has confirmed that the wave mechanical processes in the bay is not that simple and there most likely are quasi-standing wave processes occurring in the bay due to extensive wave reflection. Not only cross-sectional reflection from the cliffs and rocky outcrops but also from the steep upper beach slope at the bottom of the bay. In figure 154 it is observed how standing wave patterns from the especially the southern end of the bay has been damped significantly compared to Simulation 7. However the damped reflection from the south end has made another less energetic standing wave pattern become more visible. It is noticed how waves seem to be reflected from the beach profile itself creating a standing wave pattern with nodes and antinodes. From the H_{m0} 2D plot it looks like the model predicts an anti-node at the location of Station 3 and a weak resemblance of some something that could look like a nodal point at the location of Station 2. If this is correct it could explain why the spectral peak is amplified at Station 3 and damped at Station 2. That is of course assuming that the same standing wave pattern is not represented identically in the field data.

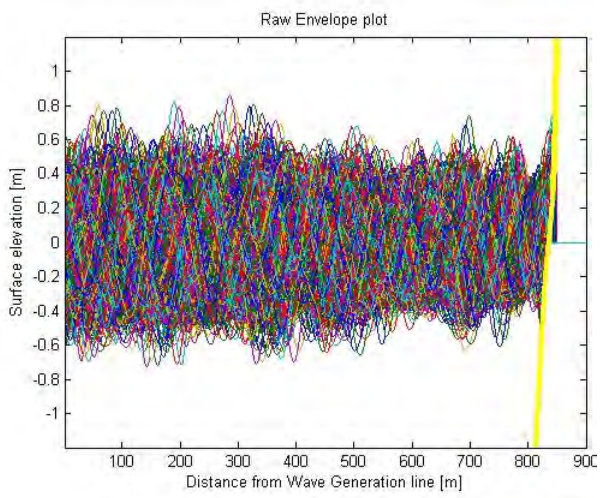

figure 155

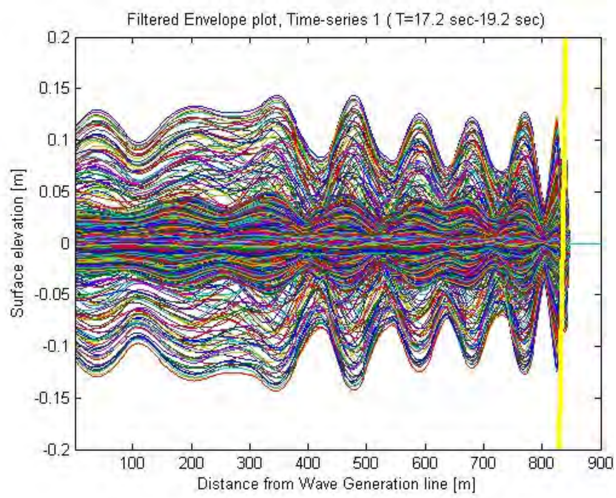

figure 156

In figure 155 an envelope plot has been constructed from the surface elevation time-series along the centerline of Waimea bay reaching from the wave generation line to the shoreline. Using Fourier analysis a narrow band (Δf = 0.006 Hz) of frequencies centered on the peak frequency corresponding to T_p=18.2 sec has be filtered out and presented in figure 156. Here it is indeed clear that a standing wave is occurring from the beach shoreline. From video recordings simultaneously recorded during Wednesdays time-series (time-series 1) it was easily visible how strong reflection and near shore wave oscillation was occurring in the bay as also predicted by the model. However given the fact that the wave conditions are highly reflective can make it very difficult to assess a models capability to simulate a real-case system only having 2 reference points (field stations). Even just a small phase-shift between the reflected waves in the field and those predicted by the model can have a significant importance to the location of nodes and anti-nodes. Also the correct prediction of the magnitude of the reflected wave brings in an additional aspect in the model assessment.

Velocities offshore						
	U_{max}	U_{min}	U_{mean}	V_{max}	V_{min}	V_{mean}
Field Data	0.53 m/s	-0.47 m/s	0.01 m/s	0.31 m/s	-0.29 m/s	-0.01 m/s
Mike21 BW	0.38 m/s	-0.38 m/s	0 m/s	0.27 m/s	-0.16 m/s	0.01 m/s

Table 49

Velocities Bay Entry						
	U_{max}	U_{min}	U_{mean}	V_{max}	V_{min}	V_{mean}
Field Data	0.59 m/s	-0.48 m/s	0.01 m/s	0.15 m/s	-0.17 m/s	-0.01 m/s
Mike21 BW	0.45 m/s	-0.44 m/s	0.00 m/s	0.16 m/s	-0.14 m/s	0.00 m/s

Table 50

Velocities Bay Middle						
	U_{max}	U_{min}	U_{mean}	V_{max}	V_{min}	V_{mean}
Field Data	1.01 m/s	-0.85 m/s	0.00 m/s	0.26 m/s	-0.25 m/s	-0.01 m/s
Mike21 BW	0.59 m/s	-0.49 m/s	0.00 m/s	0.32 m/s	-0.36 m/s	0.00 m/s

Table 51

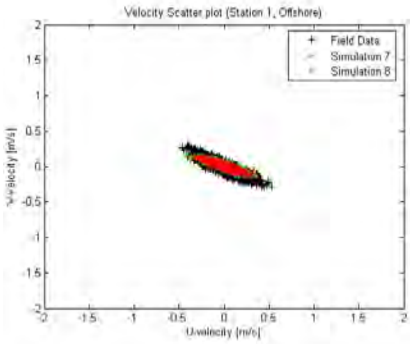

figure 157

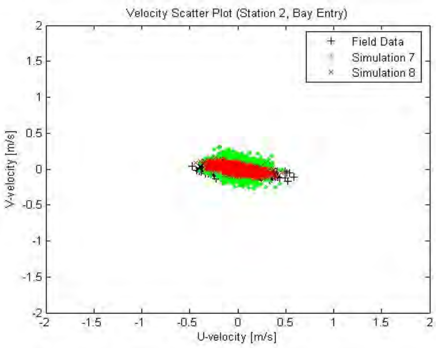

figure 158

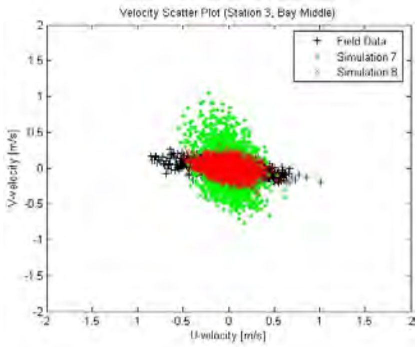

figure 159

In the velocity tables it is observed how the introduction of the porosity map helped correct the cross-sectional velocity amplitudes at station 2 and 3. The same can be observed from the velocity scatter plots, where a tremendous improvement has been obtained -Especially at Station 3 in the bay middle.

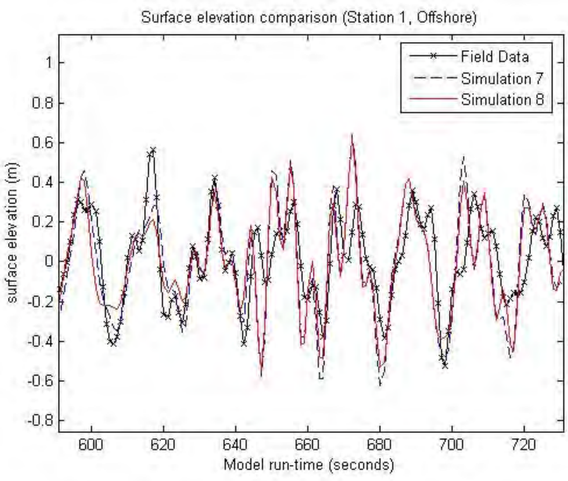

figure 160

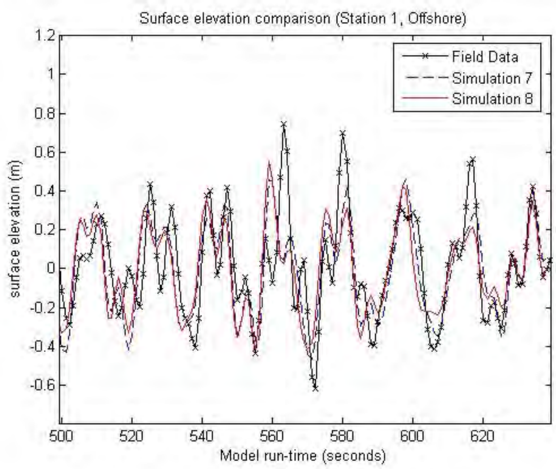

figure 161

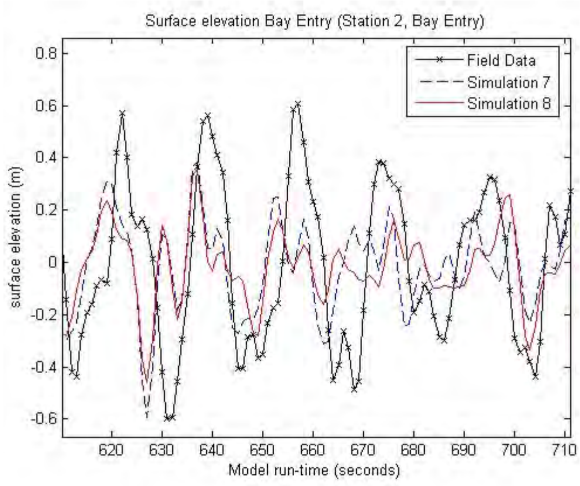

figure 162

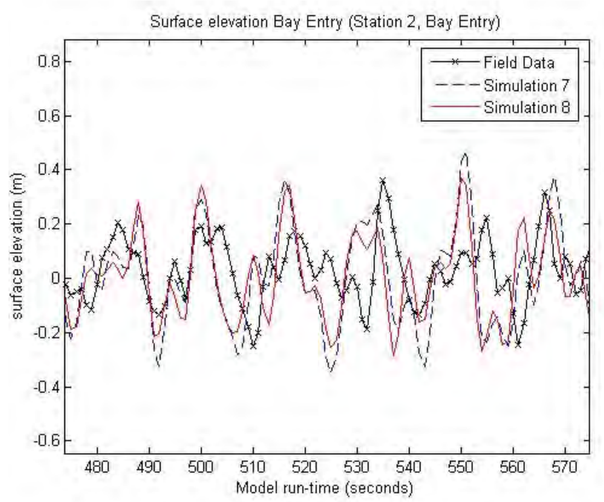

figure 163

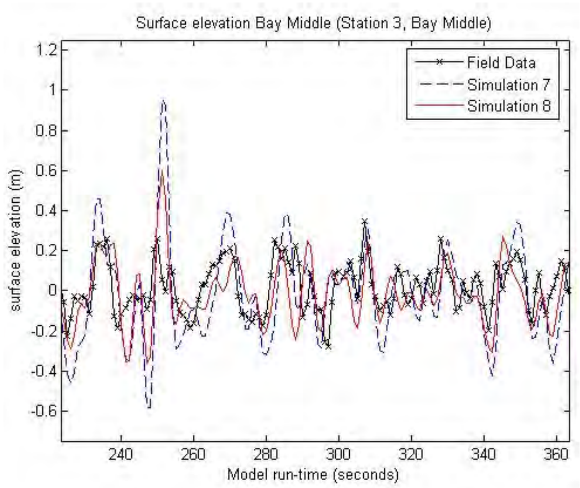

figure 164

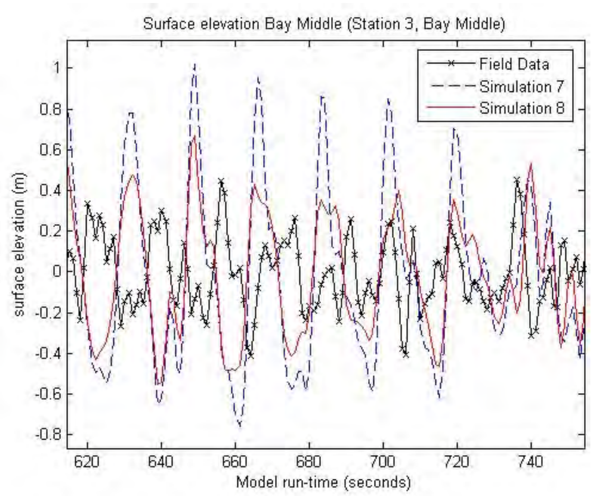

figure 165

From the time-series comparison for the 3 field stations it is observed how the implementation of the porosity layer succeeds in damping the previously overestimated cross sectional reflection affecting mostly the signal in Station 3. However even though this damping significantly improves model results there still seems to be effects in the signal at Station 2 and 3 that does not seem to be resolved well in the model.

5 Results Summary

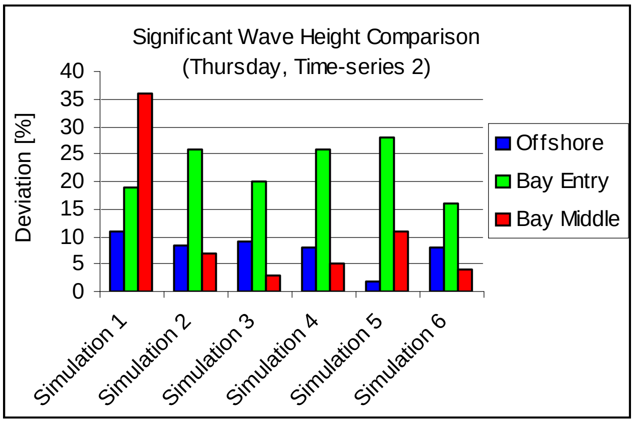

figure 166

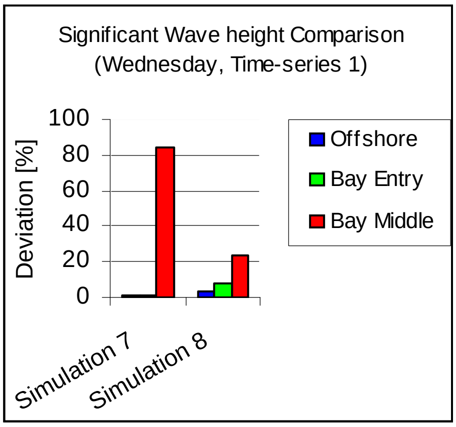

figure 167

In the previous chapter it was observed that the H_{m0}, H_{sig} and H_m all shared the same trend for each simulation, so in this result summary only a comparison of H_{sig} for the 8 simulations are listed in the figures above. As mentioned previously, the initial model setup (using time-series 2 as input) significantly overestimated the wave reflection from the steep cliffs in the domain. By applying a porosity map at these locations, it was found that a great improvement of model results offshore and especially at the bay middle was obtained. When applying a new wave input time-series (time-series 1) to the model domain the same problem with overestimated wave reflection was experienced and a similar improvement was made with respect to the bay middle when applying the model domain to the different wave conditions as given by time-series 1.

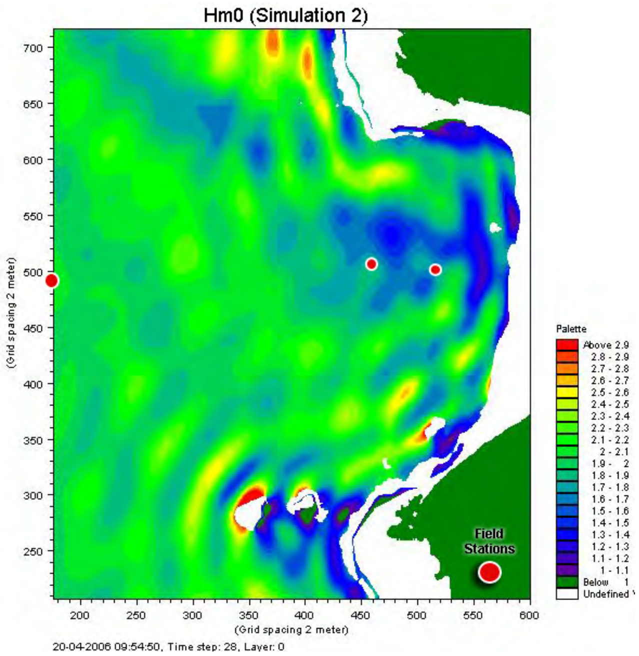

figure 168

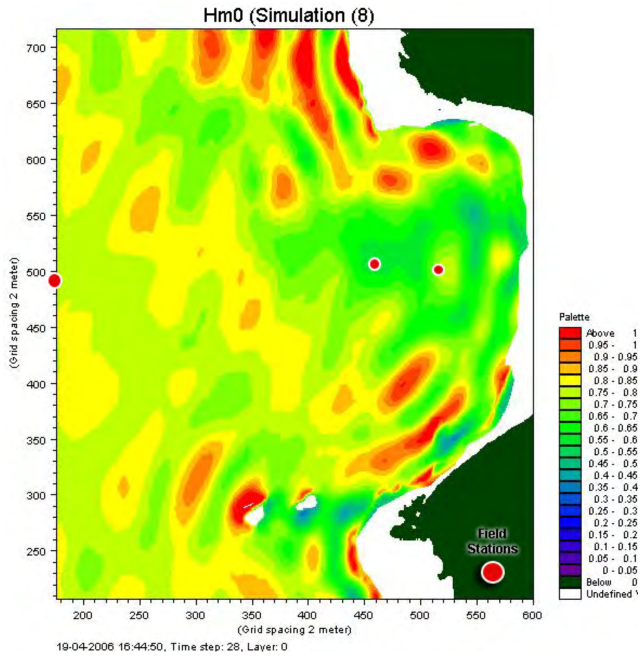

figure 169

It was found that Station 2 was located in the proximity of a small zone with smaller wave height created by the sheltering effect of the adjacent reef located off the northern end of the bay. In Simulation 7 and 8 (using time-series 1) Station 2 is located in the middle of this sheltered zone and the wave height prediction is in good agreement with field data. But in Simulation 1 to 6 (using time-series 2) Station 2 is predicted to be located on the rim of the sheltered zone and the wave height prediction is notably overestimated. This suggests that the predicted size and/or location might be slightly inaccurate. A number of simulation attempts were carried out in order to improve this prediction, but it was only by altering the wave direction (+3° N) that Station 2 became more included into the now expanded sheltered zone (due to the increased sheltering effect by the reef) and the wave height prediction was improved significantly.

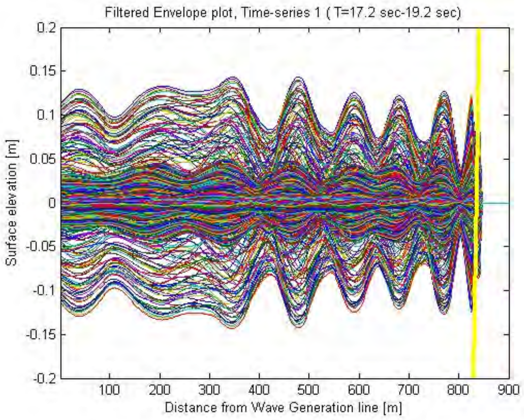

figure 170 – Simulation 7

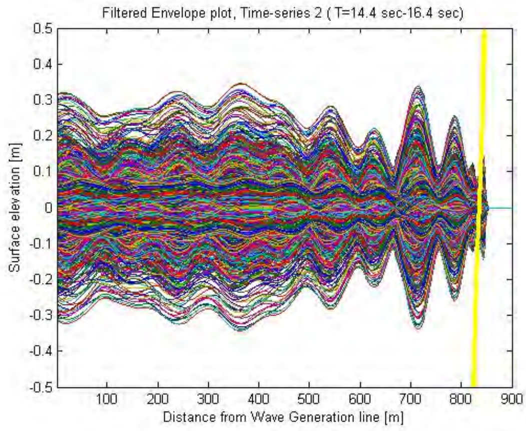

figure 171 – Simulation 2

Another phenomenon noticed in all simulations was the appearance of a standing wave pattern occurring along the centerline of the bay. The bay entry is located approximately 560 m from the wave generation line and from figure 170 and figure 171 it is observed that the standing wave pattern extend beyond this point an so effecting both the predictions at Station 2 and Station 3. While the wave height prediction at Station 3 seems in good agreement when using time-series 2 and applying a porosity map (Simulation 2-6), the wave height is notably overestimated when using time-series 1 even when applying a porosity map (Simulation 8). The best suggestion would be that the model in this case either overestimates the wave reflection occurring from the beach slope, which will be further discussed in the next chapter.

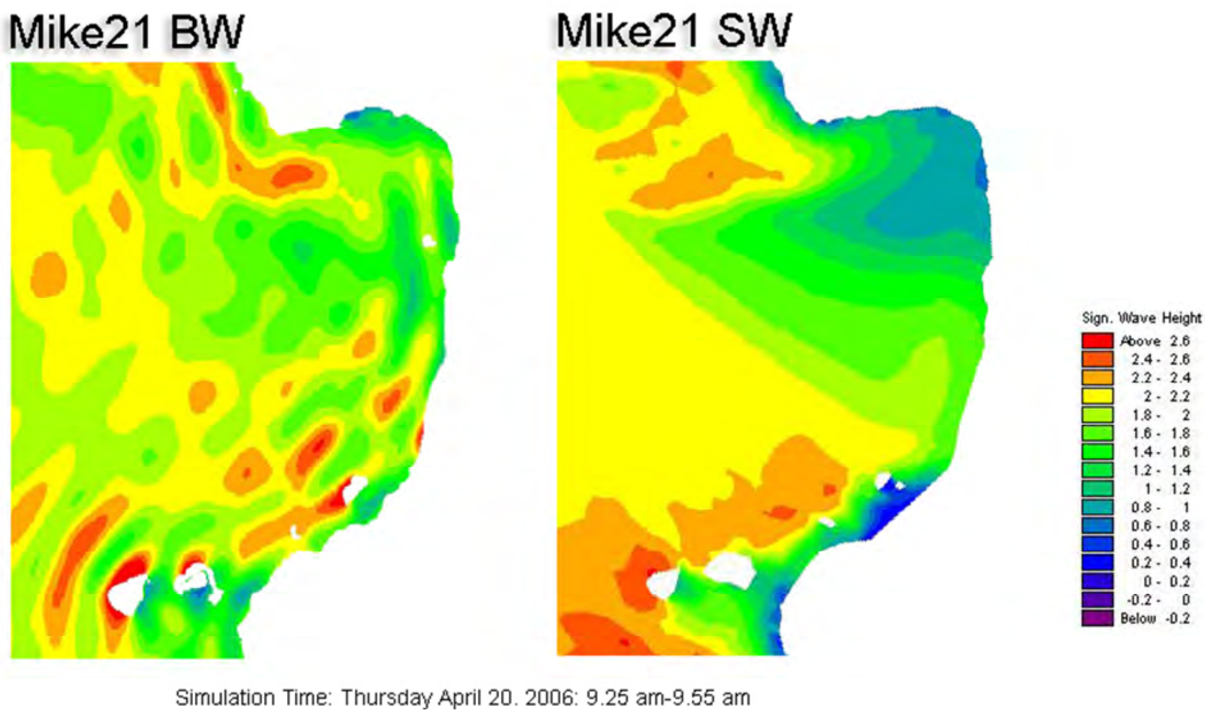

figure 172

In figure 172 a brief wave height comparison has been carried out between the Mike21 Boussinesq wave model (Mike21BW) and the Mike21 Spectral Wave model (Mike21SW). The Boundary condition used for the spectral wave model has been obtained from the wave buoy located 5.6 km offshore Waimea bay. While the application of a spectral model is not part of this study, it was found interesting to draw the comparison, as the spectral model is not capable of handling wave reflection (as opposed to BW). It is very interesting to see while both models capture the sheltering effect from the reef (at the north end), the spectral wave model does not capture the local effects due to significant wave reflection occurring from the landward boundary, which is of mayor importance to the predicted wave height distribution inside the bay.

U_{mean} Comparison, Time series 2			
	Offshore	Bay Entry	Bay Middle
Field Data	***-0,01 m/s***	***-0,02 m/s***	***-0,03 m/s***
Simulation 1	-0,05 m/s	-0,01 m/s	0,01 m/s
Simulation 2	-0,03 m/s	-0,01 m/s	-0,01 m/s
Simulation 3	-0,03 m/s	0.00 m/s	0,02 m/s
Simulation 4	-0,03 m/s	-0,01 m/s	0,01 m/s
Simulation 5	0.00 m/s	0.00 m/s	0,01 m/s
Simulation 6	-0,02 m/s	-0,01 m/s	0,01 m/s

table 52

V_{mean} Comparison, Time series 2			
	Offshore	Bay Entry	Bay Middle
Field Data	**0.00 m/s**	***0,01* m/s**	***-0,06* m/s**
Simulation 1	0,01 m/s	0,01 m/s	-0,01 m/s
Simulation 2	0,01 m/s	0.00 m/s	-0,01 m/s
Simulation 3	0,01 m/s	0.00 m/s	0.00 m/s
Simulation 4	0,01 m/s	0.00 m/s	0.00 m/s
Simulation 5	0.00 m/s	-0,01 m/s	-0,02 m/s
Simulation 6	0.00 m/s	0.00 m/s	-0,01 m/s

table 53

U_{mean} Comparison, Time series 1			
	Offshore	Bay Entry	Bay Middle
Field Data	***0,01 m/s***	***0,01 m/s***	***0,00 m/s***
Simulation 7	0,00 m/s	0,00 m/s	0,00 m/s
Simulation 8	0,00 m/s	0,00 m/s	0,00 m/s

table 54

V_{mean} Comparison, Time series 1			
	Offshore	Bay Entry	Bay Middle
Field Data	***-0,01 m/s***	***-0,01 m/s***	***-0,01 m/s***
Simulation 7	0,01 m/s	0,00 m/s	-0,01 m/s
Simulation 8	0,01 m/s	0,00 m/s	0,00 m/s

table 55

As discussed in the previous chapter and listed in the tables above, the wave driven currents at Station 1, 2 and 3 are very small and insignificant when modeling time-series 2 and basically non-existent when modeling time-series 1. The explanation for the very small wave driven currents in the bay was simply due to the lack of widespread wave breaking, which almost only occurred at the reef at the northern end and very close to the shoreline. Wave breaking only occurred with the arrival of a wave-set followed by several minutes of little or no wave breaking. As a result the wave driven currents in most part of the bay (even the most energetic part of the wave event) must be considered to be fairly small. At the 3 stations it was found that the model predictions at these locations were mostly in the correct order of magnitude but due to the extremely small values very sensitive to even small changes in the model setup.

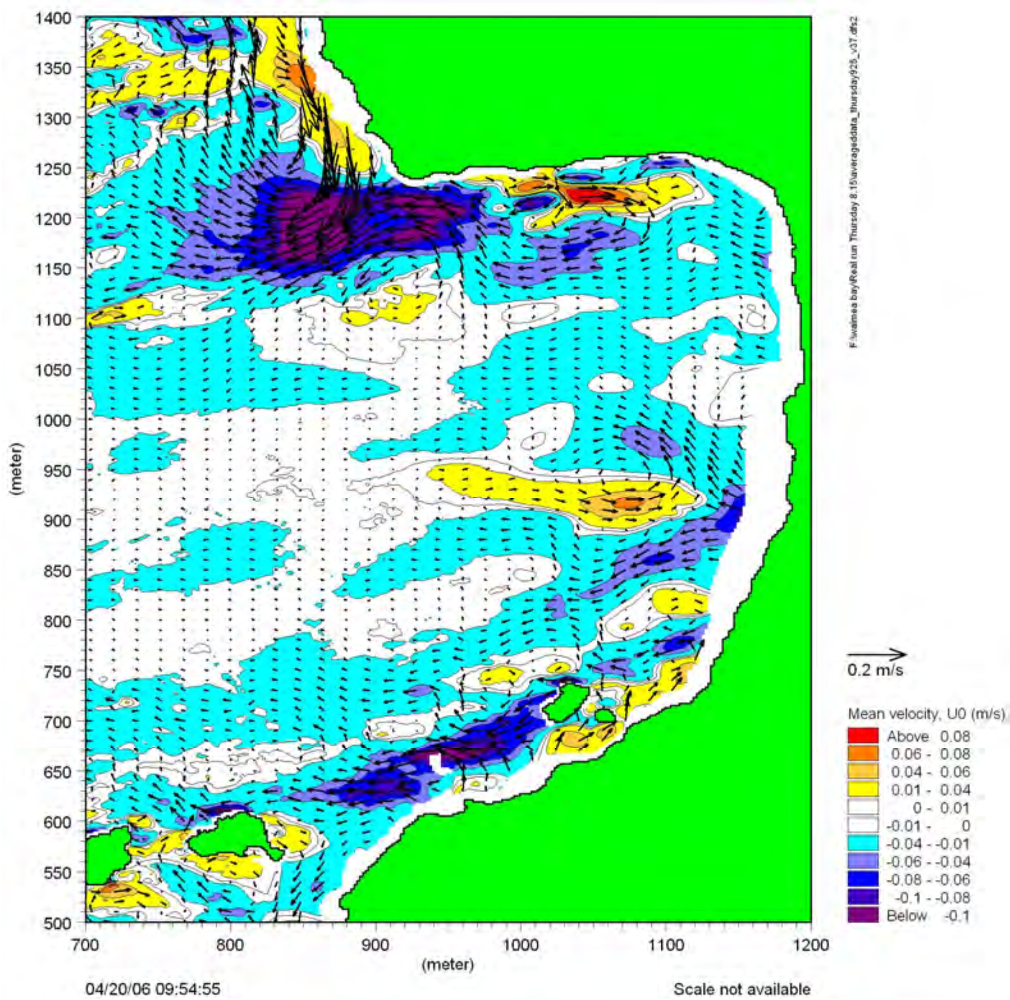

figure 173 - Wave-Driven Current Plot (Simulation 2)

From figure 173 it is observed how the most dominant current patterns occurs along northern tip of the bay due to pronounced wave breaking in this area. Also a less significant pattern appears along the south side of the bay and also a small rip current seems to be predicted at the southern end of the Waimea bay beach. However as both Station 2 and 3 are located outside any of these areas of interest it is not possible in any way to assess the performance of the model predictions of the wave driven currents.

6 Conclusion

At first it seemed like an easy task to apply a Boussinesq model to simulate the waves and wave driven currents in Waimea Bay. From the results obtained in the preliminary study it was evident that the MIKE21 BW model held an excellent capability of simulating both wave breaking, shoaling, refraction, diffraction and wave induced current circulation. So from a theoretical point of view, the usually larger deviations experienced during the Waimea Bay model simulations might initially seem less impressive.

But once realizing the complexity and sensitivity of the wave dynamical processes occurring within the domain combined with the potential sources of error associated with this study, it is in fact excessively impressive that the Boussinesq model actually succeed in providing a fair to good prediction of the wave and wave induced current conditions for all 3 stations.

The wave conditions inside the bay during simulation were far from monotonous and largely influenced by the combined effects from non-uniform wave refraction and excessive wave reflection from the steep cliffs and rocky outcrops and also from the beach itself.

When modeling time-series 2 it was found that wave height predictions could be greatly improved by just a small change in incident wave direction. In comparison it should be taken into consideration that the ADCP compass (from which the wave direction is obtained) is only accurate within 3-4°. Secondly, even though assuming the incident wave train to be unidirectional is a fair assumption for the given swell event, the velocity scatter plots does show some directional spreading (recall figure 44 and figure 45) within the magnitude of 2-5 degrees. Additionally it should be recalled that the position accuracy of the handheld GPS used to place the instruments inside the bay is only within 5-10m (sometimes even worse). For reference it should be considered that if the true position of Station 2 in fact was located 47 m North East of its assumed location, this alone would result in a perfect agreement in wave height prediction for Simulation 2 (recall figure 168). With this information in mind it would seem harsh to criticize the model for overestimating the wave height by 25% in at this location.

Another problem during simulations was the models tendency to exaggerate the magnitude of the wave reflection occurring from the steep cliffs and rocky outcrops in the domain, which is most likely due to the limitations in the method in which the model handles breaking waves. As mentioned previously, the breaker module is designed to handling spilling breakers, which assumes a gradual dissipation of wave energy. The preliminary study has shown that the breaker model also can be successfully used in modeling plunging breakers, which occurs on the reef along the north entrance of the bay. But the breaker model is not designed to handle the rapid energy dissipation occurring at the powerful collapsing breakers occurring along the steep cliffs and rocky outcrops in the domain.

(Thursday AM, April 20. 2006)
The very narrow surf zone in front of the cliffs and rocky outcrops in the south entrance of the bay.

(Thursday AM, April 20. 2006)
The Waimea Bay shore-break.

In addition the cliffs and outcrops contain rugged features that contribute to even more extensive dissipation but are not resolved in the model bathymetry due to the current 2x2 m grid resolution.

It was found that introducing a porosity map could damp the exaggerated wave reflection from the cliffs and rocky outcrops, but as concluded from the time series study the porosity map only monotonously damps the wave reflection occurring from these locations. Hence it does not capture the local wave reflection effects occurring at these areas, where full reflection might occur at some locations and perhaps not at all at other locations due to the wave response to local variations and small-scale features in the bathymetry.

Also along the shoreline of Waimea bay significant wave reflection has also been shown to occur in the model for both time-series 1 and 2. From simultaneously recorded video footage (Appendix VIII) it is easily observed that pronounced wave reflection at this location also occur in the field but from only 2 field stations inside the bay it is not possible to fully clarify if a standing wave pattern is apparent in the bay and if this in any way compares well with model predictions. It can only be concluded that it was possible to obtain a wave height prediction deviation at Station 3 of less than 5% when simulating time-series 2, while the prediction accuracy using the same model setup was more than 20% when simulating time-series 1. This could be explained by comparing the dominant breaker type occurring near the shoreline for the two simulations using the previously mentioned surf similarity parameter. First it should be advised that while the average beach slope for the entire domain is 0.04 it is 0.06 close to the shoreline. If drawing the rough assumption that the mean wave height measured at Station 3 equals the wave breaker height H_b, and using the peak period T_p to calculate the deepwater wavelength L_0, the surf similarity parameter (close to the shoreline) will be 1.2 for time-series 2 suggesting a plunging breaker and 2.3 for time-series 1 suggesting a surging or collapsing breaker. Recorded video footage during the two time-series also at least qualitatively confirms this assumption. But it could explain why the wave reflection is overestimated in time-series 1 as the breaker module does not sufficiently well simulate the energy dissipation characteristics of the collapsing wave, while the wave energy dissipation characteristics of the plunging wave breakers occurring in time-series 2 are probably more adequately described by the current breaker module.

Just from a quick glance at any of the H_{m0}-plots produced in this study, it is obvious that 2 instruments inside the bay is nowhere near sufficient to properly describe the wave conditions inside Waimea Bay and provide a adequate base for comparison and assessment of the model predictions for this domain.

In spite of this, The Mike21 BW model was actually able to produce results that agreed fairly well with field measurements even in a direct time-series comparison. It is the author’s opinion that the most dominant source of model inaccuracy was due to the way partial wave-reflection was handled in the model. In some cases due to the insufficient wave dissipation when modeling collapsing breakers and also due to the necessity to introduce artificial damping in areas with highly steep and uneven bathymetry such as in front of the steep cliffs and rocky outcrops. Unfortunately it is hard (from only two field stations inside the bay) to quantify how much the models prediction of reflection actually deviates from what is actually occurring in the bay. As mentioned previously the deviation could easily be limited to small phase shifts between the incident and reflected wave train and local effects in some problematic areas of the domain.

Again the potential complications and sources of inaccuracies associated with extracting the field data and problems in correctly resolving the near shore bathymetry (important to wave reflection) could almost be a study by its own.

But even though hindsight might suggest that some parts of this Waimea Bay study could have been carried out differently (especially with respect to the insufficient field instrumentation), the agreement between field data and model results has been satisfying not to mention that the educational gains has been more than significant. This cover a wide range of topics such as how to carry out a full-scale field campaign in the coastal zone, post-processing and interpreting the raw field data to how to apply a state-of-the-art Boussinesq wave model to simulate the highly complex wave environment in Waimea Bay. So once fully realizing the complexity and challenging aspects of this case study, it is not hard to conclude that, based on the obtained project results as well as the associated general and case-specific educational gains, the project has been a tremendous success.

Simon Brandi Mortensen

7 References

DHI Software, 2004, "***Mike21 Boussinesq Wave Modules User Guide"***, DHI Water and Environment, Hørsholm, Denmark

Kubota, S, Mizuguchi, M and Takezawa, M, 1989***,"Reflection from swash zone on natural beaches"***, Coastal Eng., 23, 570-583.

Madsen, P A, 2003, ***"An introduction to higher order spectral analysis and stochastic evolution equations"***, Lecture notes, Technical University of Denmark.

Madsen, P A and Sørensen, O R, 1992, ***"A new form for the Boussinesq equations with improved linear dispersion characteristics. Part 2: A slowl- varying Bathymetry "***. Coastal Eng., 18, 183-204.

Madsen, P A, Sørensen, O R and Scäffer, H A, 1997a, ***"Surf zone dynamics simulated by a Boussinesq type model. Part I: Model description and cross-shore motion of regular waves"***. Coastal Eng., 32, 255-288.

Madsen, P A, Sørensen, O R and Scäffer, H A, 1997b, ***"Surf zone dynamics simulated by a Boussinesq type model. Part II: Surf beat and swash zone oscillations for wave groups and irregular waves"***. Coastal Eng., 32, 289-320.

Nielsen, P, 2003, ***Teaching notes on coastal and estuarine processes***, Department of Civil Engineering, University of Queensland

Smith, S W, 1999, ***The Scientist and Engineer's Guide to Digital Signal Processing***, 2nd Edition, California Technical Publishing, San Diego California.

Sørensen, O R, Scäffer, H A and Madsen, P A, 1998, ***"Surf zone dynamics simulated by a Boussinesq type model. Part III: Wave-induced horizontal near shore circulations"***. Coastal Eng., 33, 155-176.

Web sites:
Joint Airborne Lidar Bathymetry Technical Center of Expertise (JALBTCE):
http://shoals.sam.usace.army.mil

Nortek (manufacturer of Current Profilers)
http://www.nortek-as.com

Teledyne RD Instruments – Manufacturer of ADCP
http://www.rdinstruments.com

The Coastal Data Information Program (Historic Waimea Buoy Data)
http://cdip.ucsd.edu/?pub=nonpub&stn=206&stream=p1&nav=historic&sub=data

8 Appendices

Appendix I

Matlab code used to extract velocity time-series for a chosen time frame from the ADCP data.

Appendix II

Matlab code to extract a selected surface elevation time-series from the ADCP

Appendix III

Matlab code use to calculate wave height, spectral peak period and wave direction for the 48-hour field dataset.

Appendix IV

Matlab code used to extrat selected velocity and surface elevation time-series from the AquaDopps.

Appendix V

Mablab code used for conducting time-series analysis of model results and calculate H_{sig}, H_m, U_m, V_m, U_{max} /U_{min} and V_{max}/V_{min}.

Appendix VI

Matlab code used for spectral analysis of model results.

Appendix VII

Matlab code used to calculate wave height distribution and a filtered envelope plot along the centerline of Waimea bay.

Appendix VIII

3 CD-RWs containing:

- 3D Animation of Simulation 2.
- Time-stamped video clip recorded during time-series 1
- Time-stamped video clip recorded during time-series 2 #1
- Time-stamped video clip recorded during time-series 2 #2
- Time-stamped video clip of the swash zone recorded 30 minutes after time-series 2

Appendix I

```
clear all
close all

u_input=load('u_velocity.txt');
v_input=load('v_velocity.txt');
w_input=load('w_velocity.txt');

time_vector=load('ADCP_timevector.txt')';

u_data =u_input(:,2)';
v_data =v_input(:,2)';
w_data =w_input(:,2)';

Start_date=datestr([2006 04 19 08 30 59],0);
time_origo=datenum(2006,04,19,08,59,09);

time=time_vector;


%Velocity direction during selected timeseries
%...........................................%
% Selecting the surface elevation timeseries %
%...........................................%

% Select slice
start=find(time_vector<=datenum(2006,04,20,09,25,00),1,'last');
finish=find(time_vector<=datenum(2006,04,20,09,55,00),1,'last');
duration=30*60;


% U-DATA
%Inforcing a timestep dt of 1 sec for the selected slice using
%interpolation.
time_num=time_vector*24*3600;


new_time(1)=time_num(start);
u_slice(1)=u_data(start);

for ii=2:duration;
    new_time(ii)=new_time(ii-1)+1;
    Find_pre_time=find(time_num<new_time(ii),1,'last');
    Find_next_time=find(time_num>=new_time(ii),1,'first');
    Pre_time=time_num(Find_pre_time);
    Next_time=time_num(Find_next_time);
    Pre_u=u_data(Find_pre_time);
    Next_u=u_data(Find_next_time);

    u_slice(ii)=(Next_u-Pre_u)/(Next_time-Pre_time)*(1-(Pre_time-new_time(ii-1)))+Pre_u;
end
 new_time(duration+1)=new_time(duration)+1;
 u_slice(duration+1)=u_data(finish);

% Control correct interpolation scheme
figure
```

```
plot(time_vector(start:finish),u_data(start:finish),'-o')
hold on
plot(new_time/(24*3600),u_slice,'x-')



figure
plot(time,u_data)
title('East-bound depth averaged velocity U0');
xlabel('time from 8.31 AM, Wednesday morning [hours]');
ylabel('velocity [m/s]');
saveas(gcf,'u_velocity', 'jpeg')

figure
plot(time_vector(start:finish),u_data(start:finish))
title([char('East-bound depth averaged velocity U0','Starting time: ',num2str(datestr(time_vector(start),0)),'
End time: ',num2str(datestr(time_vector(finish),0)),'')]);
xlabel('time [minutes]');
ylabel('velocity [m/s]');
saveas(gcf,'u_velocity_slice', 'jpeg')
u_velocity_slice=u_slice';
save u_slice_wednesday1615.txt u_velocity_slice -ASCII
save u_slice_wednesday1615.m u_velocity_slice -mat

% V-DATA
%Inforcing a timestep dt of 1 sec for the selected slice using
%interpolation.

v_slice(1)=v_data(start);

for ii=2:duration;
   Find_pre_time=find(time_num<new_time(ii),1,'last');
   Find_next_time=find(time_num>=new_time(ii),1,'first');
   Pre_time=time_num(Find_pre_time);
   Next_time=time_num(Find_next_time);
   Pre_v=v_data(Find_pre_time);
   Next_v=v_data(Find_next_time);

   v_slice(ii)=(Next_v-Pre_v)/(Next_time-Pre_time)*(1-(Pre_time-new_time(ii-1)))+Pre_v;
end

 v_slice(duration+1)=v_data(finish);

% Control correct interpolation scheme
figure
plot(time_vector(start:finish),v_data(start:finish),'-o')
hold on
plot(new_time/(24*3600),v_slice,'x-')


figure
plot(time,v_data)
title('North-bound depth averaged velocity V0');
xlabel('time from 8.31 AM, Wednesday morning [hours]');
ylabel('velocity [m/s]');
saveas(gcf,'v_velocity', 'jpeg')

figure
```

```
plot(time_vector(start:finish),v_data(start:finish))
title([char('North-bound depth averaged velocity V0','Starting time: ',num2str(datestr(time_vector(start),0)),' End time: ',num2str(datestr(time_vector(finish),0)),'')]);
xlabel('time [minutes]');
ylabel('velocity [m/s]');
saveas(gcf,'v_velocity_slice', 'jpeg')
v_velocity_slice=v_slice';
save v_slice_wednesday1615.txt v_velocity_slice -ASCII
save v_slice_wednesday1615.m v_velocity_slice -mat

figure
plot(time,w_data)
title('Vertical depth averaged velocity W0');
xlabel('time from 8.31 AM, Wednesday morning [hours]');
ylabel('velocity [m/s]');
saveas(gcf,'w_velocity_wednesday1615', 'jpeg')

%
% fitfunction=fit(u_data(start:finish)',v_data(start:finish)','poly1')
% Mag_correction=10.4; % correction for magnetic north
% wave_dir=abs(atan(fitfunction.p1)/pi*180)+270+Mag_correction;

%Determining Wave Direction
u=u_velocity_slice;
v=v_velocity_slice;
Mag_correction=-(10.4)*pi/180; % correction for magnetic north

u2=u*cos(Mag_correction)-v*sin(Mag_correction);
v2=v*cos(Mag_correction)+u*sin(Mag_correction);
fitfunction=fit(u2,v2,'poly1')

wave_dir=abs(atan2(1,fitfunction.p1)/pi*180)+180

figure
plot(u2,v2,'.')
hold on
plot(u2,fitfunction.p1*u2,'r')
legend('Velocity Scatter Plot','Mean wave direction')
title(['Thursday 20/04-06 9.25-9.55, \theta_m= ',num2str(round(wave_dir)),'\circ']);
xlabel('U0 [m/s], east-bound velocity');
ylabel('V0 [m/s], north-bound velocity');
axis([-2 2 -2 2])

save u_rotated_thursday925.txt u2 -ASCII
save v_rotated_thursday925.txt v2 -ASCII
```

Appendix II

Matlab code to extract a selected surface elevation time-series from the ADCP

```
clear all
close all
tic
g=9.81;
rho=1000;
ratio=10^4/(rho*g);     %conversion from dbar to pressure in [m]
data=load('ADCP_pressure.txt');
time_vector=data(:,1);
pressure=ratio*data(:,2);
time_origo=time_vector(1);

%Input remarks
adcp_offset=0.30;
dt=1;

time=[0:1:length(pressure)-1]*dt;

%Filtering out the tidal oscilation
average_length=1000;

waterdepth_fraction(1)=mean(pressure(1:average_length));
waterdepth=ones(1,average_length)*waterdepth_fraction(1);

for i=1:fix((length(pressure))/average_length)-1
   waterdepth_fraction(i+1)=mean(pressure(i*average_length:(i+1)*average_length));
   waterdepth_vector=ones(1,average_length)*waterdepth_fraction(i);
   waterdepth=[waterdepth waterdepth_vector];
end

%What is left after the last batch is assigned same waterlevel
av_length=fix((length(pressure))/average_length)*average_length;
rest=length(pressure)-av_length; %last part not included in the averaging
rest_vector=ones(1,rest)*waterdepth_fraction(fix((length(pressure))/average_length));

waterdepth=[waterdepth rest_vector];

delta_p=pressure'-waterdepth;

bins=2^13

% Compute spectrum

fn=1/(dt*2);
Y1=fft(delta_p,bins);
p_spectrum=((real(Y1(1:end)).^2+imag(Y1(1:end)).^2).^0.5)/bins*2;
p_spectrum(1)=p_spectrum(1)/2;
f=[0:bins/2]/bins*2*fn;
Find_max_total=find(p_spectrum==max(p_spectrum),1);
Tpeak_total=(f(Find_max_total))^(-1);

%plot spectrum
figure
plot(f,p_spectrum(1:length(f)))
```

```
title([char('Wave Powerspectrum (Entire timeseries)',' Tpeak: ',num2str(Tpeak_total),'Starting time:
',num2str(datestr(time_origo,0)),' End time:
',num2str(datestr(time_origo+length(pressure)/(24*3600),0)),'')],'HorizontalAlignment','center');
xlabel('frequency [Hz]');
ylabel('');
saveas(gcf,'Total_spectrum', 'jpeg')


%plotting figures
figure
plot(time,pressure,'r')
hold on
plot(time, waterdepth,'b')
title(['Starting time: ',num2str(datestr(time_origo,0)),' End time:
',num2str(datestr(time_origo+length(pressure)/(24*3600),0)),'']);
xlabel('time [seconds]');
ylabel('meters');
legend('ADCP pressure', 'Tidal motion');
saveas(gcf,'ADCP_pressure', 'jpeg')


%...........................................%
% Selecting the surface elevation timeseries %
%...........................................%

% Select slice
start=find(time_vector<=datenum(2006,04,20,09,25,00),1,'last');
finish=find(time_vector<=datenum(2006,04,20,09,55,00),1,'last');
duration=30*60;


%Inforcing a timestep dt of 1 sec for the selected slice using
%interpolation.
time_num=time_vector*24*3600;

new_time(1)=time_num(start);
p_slice(1)=delta_p(start);

for ii=2:duration;
    new_time(ii)=new_time(ii-1)+1;
    Find_pre_time=find(time_num<new_time(ii),1,'last');
    Find_next_time=find(time_num>=new_time(ii),1,'first');
    Pre_time=time_num(Find_pre_time);
    Next_time=time_num(Find_next_time);
    Pre_pressure=delta_p(Find_pre_time);
    Next_pressure=delta_p(Find_next_time);

    p_slice(ii)=(Next_pressure-Pre_pressure)/(Next_time-Pre_time)*(1-(Pre_time-new_time(ii-
1)))+Pre_pressure;
end
 new_time(duration+1)=new_time(duration)+1;
 p_slice(duration+1)=delta_p(finish);

 figure
plot(time_vector(start:finish),delta_p(start:finish),'-o')
hold on
plot(new_time/(24*3600),p_slice,'x-')
```

```
%Slice up the selected surface elevation file

time_slice=new_time;
%p_slice=delta_p(begin:stop)';
relative_t=[0:dt:length(p_slice)-1];


% Compute spectrum of selected slice
bins_slice=2^11;
Y=fft(p_slice,bins_slice);
p_slice_spectrum=((real(Y(1:end)).^2+imag(Y(1:end)).^2).^0.5)/bins*2;
p_slice_spectrum(1)=p_slice_spectrum(1)/2;
f_slice=[0:bins_slice/2]/bins_slice*2*fn;

Find_max=find(p_slice_spectrum==max(p_slice_spectrum),1);
Tpeak=(f_slice(Find_max))^(-1);
water_level=mean(waterdepth(start:finish))+adcp_offset;

% Plot spectrum of selected slice
figure
plot(f_slice,p_slice_spectrum(1:length(f_slice)))
title([char('Wave Powerspectrum (Selected timeseries) Tpeak: ',num2str(Tpeak),'Starting time:
',num2str(datestr(new_time(1)/(24*3600),0)),' End time: ',num2str(datestr(new_time(end)/(24*3600),0)),' ')]);
xlabel('frequency [Hz]');
ylabel('');
saveas(gcf,'wavespectrum_slice', 'jpeg')


%%%%%%%%%%%%%%%%%%%%%%%%%%%%%%%%%%%%%%%%%%%%%%%
% Syntesize Untransformed Wavespectrum: Frequency space => Time Series
%%%%%%%%%%%%%%%%%%%%%%%%%%%%%%%%%%%%%%%%%%%%%

Re_Y1=real(Y(1))/bins_slice;
Re_Y2=real(Y(2:end-1))/(bins_slice/2); %Correcting the real parts.
Re_Y3=real(Y(bins_slice/2))/bins_slice;
Re_Y=[Re_Y1 Re_Y2 Re_Y3];

Im_Y=-imag(Y(1:end))/(bins_slice/2);

%Create low-pass filter
fmin=0.1928; %Hz
bandwidth=1/(fmin^(-1)-2); %Hz
Find_cutoff=find(f_slice>=fmin & f_slice<=bandwidth);
L_band=[0:length(Find_cutoff)-1]*pi/(2*length(Find_cutoff));
Lowpass_fx=(cos(L_band).^2)';

for kk=1:Find_cutoff(1)
   merged(kk,:)=Re_Y(kk).*cos(2*pi*f_slice(kk)*relative_t)+Im_Y(kk)*sin(2*pi*f_slice(kk)*relative_t);
end

% %Apply Lowpass filter
%
% jj=1;
% for pp=Find_cutoff(1):Find_cutoff(end)
% merged(pp,:)=merged(pp,:)*Lowpass_fx(jj);
% jj=jj+1;
% end
```

```
reform_wave=sum(merged);

% CONTROLING CORRECT FOURIER ANALYSIS
figure
plot(time_slice,p_slice,'r')
title('Original signal compared to fourier synthesis');
hold on
plot(time_slice,reform_wave+2.5,'b')
saveas(gcf,'slice_control', 'jpeg')


%%%%%%%%%%%%%%%%%%%%%%%%%%%%%%%%%%%%%%%%%%%%%%%%%
% Syntesize The transformed Wavespectrum: Frequency space => Time Series
%%%%%%%%%%%%%%%%%%%%%%%%%%%%%%%%%%%%%%%%%%%%%%%

%calc k
omega=f_slice*2*pi;
L0=g*f_slice.^(-2)/(2*pi);
k_guess=2*pi*L0.^(-1);

for pp=1:length(f_slice)
   delta=1;
   while delta>10^(-6)
   L(pp)=L0(pp)*tanh(k_guess(pp)*water_level);
   k(pp)=2*pi/L(pp);
   delta=abs(k(pp)^2-k_guess(pp)^2);
   k_guess(pp)=k(pp);
   end
end

GN_function=(cosh(k*water_level)./cosh(k*adcp_offset))';

figure
plot(k,GN_function)
title('The ''pressure=>surface elevation transfer function');
xlabel('k');
ylabel('GN');
saveas(gcf,'GN_function', 'fig')
%plot(k)

   merged_trans(1,:)=merged(1,:)
for vv=2:Find_cutoff(1)
   merged_trans(vv,:)=merged(vv,:)*GN_function(vv);
end

surf_elevation=sum(merged_trans);

%%%%%%%%%%%%%%%%%%%%%%%%%%%%%%%%%%%%%%%%%%%%%%%%%%%%
% Wave Stats
%%%%%%%%%%%%%%%%%%%%%%%%%%%%%%%%%%%%%%%%%%%%%%%%%%%%
   f_band=0.01;
   df=(bins_slice*2*fn)^(-1);
   bin_size=round(f_band/df);
   f_slice=[0:bins_slice/2]/bins_slice*2*fn;

   bin_number=fix(length(f_slice)/bin_size);
```

```
   f_new=[0.5:bin_number-0.5]*f_band;
   Y2=fft(surf_elevation,bins_slice);
   p_slice_spectrum=((real(Y2(1:end)).^2+imag(Y2(1:end)).^2).^0.5)/bins_slice*2;
   p_slice_spectrum(1)=p_slice_spectrum(1)/2;

   for cc=1:bin_number
      new_spect(cc)=mean(p_slice_spectrum((cc-1)*bin_size+1:cc*bin_size));
   end
   Tpeak=f_new(find(new_spect==max(new_spect)))^(-1);
%locate upcrossings

 %   surf_elevation=surf_elevation_log(47,:);

   for ss =1:length(surf_elevation)-1
      if surf_elevation(ss)<0 & surf_elevation(ss+1)>0;
         nm_log(ss)=ss;
      end
   end
   Finder=find(nm_log>0);

   % find wavecrest and wavetroughs
   tt=1;
   for tt = 1:length(Finder)-1
      crest(tt)=max(surf_elevation(Finder(tt):Finder(tt+1)));
      trough(tt)=min(surf_elevation(Finder(tt):Finder(tt+1)));
   end

   Waveheight=crest-trough;
   Hm=mean(Waveheight);

   sort_fx=sort(Waveheight,'descend');
   length_vector=round(length(sort_fx)/3);
   Hsig=mean(sort_fx(1:length_vector));

   figure
   plot(f_new,new_spect)
   title([char('Powerspectrum: [16.15-16.45] Wednesday April 19 2006')]);
   xlabel('frequency [Hz]');
   ylabel('m^2/Hz');
   saveas(gcf,'wavespectrum_slice', 'jpeg')
   axis([0 0.5 0 0.03])
   save powerspectrum_thursday925.txt new_spect -ASCII
   save F_new.txt f_new -ASCII

   %Log values
   Tpeak
   Hm
   Hsig
   Hmax=max(Waveheight)


figure
plot(surf_elevation,'-.')
hold on
plot(p_slice,'r')
title(['Starting time: ',num2str(datestr(new_time(1)/(24*3600),0)),' End time:
',num2str(datestr(new_time(end)/(24*3600),0)),' ']);
xlabel('time [seconds]');
```

```
ylabel('meters');
axis([0 1800 -2 2.2])
legend('\eta(t),  f = 0 - 0.19 Hz',' p^+(t), ADCP)');
saveas(gcf,'surfelevation_slice', 'fig')

surf_elevation=surf_elevation';
save input_surfelevation_thursday925_955.txt surf_elevation -ASCII
%save surf_slice_thursday925_955.m surf_elevation -mat

disp(['Starting time: ',num2str(datestr(new_time(1)/(24*3600),0)),''])
disp(['Ending time: ',num2str(datestr(new_time(end)/(24*3600),0)),''])
disp(['Number of timesteps: ',num2str(length(p_slice)),''])
disp(['Average Waterlevel: ',num2str(water_level),'meters'])
disp(['Waterlevel diff: ',num2str(waterdepth(start)-waterdepth(finish)),'meter'])
disp(['Wave peak period: ',num2str(Tpeak),'sec'])

p_slice=p_slice';

%Save pressure
save pressure_ADCP_thursday925.txt p_slice -ASCII

figure
plot(surf_elevation,'-.','LineWidth',1.5)
hold on
plot(p_slice,'r','LineWidth',1.5)
title('Transformation from intrument measured pressure to surface elevation (ADCP)');
xlabel('time [seconds]');
ylabel('meters');
legend('\eta(t), f = 0 - 0.19 Hz',' p^+(t)');
saveas(gcf,'surfelevation_slice', 'fig')
axis([100 200 -1.5 2])
```

Appendix III

Matlab code use to calculate wave height, spectral peak period and wave direction for the 48-hour field dataset.

```
clear all
close all

g=9.81;
rho=1024;
ratio=10^4/(rho*g);     %conversion from dbar to pressure in [m]
pressure=ratio*load('pressure.txt');
u_input=load('u_velocity.txt');
v_input=load('v_velocity.txt');
u_data =u_input(:,2)';
v_data =v_input(:,2)';

time_origo=datenum(2006,04,19,08,59,09);

%Input remarks
adcp_offset=0.30;
dt=1;
%resolution for spectrum calc;
bins_slice=2^12;
   f_band=0.01;

time=[0:1:length(pressure)-1]*dt;

%Filtering out the tidal oscilation
average_length=1000;

waterdepth_fraction(1)=mean(pressure(1:average_length));
waterdepth=ones(1,average_length)*waterdepth_fraction(1);

for i=1:fix((length(pressure))/average_length)-1
   waterdepth_fraction(i+1)=mean(pressure(i*average_length:(i+1)*average_length));
   waterdepth_vector=ones(1,average_length)*waterdepth_fraction(i);
   waterdepth=[waterdepth waterdepth_vector];
end

%What is left after the last batch is assigned same waterlevel
av_length=fix((length(pressure))/average_length)*average_length;
rest=length(pressure)-av_length; %last part not included in the averaging
rest_vector=ones(1,rest)*waterdepth_fraction(fix((length(pressure))/average_length));

waterdepth=[waterdepth rest_vector];

delta_p=pressure'-waterdepth;



%Number of 30 min segments
segment=60 %minutes
seg_num=fix(length(delta_p)/(segment*60))

tic
for bb = 1:seg_num

   bb % show progress
```

```
   %..........................................%
   % Selecting the surface elevation timeseries %
   %..........................................%

   %Slice up the selected surface elevation file
   duration=segment*60;
   begin=1+(bb-1)*duration
   stop=begin+duration
   time_slice=time(begin:stop);
   p_slice=delta_p(begin:stop)';
   u_slice=u_data(begin:stop)';
   v_slice=v_data(begin:stop)';

   fitfunction=fit(u_slice,v_slice,'poly1')
   Mag_correction=10.4; % correction for magnetic north
   wave_dir(bb)=abs(atan(fitfunction.p1)/pi*180)+270+Mag_correction;


   relative_t=[0:dt:length(p_slice)-1];

   % Compute spectrum of selected slice
   fn=1/(dt*2);

   df=(bins_slice*2*fn)^(-1);
   bin_size=round(f_band/df);
   f_slice=[0:bins_slice/2]/bins_slice*2*fn;

   bin_number=fix(length(f_slice)/bin_size);

   f_new=[0.5:bin_number-0.5]*f_band;
   Y=fft(p_slice,bins_slice);
   p_slice_spectrum=((real(Y(1:end)).^2+imag(Y(1:end)).^2).^0.5)/bins_slice*2;
   p_slice_spectrum(1)=p_slice_spectrum(1)/2;

   for cc=1:bin_number
      new_spect(cc)=mean(p_slice_spectrum((cc-1)*bin_size+1:cc*bin_size));
   end
   Tpeak=f_new(find(new_spect==max(new_spect)))^(-1);


   p_slice_spectrum_log(bb,:)=p_slice_spectrum;
   %f_slice=[0:bins_slice/2]/bins_slice*2*fn;


%    Find_max=find(p_slice_spectrum==max(p_slice_spectrum),1);
%    Tpeak=(f_slice(Find_max))^(-1);
   water_level=mean(waterdepth(begin:stop))+adcp_offset;


   %%%%%%%%%%%%%%%%%%%%%%%%%%%%%%%%%%%%%%%%%%%%%%%%%
   % Syntesize The transformed Wavespectrum: Frequency space => Time Series
   %%%%%%%%%%%%%%%%%%%%%%%%%%%%%%%%%%%%%%%%%%%%%%%

   Re_Y1=real(Y(1))/bins_slice;
   Re_Y2=real(Y(2:end-1))/(bins_slice/2); %Correcting the real parts.
   Re_Y3=real(Y(bins_slice/2))/bins_slice;
   Re_Y=[Re_Y1' Re_Y2' Re_Y3'];
```

```
  Im_Y=-imag(Y(1:end))/(bins_slice/2);

  kk=1;
  for kk=1:bins_slice/2
     merged(kk,:)=Re_Y(kk).*cos(2*pi*f_slice(kk)*relative_t)+Im_Y(kk)*sin(2*pi*f_slice(kk)*relative_t);
  end

  %Frequency cutt-off
  fmin=0.1928; %Hz
  Find_cutoff=find(f_slice>=fmin,1);

  %calc k
  omega=f_slice*2*pi;
  L0=g*f_slice.^(-2)/(2*pi);
  k_guess=2*pi*L0.^(-1);

  pp=1;
  for pp=1:length(f_slice)
     delta=1;
     while delta>10^(-6)
        L(pp)=L0(pp)*tanh(k_guess(pp)*water_level);
        k(pp)=2*pi/L(pp);
        delta=abs(k(pp)^2-k_guess(pp)^2);
        k_guess(pp)=k(pp);
     end
  end

  GN_function=cosh(k*(water_level+adcp_offset))./cosh(k*adcp_offset);

  vv=2;
  for vv=2:Find_cutoff
     merged_trans(vv,:)=merged(vv,:)*GN_function(vv);
  end

  surf_elevation=sum(merged_trans);
  surf_elevation_log(bb,:)=surf_elevation;

  %locate upcrossings

%   surf_elevation=surf_elevation_log(47,:);

  for ss =1:length(surf_elevation)-1
     if surf_elevation(ss)<0 & surf_elevation(ss+1)>0;
        nm_log(ss)=ss;
     end
  end
  Finder=find(nm_log>0);

  % find wavecrest and wavetroughs
  tt=1;
  for tt = 1:length(Finder)-1
     crest(tt)=max(surf_elevation(Finder(tt):Finder(tt+1)));
     trough(tt)=min(surf_elevation(Finder(tt):Finder(tt+1)));
  end

  Waveheight=crest-trough;
  Hm=mean(Waveheight)
```

```
    sort_fx=sort(Waveheight,'descend');
    length_vector=round(length(sort_fx)/3);
    Hsig=mean(sort_fx(1:length_vector));

    %Log values
    Tp(bb)=Tpeak;
    Hmean(bb)=Hm;
    Hs(bb)=Hsig;
    Hmax(bb)=max(Waveheight);

   clear Waveheight Hm Finder tt ii crest trough nm_log new_spec Tpeak
    end


time_vector=[1:seg_num]*segment/60;

figure
plot(time_vector,Tp,'-.')
title([char('Peak wave period, Offshore ADCP, h=21 m','averaging segment size (in minutes):
',num2str(segment),' Origin:',datestr(time_origo,0),'')])
xlabel('time [hours]');
ylabel('seconds');
%dateaxis('x',13,time_origo)
axis([0 50 0 20])
saveas(gcf,'Tp_ADCP_48hours', 'fig')

Tp=Tp';
save Tp_48hours.txt Tp -ASCII

figure
plot(time_vector,Hmean,'r')
title([char('Wave Height, Offshore ADCP, h=21 m','averaging segment size (in minutes): ',num2str(segment),'
Origin:',datestr(time_origo,0),'')])
hold on
plot(time_vector,Hs,'-.')
hold on
plot(time_vector,Hmax,'-og')
xlabel('time [hours]');
ylabel('meters');
legend('Hmean','Hsig','Hmax')
saveas(gcf,'Waveheight_ADCP_48hours', 'fig')

figure
plot(time_vector,wave_dir,'rx-')
title([char('Wave Direction, Offshore ADCP, h=21 m','averaging segment size (in minutes):
',num2str(segment),' Origin:',datestr(time_origo,0),'')])
xlabel('time [hours]');
ylabel('Direction');
saveas(gcf,'Wavedirection_ADCP_48hours', 'fig')
axis([0 48 310 340]);

figure
plot(time/3600,delta_p)
hold on
title('Pressure timeseries ADCP (tidal variation extracted)')
plot(time/3600,waterdepth-mean(waterdepth),'r--','LineWidth',4)
xlabel('time [hours]');
ylabel('pressure [dBar]');
```

```
legend('Pressure flucturation due to wave motion','Pressure flucturation due to tidal motion')
axis([0 50 -2 2]);

figure
plot(time/3600,pressure)
title('Pressure timeseries ADCP (Raw)')
xlabel('time [hours]');
ylabel('pressure [dBar]');
axis([0 50 19 23]);


Hmean=Hmean';
Hs=Hs';
Hmax=Hmax';
wave_dir=wave_dir';

save Hm_48hours.txt Hmean -ASCII
save Hsig_48hours.txt Hs -ASCII
save Hmax_48hours.txt Hmax -ASCII
save wavedir_48hours.txt wave_dir -ASCII
toc
```

Appendix IV

Matlab code used to extrat selected velocity and surface elevation time-series from the AquaDopps.

```
clear all
close all
tic
g=9.81;
rho=1000;
ratio=10^4/(rho*g);     %conversion from dbar to pressure in [m]
data06=load('waimea_6m_may06.dat');
pressure=ratio*data06(:,6)
u=data06(:,7);
v=data06(:,8);
time_origo=datenum(2006,04,19,09,00,00);

%Input remarks
adcp_offset=0.30;
dt=1;

time=[0:1:length(pressure)-1]*dt;

%Filtering out the tidal oscilation
average_length=1000;

waterdepth_fraction(1)=mean(pressure(1:average_length));
waterdepth=ones(1,average_length)*waterdepth_fraction(1);

for i=1:fix((length(pressure))/average_length)-1
   waterdepth_fraction(i+1)=mean(pressure(i*average_length:(i+1)*average_length));
   waterdepth_vector=ones(1,average_length)*waterdepth_fraction(i);
   waterdepth=[waterdepth waterdepth_vector];
end

%What is left after the last batch is assigned same waterlevel
av_length=fix((length(pressure))/average_length)*average_length;
rest=length(pressure)-av_length; %last part not included in the averaging
rest_vector=ones(1,rest)*waterdepth_fraction(fix((length(pressure))/average_length));

waterdepth=[waterdepth rest_vector];

delta_p=pressure'-waterdepth;

bins=2^17

% Compute spectrum

fn=1/(dt*2);
Y1=fft(delta_p,bins);
p_spectrum=((real(Y1(1:end)).^2+imag(Y1(1:end)).^2).^0.5)/bins*2;
p_spectrum(1)=p_spectrum(1)/2;
f=[0:bins/2]/bins*2*fn;
Find_max_total=find(p_spectrum==max(p_spectrum),1);
Tpeak_total=(f(Find_max_total))^(-1);

%plot spectrum
figure
plot(f,p_spectrum(1:length(f)))
```

```
title([char('Wave Powerspectrum (Entire timeseries)',' Tpeak: ',num2str(Tpeak_total),'Starting time:
',num2str(datestr(time_origo,0)),' End time:
',num2str(datestr(time_origo+length(pressure)/(24*3600),0)),'')],'HorizontalAlignment','center');
xlabel('frequency [Hz]');
ylabel('');
saveas(gcf,'Total_spectrum', 'jpeg')

%plotting figures
figure
plot(time,pressure,'r')
hold on
plot(time, waterdepth,'b')
title(['Starting time: ',num2str(datestr(time_origo,0)),' End time:
',num2str(datestr(time_origo+length(pressure)/(24*3600),0)),'']);
xlabel('time [seconds]');
ylabel('meters');
legend('ADCP pressure', 'Tidal motion');
saveas(gcf,'ADCP_pressure', 'jpeg')
%..........................................%
% Selecting the surface elevation timeseries %
%..........................................%

%Slice up the selected surface elevation file
begin=83700+4200;
duration=30*60;
stop=begin+duration;

time_slice=time(begin:stop);
p_slice=delta_p(begin:stop)';
relative_t=[0:dt:length(p_slice)-1];


%Extract velocities
u_slice_thursday_925=u(begin:stop);
v_slice_thursday_925=v(begin:stop);

fitfunction=fit(u_slice_thursday_925,v_slice_thursday_925,'poly1');
Mag_correction=10.4; % correction for magnetic north
wave_dir=abs(atan2(1,fitfunction.p1)/pi*180)+180+Mag_correction;

figure
plot(u_slice_thursday_925,v_slice_thursday_925,'.')
hold on
title(['AQDP06 wave direction: ',num2str(wave_dir),' degrees'])
plot(u_slice_thursday_925,fitfunction.p1*u_slice_thursday_925,'r')
axis([-1.5 1.5 -1.5 1.5])

save u_AQDP06_thursday_925.mat u_slice_thursday_925 -MAT
save v_AQDP06_thursday_925.mat v_slice_thursday_925 -MAT


% save pressure file
save pressure_AQDP06_thursday925_v2.txt p_slice -ASCII
save pressure_AQDP06_thursday925_v2.mat p_slice -mat

% Compute spectrum of selected slice
bins_slice=2^12;
Y=fft(p_slice,bins_slice);
```

```
p_slice_spectrum=((real(Y(1:end)).^2+imag(Y(1:end)).^2).^0.5)/bins*2;
p_slice_spectrum(1)=p_slice_spectrum(1)/2;
f_slice=[0:bins_slice/2]/bins_slice*2*fn;


Find_max=find(p_slice_spectrum==max(p_slice_spectrum),1);
Tpeak=(f_slice(Find_max))^(-1);
water_level=mean(waterdepth(begin:stop))+adcp_offset;

% Plot spectrum of selected slice
figure
plot(f_slice,p_slice_spectrum(1:length(f_slice)))
title([char('Wave Powerspectrum (Selected timeseries) Tpeak: ',num2str(Tpeak),'Starting time:
',num2str(datestr(time_origo+begin/(24*3600),0)),' End time:
',num2str(datestr(time_origo+stop/(24*3600),0)),' ')]);
xlabel('frequency [Hz]');
ylabel('');
saveas(gcf,'wavespectrum_slice', 'jpeg')

%%%%%%%%%%%%%%%%%%%%%%%%%%%%%%%%%%%%%%%%%%%%%%%
% Syntesize Untransformed Wavespectrum: Frequency space => Time Series
%%%%%%%%%%%%%%%%%%%%%%%%%%%%%%%%%%%%%%%%%%%%%

Re_Y1=real(Y(1))/bins_slice;
Re_Y2=real(Y(2:end-1))/(bins_slice/2); %Correcting the real parts.
Re_Y3=real(Y(bins_slice/2))/bins_slice;
Re_Y=[Re_Y1' Re_Y2' Re_Y3'];

Im_Y=-imag(Y(1:end))/(bins_slice/2);

f_cutoff=find(f_slice>=0.22,1)%0.337,1);
for kk=1:f_cutoff
   merged(kk,:)=Re_Y(kk).*cos(2*pi*f_slice(kk)*relative_t)+Im_Y(kk)*sin(2*pi*f_slice(kk)*relative_t);
end

reform_wave=sum(merged);

% CONTROLING CORRECT FOURIER ANALYSIS
figure
plot(time_slice,p_slice,'r')
title('Original signal compared to fourier synthesis');
hold on
plot(time_slice,reform_wave+2.5,'b')
saveas(gcf,'slice_control', 'jpeg')

%%%%%%%%%%%%%%%%%%%%%%%%%%%%%%%%%%%%%%%%%%%%%%%
% Syntesize The transformed Wavespectrum: Frequency space => Time Series
%%%%%%%%%%%%%%%%%%%%%%%%%%%%%%%%%%%%%%%%%%%%%

%calc k
omega=f_slice*2*pi;
L0=g*f_slice.^(-2)/(2*pi);
k_guess=2*pi*L0.^(-1);

for pp=1:length(f_slice)
   delta=1;
   while delta>10^(-6)
   L(pp)=L0(pp)*tanh(k_guess(pp)*water_level);
```

```
    k(pp)=2*pi/L(pp);
    delta=abs(k(pp)^2-k_guess(pp)^2);
    k_guess(pp)=k(pp);
    end
end

GN_function=cosh(k*water_level)./cosh(k*adcp_offset);

figure
plot(k,GN_function)
title('The ''pressure=>surface elevation transfer function');
xlabel('k');
ylabel('GN');
saveas(gcf,'GN_function', 'fig')
%plot(k)

merged_trans(1,:)=merged(1,:);
for vv=2:f_cutoff
    merged_trans(vv,:)=merged(vv,:)*GN_function(vv);
end

surf_elevation=sum(merged_trans);

%%%%%%%%%%%%%%%%%%%%%%%%%%%%%%%%%%%%%%%%%%%%%%%%%%%%%%%%%%%%%%%


figure
plot(surf_elevation,'-.')
hold on
plot(p_slice,'r')
title(['Starting time: ',num2str(datestr(time_origo+begin/(24*3600),0)),' End time:
',num2str(datestr(time_origo+stop/(24*3600),0)),'']);
xlabel('time [seconds]');
ylabel('meters');
legend('Surface elevation f = 0 - 0.15 Hz', 'Pressure (ADCP)');
saveas(gcf,'surfelevation_slice', 'fig')
save surf_slice.mat surf_elevation

disp(['Starting time: ',num2str(datestr(time_origo+begin/(24*3600),0)),''])
disp(['Ending time: ',num2str(datestr(time_origo+stop/(24*3600),0)),''])
disp(['Number of timesteps: ',num2str(length(p_slice)),''])
disp(['Average Waterlevel: ',num2str(water_level),'meters'])
disp(['Waterlevel diff: ',num2str(waterdepth(begin)-waterdepth(stop)),'meter'])
disp(['Wave peak period: ',num2str(Tpeak),'sec'])

%%%%%%%%%%%%%%%%%%%%%%%%%%%%%%%%%%%%%%%%%%%%%%%%
surf_elevation=surf_elevation'
save etha_AQDP06_thursday925_v_cutoff022.txt surf_elevation -ASCII
```

Appendix V

Mablab code used for conducting time-series analysis of model results and calculate H_{sig}, H_m, U_m, V_m, U_{max} /U_{min} and V_{max}/V_{min}.

```
close all
clear all

phase_shift=69;
time_length=1799;
Magnetic_North=10.4;

% Load Data from AQDP 06
AQDP06=load('etha_AQDP06_thursday925_v3.txt');
AQDP06_u_load=load('-mat','u_AQDP06_thursday_925.mat');
AQDP06_v_load=load('-mat','v_AQDP06_thursday_925.mat');

AQDP06_u=AQDP06_u_load.u_slice_thursday_925;
AQDP06_v=AQDP06_v_load.v_slice_thursday_925;
%%%%%%%%%%%%%%%%%%%%%%%%%%%%%%%%%%%

% Load Data from AQDP 10
AQDP10=load('etha_AQDP10_thursday925_v3.txt')';

AQDP10_u_load=load('-mat','u_AQDP10_thursday_925.mat');
AQDP10_v_load=load('-mat','v_AQDP10_thursday_925.mat');

AQDP10_u=AQDP10_u_load.u_slice_thursday_925;
AQDP10_v=AQDP10_v_load.v_slice_thursday_925;

%%%%%%%%%%%%%%%%%%%%%%%%%

% Load ADCP Velocities
ADCP_u_load=load('-mat','u_slice_thursday925.m');
ADCP_v_load=load('-mat','v_slice_thursday925.m');

ADCP_u=ADCP_u_load.u_velocity_slice./1.75;
ADCP_v=ADCP_v_load.v_velocity_slice./1.75;

%¤¤¤¤¤¤¤¤¤¤¤¤¤¤¤¤
% Velocity Rotation
%%%%%%%%%%%%%%%%%%%%%%%

rotation=(30-Magnetic_North)*pi/180;

AQDP06_u_rot = AQDP06_u * cos(rotation) - AQDP06_v * sin(rotation);
AQDP06_v_rot = AQDP06_v * cos(rotation) + AQDP06_u * sin(rotation);

AQDP10_u_rot = AQDP10_u * cos(rotation) - AQDP10_v * sin(rotation);
AQDP10_v_rot = AQDP10_v * cos(rotation) + AQDP10_u * sin(rotation);

ADCP_u_rot = ADCP_u * cos(rotation) - ADCP_v * sin(rotation);
ADCP_v_rot = ADCP_v * cos(rotation) + ADCP_u * sin(rotation);



%Version 28
Mike_input_v6=load('ADCPinput_raw_v4.txt');
Mike_offshore_v6=load('etha_offshore_MIKE21_v28.txt');
```

```
Mike_bayentry_v6=load('etha_bayentry_MIKE21_v28.txt');
Mike_baymiddle_v6=load('etha_baymiddle_MIKE21_v28.txt');

%Version 31
Mike_input_v7=load('ADCPinput_raw_v4.txt');
Mike_offshore_v7=load('etha_offshore_MIKE21_v31.txt');
Mike_bayentry_v7=load('etha_bayentry_MIKE21_v31.txt');
Mike_baymiddle_v7=load('etha_baymiddle_MIKE21_v31.txt');

% Load Mike21 Velocities
h_input=20.98;
Mike_input_u_v6=load('pflux_offshore_MIKE21_v28.txt')/h_input;
Mike_input_v_v6=load('qflux_offshore_MIKE21_v28.txt')/h_input;

h10=10.8;
Mike_bayentry_u_v6=load('pflux_bayentry_MIKE21_v28.txt')./(Mike_bayentry_v6+h10);
Mike_bayentry_v_v6=load('qflux_bayentry_MIKE21_v28.txt')./(Mike_bayentry_v6+h10);

h06=7.4;
Mike_baymiddle_u_v6=load('pflux_baymiddle_MIKE21_v28.txt')./(Mike_baymiddle_v6+h06);
Mike_baymiddle_v_v6=load('qflux_baymiddle_MIKE21_v28.txt')./(Mike_baymiddle_v6+h06);


Mike_input_u_v7=load('pflux_offshore_MIKE21_v31.txt')./(h_input+Mike_input_v7(1:time_length));
Mike_input_v_v7=load('qflux_offshore_MIKE21_v31.txt')./(h_input+Mike_input_v7(1:time_length));

Mike_bayentry_u_v7=load('pflux_bayentry_MIKE21_v31.txt')./(h10+Mike_bayentry_v7+1);
Mike_bayentry_v_v7=load('qflux_bayentry_MIKE21_v31.txt')./(h10+Mike_bayentry_v7+1);

Mike_baymiddle_u_v7=load('pflux_baymiddle_MIKE21_v31.txt')./(h06+Mike_baymiddle_v7+1);
Mike_baymiddle_v_v7=load('qflux_baymiddle_MIKE21_v31.txt')./(h06+Mike_baymiddle_v7+1);


%Intercorrelation between MIKE21 Output
correlation1_v6=lagcor(Mike_input_v6(1:time_length),Mike_offshore_v6(1:time_length),220);
correlation1_v7=lagcor(Mike_input_v7(1:time_length),Mike_offshore_v7(1:time_length),220);

t_vector=[1:time_length]-1;
x_vector=[1:length(correlation1_v7)]-220;


%Plot inputwaveseries vs directional wave series
figure
plot(x_vector,correlation1_v6,'b')
title(char('Correlation between input wave vs resultant directional ','wave at deployment location of ADCP'))
hold on
plot(x_vector,correlation1_v7,'r')
legend('ver 6','ver 11')
xlabel('seconds')

figure
plot(t_vector,Mike_input_v6(1:time_length))
hold on
title('\eta calculated from p^+ ver6 (frequency cutoff = 0.19 Hz)')
plot(t_vector-69,Mike_offshore_v6(1:time_length),'r')
legend('Input timeseries from ADCP','Mike21 prediction at ADCP location')
axis([-70 70 -2.5 2.5])
xlabel('Model run-time (seconds)')
```

```
ylabel('surface elevation (m)')

figure
plot(t_vector,Mike_input_v7(1:time_length))
hold on
title('\eta calculated from p^+ ver11 (frequency cutoff = 0.19 Hz)')
plot(t_vector-66,Mike_offshore_v7(1:time_length),'r')
legend('Input timeseries from ADCP','Mike21 prediction at ADCP location')
axis([-70 70 -2.5 2.5])
xlabel('Model run-time (seconds)')
ylabel('surface elevation (m)')

figure
plot(t_vector-69,Mike_offshore_v6(1:time_length),'r')
hold on
title('wave-input comparison')
plot(t_vector-66,Mike_offshore_v7(1:time_length),'g')
legend('ver6','ver11 (corrected for reflection)')
axis([-70 70 -2.5 2.5])
xlabel('Model run-time (seconds)')
ylabel('surface elevation (m)')

correlation7_v7=lagcor(Mike_bayentry_v7(1:time_length),AQDP10(1:time_length),220);
correlation7_v6=lagcor(Mike_bayentry_v6(1:time_length),AQDP10(1:time_length),220);

figure
plot(x_vector,correlation7_v6,'r')
hold on
plot(x_vector,correlation7_v7,'g')
title(char('Correlation between Mike21 ver 11 vs field ',' measurements (from Aquadopp) in the bay entry'))
xlabel('seconds')
xlabel('seconds')
legend('ver6','ver9')

figure
plot(t_vector,AQDP10(1:time_length),'k')
hold on
title('\eta calculated from p^+ (frequency cutoff = 0.28 Hz)')
plot(t_vector-70,Mike_bayentry_v6(1:time_length),'b')
hold on
plot(t_vector-72,Mike_bayentry_v7(1:time_length),'r')
legend('AquaDopp placed at Bay Entry (h = 10 m)','Mike21s prediction at same location (ver. 6)','Mike21s
prediction at same location (ver. 11)')
axis([-70 70 -1.5 1.5])
xlabel('Model run-time (seconds)')
ylabel('surface elevation (m)')


correlation8_v6=lagcor(Mike_baymiddle_v6(1:time_length),AQDP06(1:time_length),220);
correlation8_v7=lagcor(Mike_baymiddle_v7(1:time_length),AQDP06(1:time_length),220);

figure
plot(x_vector,correlation8_v6,'b')
hold on
plot(x_vector,correlation8_v7,'r')
title(char('Correlation between Mike21 vs field ',' measurements (from Aquadopp) at the bay middle'))
xlabel('seconds')
xlabel('seconds')
```

```
legend('ver6','ver 9')
figure
plot(t_vector,AQDP06(1:time_length),'k')
hold on
title('\eta calculated from p^+ (frequency cutoff = 0.34 Hz)')
plot(t_vector-48,Mike_baymiddle_v6(1:time_length),'b')
hold on
plot(t_vector-48,Mike_baymiddle_v7(1:time_length),'r')
legend('AquaDopp placed in the Bay middle (h = 6.8 m)','Mike21s prediction at same location (ver.
6)','Mike21s prediction at same location (ver. 11)')
axis([-70 70 -2.5 2.5])
xlabel('Model run-time (seconds)')
ylabel('surface elevation (m)')

%%%%%%%%%%%%%%%%%%%%%%%%%%%%%%%%%%%%%%%%%%%%%%%%%%%%%%%%%%%%
% Bayentry velocity comparison
%%%%%%%%%%%%%%%%%%%%%%%%%%%%%%%%%%%%%%%%%%%%%%%%%%%%%%%%%%%%

figure
plot(t_vector,AQDP10_u_rot(1:time_length),'k')
title('UO comparison, Bay Entry')
hold on
plot(t_vector-69,Mike_bayentry_u_v6(1:time_length),'b')
hold on
plot(t_vector-66,Mike_bayentry_u_v7(1:time_length),'r')
legend('AquaDopp (h = 10.8 m)','Mike21s prediction at same location (ver. 6)','Mike21s prediction at same
location (ver. 11)')
xlabel('Model run-time (seconds)')
axis([-70 70 -2.5 2.5])
ylabel('velocity (m/s)')

figure
plot(t_vector,AQDP10_v_rot(1:time_length),'k')
title('VO comparison, Bay Entry')
hold on
plot(t_vector-69,Mike_bayentry_v_v6(1:time_length),'b')
hold on
plot(t_vector-66,Mike_bayentry_v_v7(1:time_length),'r')
legend('AquaDopp (h = 10.8 m)','Mike21s prediction at same location (ver. 6)','Mike21s prediction at same
location (ver. 11)')
xlabel('Model run-time (seconds)')
axis([-70 70 -2.5 2.5])
ylabel('velocity (m/s)')
%%%%%%%%%%%%%%%%%%%%%%%%%%%%%%%%%%%%%%%%%%%%%%%%%%%%%%%%%%%
% Baymiddle velocity comparison
%%%%%%%%%%%%%%%%%%%%%%%%%%%%%%%%%%%%%%%%%%%%%%%%%%%%%%%%%%%

figure
plot(t_vector,AQDP06_u_rot(1:time_length),'k')
title('UO comparison, Bay middle')
hold on
plot(t_vector-69,Mike_baymiddle_u_v6(1:time_length),'b')
hold on
plot(t_vector-48,Mike_baymiddle_u_v7(1:time_length),'r')
legend('AquaDopp (h = 7.8 m)','Mike21s prediction at same location (ver. 6)','Mike21s prediction at same
location (ver. 11)')
xlabel('Model run-time (seconds)')
axis([-70 70 -2.5 2.5])
```

```
ylabel('velocity (m/s)')

figure
plot(t_vector,AQDP06_v_rot(1:time_length),'k')
title('VO comparison, Bay middle')
hold on
plot(t_vector-69,Mike_baymiddle_v_v6(1:time_length),'b')
hold on
plot(t_vector-48,Mike_baymiddle_v_v7(1:time_length),'r')
legend('AquaDopp (h = 7.8 m)','Mike21s prediction at same location (ver. 6)','Mike21s prediction at same
location (ver. 11)')
xlabel('Model run-time (seconds)')
axis([-70 70 -2.5 2.5])
ylabel('velocity (m/s)')

%%%%%%%%%%%%%%%%%%%%%%%%%%%%%%%%%%%%%%%%%%%%%%%%%%%%%%%%%
%Wave direction comparison
%%%%%%%%%%%%%%%%%%%%%%%%%%%%%%%%%%%%%%%%%%%%%%%%%%%%%%%%%
figure

% hold on
% plot(Mike_input_u_v7,fitfunction1.p1*Mike_input_u_v7,'r')
% wave_dir(1)=abs(atan2(1,fitfunction1.p1)/pi*180)+210;
plot(Mike_input_u_v6,Mike_input_v_v6,'.g')
hold on
plot(Mike_input_u_v7,Mike_input_v_v7,'xr')
title('Velocity Scatter plot (Station 1, Offshore)')
fitfunction1=fit(-Mike_input_u_v7,Mike_input_v_v7,'poly1');
axis([-2 2 -2 2])
hold on
plot(ADCP_u_rot,ADCP_v_rot,'k+')
legend('Simulation 1','Simulation 2','Field Data')
xlabel('U-velocity [m/s]')
ylabel('V-velocity [m/s]')

% fitfunction2=fit(ADCP_u_rot,ADCP_v_rot,'poly1');
% wave_dir(2)=abs(atan2(1,fitfunction2.p1)/pi*180)+210;

figure
plot(Mike_bayentry_u_v7,Mike_bayentry_v_v7,'x')
axis([-2 2 -2 2])
title('velocity direction, Mike21 Bay Entry ver 7')
fitfunction3=fit(Mike_bayentry_u_v7,Mike_bayentry_v_v7,'poly1');
wave_dir(3)=abs(atan2(1,fitfunction3.p1)/pi*180)+210;
hold on
plot(AQDP10_u_rot,AQDP10_v_rot,'xr')
fitfunction4=fit(AQDP10_u_rot,AQDP10_v_rot,'poly1');
wave_dir(4)=abs(atan2(1,fitfunction4.p1)/pi*180)+210;
legend('v24','AQDP10')

figure
plot(Mike_baymiddle_u_v7,Mike_baymiddle_v_v7,'x')
title('velocity direction, Mike21 Baymiddle ver 17')
axis([-2 2 -2 2])
fitfunction5=fit(Mike_baymiddle_u_v7,Mike_baymiddle_v_v7,'poly1');
wave_dir(5)=abs(atan2(1,fitfunction5.p1)/pi*180)+210;
hold on
plot(AQDP06_u_rot,AQDP06_v_rot,'xr')
```

```
fitfunction6=fit(AQDP06_u_rot,AQDP06_v_rot,'poly1');
wave_dir(6)=abs(atan2(1,fitfunction6.p1)/pi*180)+210;
legend('v24','AQDP06')

figure
plot(Mike_baymiddle_u_v6,Mike_baymiddle_v_v6,'.g')
title('velocity direction, Mike21 Baymiddle ver 17')
axis([-2 2 -2 2])
hold on
plot(Mike_baymiddle_u_v7,Mike_baymiddle_v_v7,'xr')
title('Velocity Scatter Plot (Station 3, Bay Middle)')
hold on
fitfunction5=fit(Mike_baymiddle_u_v6,Mike_baymiddle_v_v6,'poly1');
wave_dir(5)=abs(atan2(1,fitfunction5.p1)/pi*180)+210;
plot(AQDP06_u_rot,AQDP06_v_rot,'+k')
fitfunction6=fit(AQDP06_u_rot,AQDP06_v_rot,'poly1');
wave_dir(6)=abs(atan2(1,fitfunction6.p1)/pi*180)+210;
legend('Simulation 2','Simulation 3','Field Data')
xlabel('U-velocity [m/s]')
ylabel('V-velocity [m/s]')

figure
plot(Mike_bayentry_u_v6,Mike_bayentry_v_v6,'.g')
title('velocity direction, Mike21 Baymiddle ver 17')
axis([-2 2 -2 2])
hold on
plot(Mike_bayentry_u_v7,Mike_bayentry_v_v7,'xr')
title('Velocity Scatter Plot (Station 2, Bay Entry)')
hold on
fitfunction5=fit(Mike_bayentry_u_v6,Mike_bayentry_v_v6,'poly1');
wave_dir(5)=abs(atan2(1,fitfunction5.p1)/pi*180)+210;
plot(AQDP10_u_rot,AQDP10_v_rot,'+k')
fitfunction6=fit(AQDP06_u_rot,AQDP06_v_rot,'poly1');
wave_dir(6)=abs(atan2(1,fitfunction6.p1)/pi*180)+210;
legend('Simulation 2','Simulation 3','Field Data')
xlabel('U-velocity [m/s]')
ylabel('V-velocity [m/s]')


%% PRESENTATION
figure
plot(t_vector,Mike_input_v7(1:time_length),'k-x','Markersize',6)
hold on
title('Surface elevation comparison (Station 1, Offshore)')
plot(t_vector-73,Mike_offshore_v6(1:time_length),'b--')
hold on
plot(t_vector-73,Mike_offshore_v7(1:time_length),'r')
legend('Field Data','Simulation 2','Simulation 3')
axis([-70 70 -2.5 2.5])
xlabel('Model run-time (seconds)')
ylabel('surface elevation (m)')

figure
plot(t_vector,AQDP10(1:time_length),'k-x','Markersize',5)
hold on
title('Surface elevation Bay Entry (Station 2, Bay Entry)')
% plot(t_vector-70,Mike_bayentry_v6(1:time_length),'b')
% hold on
```

```
plot(t_vector-73,Mike_bayentry_v6(1:time_length),'b--')
hold on
plot(t_vector-73,Mike_bayentry_v7(1:time_length),'r')
legend('Field Data','Simulation 2','Simulation 3')
axis([-70 70 -2.5 2.5])
xlabel('Model run-time (seconds)')
ylabel('surface elevation (m)')

figure
plot(t_vector,AQDP06(1:time_length),'k-x','Markersize',5)
hold on
title('Surface elevation Bay Middle (Station 3, Bay Middle)')
% plot(t_vector-70,Mike_bayentry_v6(1:time_length),'b')
% hold on
plot(t_vector-73,Mike_baymiddle_v6(1:time_length),'b--')
hold on
plot(t_vector-73,Mike_baymiddle_v7(1:time_length),'r')
legend('Field Data','Simulation 2','Simulation 3')
axis([-70 70 -2.5 2.5])
xlabel('Model run-time (seconds)')
ylabel('surface elevation (m)')

%%%%%%%%%%%%%%%%%%%%%%%%%%%%%%%%%%%%%%%%%%%%%%%%%%%%%%%%%%%%

% Input u velocity comparison
figure
plot(t_vector,ADCP_u_rot(1:time_length),'k')
title('offshore u-velocity comparison')
hold on
plot(t_vector-69,Mike_input_u_v6(1:time_length),'b')
hold on
plot(t_vector-66,Mike_input_u_v7(1:time_length),'r')
legend('ADCP','ver 6','ver 11')

%%%%%%%%%%%%%%%%%%%%%%%%%%%%%%%%%%%%%%%%%%%%%%%%%%%%%%%%%%%%

% Input v velocity comparison
figure
plot(t_vector,ADCP_v_rot(1:time_length),'k')
title('offshore v-velocity comparison')
hold on
plot(t_vector-66,Mike_input_v_v7(1:time_length),'r')
legend('ADCP','ver 11')


%%%%%%%%%%%%%%%%%%%%%%%%%%%%%%%%%%%%%%
% Wave statistics
%%%%%%%%%%%%%%%%%%%%%%%%%%%%%%%%%%%%%%
extra=40;

Surf_matrix=[...
	AQDP06(extra:time_length-phase_shift)...
	AQDP10(extra:time_length-phase_shift)...
	Mike_bayentry_v6(phase_shift+extra:time_length)...
	Mike_bayentry_v7(phase_shift+extra:time_length)...
	Mike_baymiddle_v6(phase_shift+extra:time_length)...
	Mike_baymiddle_v7(phase_shift+extra:time_length)...
	Mike_input_v6(phase_shift+extra:time_length)...
```

```
            Mike_input_v7(phase_shift+extra:time_length)...
            Mike_offshore_v6(phase_shift+extra:time_length)...
            Mike_offshore_v7(phase_shift+extra:time_length)...
            ];
for ff=1:size(Surf_matrix,2)

    surf_elevation=Surf_matrix(:,ff);

    %locate upcrossings
    for ii =1:length(surf_elevation)-1
        if surf_elevation(ii)<0 & surf_elevation(ii+1)>0;
            log(ii)=ii;
        end
    end
    Finder=find(log>0);

    % find wavecrest and wavetroughs
    for kk = 1:length(Finder)-1
        crest(kk)=max(surf_elevation(Finder(kk):Finder(kk+1)));
        trough(kk)=min(surf_elevation(Finder(kk):Finder(kk+1)));
    end

    Waveheight=crest-trough;
    Hm(ff)=mean(Waveheight);

    sort_fx=sort(Waveheight,'descend');
    length_vector=round(length(sort_fx)/3);
    Hsig(ff)=mean(sort_fx(1:length_vector));

    clear Finder Waveheight ii kk crest trough nm_log surf_elevation log
end
%Wave direction Comparison

%Mean waveheight Comparison
disp(['************************************'])
disp(['* Mean wave height                  *'])
disp(['************************************'])
disp(['ADCP, Hmean = ',num2str(Hm(7),3), ' m'])
disp(['Offshore v6, Hmean = ',num2str(Hm(9),3), ' m'])
disp(['Offshore v22, Hmean = ',num2str(Hm(10),3), ' m'])
disp([' '])
disp(['AQDP10, Hmean = ',num2str(Hm(2),2), ' m'])
disp(['Bayentry Mike21 v6, Hmean = ',num2str(Hm(3),2), ' m'])
disp(['Bayentry Mike21 v22, Hmean = ',num2str(Hm(4),2), ' m'])
disp([''])
disp(['AQDP06, Hmean = ',num2str(Hm(1),3), ' m'])
disp(['Baymiddle Mike21 v6, Hmean = ',num2str(Hm(5),3), ' m'])
disp(['Baymiddle Mike21 v22, Hmean = ',num2str(Hm(6),3), ' m'])
disp([' '])
disp(['*************************************'])
disp(['* Significant wave height           *'])
disp(['*************************************'])
%Sig waveheight Comparison
disp(['ADCP, Hsig = ',num2str(Hsig(7),3), ' m'])
disp(['Offshore v6, Hsig = ',num2str(Hsig(9),3), ' m'])
disp(['Offshore v22, Hsig = ',num2str(Hsig(10),3), ' m'])
disp([' '])
disp(['AQDP10, Hsig = ',num2str(Hsig(2),3), ' m'])
```

```
disp(['Bayentry Mike21 v6, Hsig = ',num2str(Hsig(3),3), ' m'])
disp(['Bayentry Mike21 v22, Hsig = ',num2str(Hsig(4),3), ' m'])
disp([' '])
disp(['AQDP06, Hsig = ',num2str(Hsig(1),3), ' m'])
disp(['Baymiddle Mike21 v6, Hsig = ',num2str(Hsig(5),3), ' m'])
disp(['Baymiddle Mike21 v22, Hsig = ',num2str(Hsig(6),3), ' m'])
disp([' '])
disp(['*************************************'])
disp(['* Mean Velocities  Bay Entry       *'])
disp(['*************************************'])
disp(['Um_{AQDP} =', num2str(mean(AQDP10_u_rot),1),'m/s'])
disp(['Um_{Mike21} v6=', num2str(mean(Mike_bayentry_u_v6),1),'m/s'])
disp(['Um_{Mike21} v11=', num2str(mean(Mike_bayentry_u_v7),1),'m/s'])
disp([' '])
disp(['Vm_{AQDP} =', num2str(mean(AQDP10_v_rot),1),'m/s'])
disp(['Vm_{Mike21} v6=', num2str(mean(Mike_bayentry_v_v6),1),'m/s'])
disp(['Vm_{Mike21} v11=', num2str(mean(Mike_bayentry_v_v7),1),'m/s'])
disp([' '])
disp(['*************************************'])
disp(['* Max/Min Velocities  Bay Entry    *'])
disp(['*************************************'])
disp(['Umax_{AQDP} =', num2str(max(AQDP10_u_rot),3),'m/s'])
disp(['Umin_{AQDP} =', num2str(min(AQDP10_u_rot),2),'m/s'])
disp([' '])
disp(['Umax_{Mike21} v6 =', num2str(max(Mike_bayentry_u_v6),3),'m/s'])
disp(['Umin_{Mike21} v6=', num2str(min(Mike_bayentry_u_v6),2),'m/s'])
disp([' '])
disp(['Umax_{Mike21} v11=', num2str(max(Mike_bayentry_u_v7),3),'m/s'])
disp(['Umin_{Mike21} v11=', num2str(min(Mike_bayentry_u_v7),2),'m/s'])
disp([' '])
disp(['Vmax_{AQDP} =', num2str(max(AQDP10_v_rot),2),'m/s'])
disp(['Vmin_{AQDP} =', num2str(min(AQDP10_v_rot),2),'m/s'])
disp([' '])
disp(['Vmax_{Mike21} v6 =', num2str(max(Mike_bayentry_v_v6),3),'m/s'])
disp(['Vmin_{Mike21} v6=', num2str(min(Mike_bayentry_v_v6),3),'m/s'])
disp([' '])
disp(['Vmax_{Mike21} v11=', num2str(max(Mike_bayentry_v_v7),3),'m/s'])
disp(['vmin_{Mike21} v11=', num2str(min(Mike_bayentry_v_v7),2),'m/s'])
disp([' '])
disp(['*************************************'])
disp(['* Mean Velocities  Bay Middle      *'])
disp(['*************************************'])
disp(['Um_{AQDP} =', num2str(mean(AQDP06_u_rot),2),'m/s'])
disp(['Um_{Mike21} v6=', num2str(mean(Mike_baymiddle_u_v6),1),'m/s'])
disp(['Um_{Mike21} v11=', num2str(mean(Mike_baymiddle_u_v7),1),'m/s'])
disp([' '])
disp(['Vm_{AQDP} =', num2str(mean(AQDP06_v_rot),1),'m/s'])
disp(['Vm_{Mike21} v6=', num2str(mean(Mike_baymiddle_v_v6),1),'m/s'])
disp(['Vm_{Mike21} v11=', num2str(mean(Mike_baymiddle_v_v7),1),'m/s'])
disp([' '])
disp(['*************************************'])
disp(['* Max/Min Velocities  Bay Middle    *'])
disp(['*************************************'])
disp(['Umax_{AQDP} =', num2str(max(AQDP06_u_rot),3),'m/s'])
disp(['Umin_{AQDP} =', num2str(min(AQDP06_u_rot),3),'m/s'])
```

```
disp([' '])
```

```
disp(['Umax_{Mike21} v6 =', num2str(max(Mike_baymiddle_u_v6),3),'m/s'])
disp(['Umin_{Mike21} v6=', num2str(min(Mike_baymiddle_u_v6),3),'m/s'])
disp([' '])
disp(['Umax_{Mike21} v11=', num2str(max(Mike_baymiddle_u_v7),3),'m/s'])
disp(['Umin_{Mike21} v11=', num2str(min(Mike_baymiddle_u_v7),3),'m/s'])
disp([' '])
disp(['Vmax_{AQDP} =', num2str(max(AQDP06_v_rot),2),'m/s'])
disp(['Vmin_{AQDP} =', num2str(min(AQDP06_v_rot),2),'m/s'])
disp([' '])
disp(['Vmax_{Mike21} v6 =', num2str(max(Mike_baymiddle_v_v6),3),'m/s'])
disp(['Vmin_{Mike21} v6=', num2str(min(Mike_baymiddle_v_v6),3),'m/s'])
disp([' '])
disp(['Vmax_{Mike21} v11=', num2str(max(Mike_baymiddle_v_v7),3),'m/s'])
disp(['Vmin_{Mike21} v11=', num2str(min(Mike_baymiddle_v_v7),3),'m/s'])
disp([' '])
disp(['***********************************'])
disp(['* Mean Velocities Offshore        *'])
disp(['***********************************'])
disp(['Um_{AQDP} =', num2str(mean(ADCP_u_rot),2),'m/s'])
disp(['Um_{Mike21} v6=', num2str(mean(Mike_input_u_v6),1),'m/s'])
disp(['Um_{Mike21} v11=', num2str(mean(Mike_input_u_v7),1),'m/s'])
disp([' '])
disp(['Vm_{AQDP} =', num2str(mean(ADCP_v_rot),1),'m/s'])
disp(['Vm_{Mike21} v6=', num2str(mean(Mike_input_u_v6),1),'m/s'])
disp(['Vm_{Mike21} v11=', num2str(mean(Mike_input_v_v7),1),'m/s'])
disp([' '])
disp(['***********************************'])
disp(['* Max/Min Velocities  Offshore    *'])
disp(['***********************************'])
disp(['Umax_{AQDP} =', num2str(max(ADCP_u_rot),3),'m/s'])
disp(['Umin_{AQDP} =', num2str(min(ADCP_u_rot),3),'m/s'])
disp([' '])
disp(['Umax_{Mike21} v6 =', num2str(max(Mike_input_u_v6),3),'m/s'])
disp(['Umin_{Mike21} v6=', num2str(min(Mike_input_u_v6),3),'m/s'])
disp([' '])
disp(['Umax_{Mike21} v11=', num2str(max(Mike_input_u_v7),3),'m/s'])
disp(['Umin_{Mike21} v11=', num2str(min(Mike_input_u_v7),3),'m/s'])
disp([' '])
disp(['Vmax_{AQDP} =', num2str(max(ADCP_v_rot),2),'m/s'])
disp(['Vmin_{AQDP} =', num2str(min(ADCP_v_rot),2),'m/s'])
disp([' '])
disp(['Vmax_{Mike21} v6 =', num2str(max(Mike_input_v_v6),3),'m/s'])
disp(['Vmin_{Mike21} v6=', num2str(min(Mike_input_v_v6),3),'m/s'])
disp([' '])
disp(['Vmax_{Mike21} v11=', num2str(max(Mike_input_v_v7),3),'m/s'])
disp(['Vmin_{Mike21} v11=', num2str(min(Mike_input_v_v7),3),'m/s'])
disp([' '])
```

Appendix VI

Matlab code used for spectral analysis of model results.

```
close all
clear all


dt=1;
fn=1/(dt*2);
bins=2^12
f=[1:bins/2]/bins*2*fn;
df=(bins*2*fn)^(-1);
f_band=0.01;
bin_size=round(f_band/df);
bin_number=fix(length(f)/bin_size);
f_new=[0.5:bin_number-0.5]*f_band;

% Load Field data
ADCP=load('ADCPinput_raw_v4.txt');
AQDP10=load('etha_AQDP10_thursday925_v3.txt')';
AQDP06=load('etha_AQDP06_thursday925_v3.txt');

% Load Mike21 Data
Mike_offshore=load('etha_offshore_MIKE21_v28.txt');
Mike_bayentry=load('etha_bayentry_MIKE21_v28.txt');
Mike_baymiddle=load('etha_baymiddle_MIKE21_v28.txt');

l_diff=length(ADCP)-length(Mike_offshore);
phase(1)=73;
phase(2)=73;
phase(3)=73;

Surf_matrix=[...
        ADCP(1:end-phase(1)-l_diff+1)...
        Mike_offshore(phase(1):end)...
        AQDP10(1:end-phase(2)-l_diff+1)...
        Mike_bayentry(phase(2):end)...
        AQDP06(1:end-phase(3)-l_diff+1)...
        Mike_baymiddle(phase(3):end)...
        ];
%plot(Surf_matrix(:,5:6))

for ii=1:size(Surf_matrix,2)

  surf=Surf_matrix(:,ii);

  Y=abs(fft(surf,bins));

  A=2*Y(2:bins/2+1)./bins;
  Power=Y(2:bins/2+1).^2;
  Power_scale=Power*2/bins^2/df;

  for cc=1:bin_number
    new_spect(cc)=mean(Power_scale((cc-1)*bin_size+1:cc*bin_size));
    new_A(cc)=mean(A((cc-1)*bin_size+1:cc*bin_size));
  end

  M0=sum(new_spect*bin_size)/length(AQDP06);
```

```
    Hm0(ii)=4*M0.^0.5;
    spect(:,ii)=new_spect;
    amp(:,ii)=new_A;
end
thursday=spect(:,1);
figure

subplot(2,2,1),semilogy(f_new,spect(:,1),'-k')
hold on
semilogy(f_new,spect(:,2),'-r')
xlabel('Frequency [Hz]')
ylabel('Power [m^2/Hz]')
title('Offshore (h = 21 m)')
legend('Field Data','Mike21 BW')
save thursday925_spect.txt thursday -ASCII

subplot(2,2,2),semilogy(f_new,spect(:,3),'-k')
hold on
semilogy(f_new,spect(:,4),'-r')
xlabel('Frequency [Hz]')
ylabel('Power [m^2/Hz]')
title('Bay Entry (h = 10.8 m)')
legend('Field Data','Mike21 BW')

subplot(2,2,3),semilogy(f_new,spect(:,5),'-k')
hold on
semilogy(f_new,spect(:,6),'-r')
xlabel('Frequency [Hz]')
ylabel('Power [m^2/Hz]')
title('Bay Middle (h = 7.4 m)')
legend('Field Data','Mike21 BW')

subplot(2,2,4), plot([0 568 683],[Hm0(1) Hm0(3) Hm0(5)],'k-o')
hold on
plot([0 568 683],[Hm0(2) Hm0(4) Hm0(6)],'r-x')
title('Significant waveheight')
xlabel('Distance from generation line [m]')
ylabel('Hm0 [m]')
legend('Field Data','Mike21 BW')

%%%%%%%%%%%%%%%%%%%%%%%%%%%%%%%%%%%%%%%%
figure

subplot(2,2,1),plot(f_new,spect(:,1),'-k')
hold on
plot(f_new,spect(:,2),'-r')
xlabel('Frequency [Hz]')
ylabel('Power [m^2/Hz]')
title('Offshore (h = 21 m)')
legend('Field Data','Mike21 BW')

subplot(2,2,2),plot(f_new,spect(:,3),'-k')
hold on
plot(f_new,spect(:,4),'-r')
xlabel('Frequency [Hz]')
ylabel('Power [m^2/Hz]')
title('Bay Entry (h = 10.8 m)')
```

```
legend('Field Data','Mike21 BW')

subplot(2,2,3),plot(f_new,spect(:,5),'-k')
hold on
plot(f_new,spect(:,6),'-r')
xlabel('Frequency [Hz]')
ylabel('Power [m^2/Hz]')
title('Bay Middle (h = 7.4 m)')
legend('Field Data','Mike21 BW')

subplot(2,2,4), plot([0 568 683],[Hm0(1) Hm0(3) Hm0(5)],'k-o')
hold on
plot([0 568 683],[Hm0(2) Hm0(4) Hm0(6)],'r-x')
title('Significant waveheight')
xlabel('Distance from generation line [m]')
ylabel('Hm0 [m]')
legend('Field Data','Mike21 BW')

%%%%%%%%%%%%%%%%%%%%%%%%%%%%%%%%%%%%%%%%%%%%%%
figure
set(gcf, 'PaperUnits', 'inches');
set(gcf, 'PaperSize', [50 7]);
subplot(2,2,1),plot(f_new,amp(:,1),'-ok','LineWidth',1,'MarkerSize',5)
hold on
plot(f_new,amp(:,2),'-xr','LineWidth',1)
xlabel('Frequency [Hz]','FontSize',8)
ylabel('Harmonic Amplitude [m]','FontSize',8)
title('Offshore (h = 21 m)')
axis([0 0.5 0 0.06])
legend('Field Data','Mike21 BW')

subplot(2,2,2),plot(f_new,amp(:,3),'-ok','LineWidth',1,'MarkerSize',5)
hold on
plot(f_new,amp(:,4),'-xr','LineWidth',1)
xlabel('Frequency [Hz]','FontSize',8)
ylabel('Harmonic Amplitude [m]','FontSize',8)
title('Bay Entry (h = 10.8 m)')
axis([0 0.5 0 0.06])
legend('Field Data','Mike21 BW')

subplot(2,2,3),plot(f_new,amp(:,5),'-ok','LineWidth',1,'MarkerSize',5)
hold on
plot(f_new,amp(:,6),'-xr','LineWidth',1)
xlabel('Frequency [Hz]','FontSize',8)
ylabel('Harmonic Amplitude [m]','FontSize',8)
title('Bay Middle (h = 7.4 m)')
axis([0 0.5 0 0.06])
legend('Field Data','Mike21 BW')

subplot(2,2,4), plot([0 568 683],[Hm0(1) Hm0(3) Hm0(5)],'k-o','LineWidth',1,'MarkerSize',5)
hold on
plot([0 568 683],[Hm0(2) Hm0(4) Hm0(6)],'r-x','LineWidth',1)
title('Significant Waveheight')
xlabel('Distance from generation line [m]','FontSize',8)
ylabel('Hm0 [m]','FontSize',8)
axis([0 900 0 3.5])
legend('Field Data','Mike21 BW')
```

Appendix VII

Matlab code used to calculate wave height distribution and a filtered envelope plot along the centerline of Waimea bay.

```
close all
clear all


dt=1;
fn=1/(dt*2);
bins=2^12
f=[1:bins/2]/bins*2*fn;
df=(bins*2*fn)^(-1);
f_band=0.01;
bin_size=round(f_band/df);
bin_number=fix(length(f)/bin_size);
f_new=[0.5:bin_number-0.5]*f_band;
phase=73;

%%%%%%%%%%%%%%%%%%%%%%%%%%%
% SURFLINE CALC
%%%%%%%%%%%%%%%%%%%%%%%%%

Surfline=load('surfline_thursday925_v28.txt');

for ii=1:size(Surfline,2)
   ii;
   surf=Surfline(:,ii);

   Y=abs(fft(surf,bins));


%%%%%%%%%%%%%%%%%%%%%%%%%%%%%%%%%%%%%%%%%%%%%%%%%
% Syntesize Untransformed Wavespectrum: Frequency space => Time Series
%%%%%%%%%%%%%%%%%%%%%%%%%%%%%%%%%%%%%%%%%%%%%%%
relative_t=[1:1798];

Re_Y1=real(Y(1))/bins;
Re_Y2=real(Y(2:end-1))/(bins/2); %Correcting the real parts.
Re_Y3=real(Y(bins/2))/bins;
Re_Y=[Re_Y1 Re_Y2' Re_Y3];

Im_Y=-imag(Y(1:end))/(bins/2);

%Create low-pass filter
fmin=0.061;%0.05;
fmax=0.069;%0.06; %Hz
f2=0.083;
f3=0.19;
Find_fmax=find(f>=fmax,1);
Find_fmin=find(f>=fmin,1);

Find_f2=find(f>=f2,1);
Find_f3=find(f>=f3,1);

for kk=Find_fmin:Find_fmax
   merged(kk,:)=Re_Y(kk).*cos(2*pi*f(kk)*relative_t)+Im_Y(kk)*sin(2*pi*f(kk)*relative_t);
end
```

```
for tt=Find_f2:Find_f3
   merged2(tt,:)=Re_Y(tt).*cos(2*pi*f(tt)*relative_t)+Im_Y(tt)*sin(2*pi*f(tt)*relative_t);
end

filter_surf(:,ii)=sum(merged);

filter_surf2(:,ii)=sum(merged2);
end

Bat=load('bathymetry_final1.txt');


%%%%%%%%%%%%%%%%%%
% Plot figure
%%%%%%%%%%%%%%%%%%
wall=0;
x_vector=[1:699]*2;

figure
plot(x_vector-352,Surfline(500:1798,:))
% hold on
% plot(x_vector(1:593),etha,'k','Linewidth',3)
axis([1 900 -2.6 2.6])
hold on
plot(x_vector-352,Bat(1:699),'y','Linewidth',3)
ylabel('Surface elevation [m]')
xlabel('Distance from Wave Generation line [m]')
hold on
plot(x_vector-352,Bat(1:699),'y','Linewidth',3)

figure
plot(x_vector-352,filter_surf(500:1798,:)')
% hold on
% plot(x_vector(1:593)-352,etha,'k','Linewidth',3)
axis([1 900 -0.5 0.5])
hold on
plot(x_vector-352,Bat(1:699),'y','Linewidth',3)
title('Filtered Envelope plot, Time-series 2 ( T=14.4 sec-16.4 sec)')
ylabel('Surface elevation [m]')
xlabel('Distance from Wave Generation line [m]')

figure
plot(x_vector-352,filter_surf2(500:1798,:)')
% hold on
% plot(x_vector(1:593)-352,etha,'k','Linewidth',3)
axis([1 900 -0.5 0.5])
hold on
plot(x_vector-352,Bat(1:699),'y','Linewidth',3)
ylabel('Surface elevation [m]')
xlabel('Distance from Wave Generation line [m]')
```

Appendix VIII
3 CD-RWs containing:

CD 1
- 3D Animation of Simulation 2.

CD 2
- Time-stamped video clip recorded during time-series 1 ***(Tape1 Clip2.avi)***
- Time-stamped video clip recorded during time-series 2 #1 ***(Tape2 Clip1 Sub1.avi)***

CD 3
- Time-stamped video clip recorded during time-series 2 #2 ***(Tape2 Clip1 Sub2.avi)***
- Time-stamped video clip of the swash zone recorded 30 minutes after time-series 2 ***(Tape2 Clip2 Sub1.avi)***